HIGH PRESSURE PHASE EQUILIBRIUM STUDIES OF NEAR-PRIMARY PLANETARY BASALTS

by

Karen Susan Bartels

B.S. Geology, Iowa State University
(1985)

Submitted to the Department of Earth, Atmospheric and Planetary Sciences in Partial Fulfillment of the Requirements for the Degree of

DOCTOR OF PHILOSOPHY

in

GEOLOGY

at the

MASSACHUSETTS INSTITUTE OF TECHNOLOGY

February, 1991

Signature of Author: _____
Department of Earth, Atmospheric, & Planetary Sciences, MIT
14 November 1990

Certified by: _____
Dr. Timothy L. Grove
Thesis Supervisor

Accepted by: _____
Dr. Thomas H. Jordan
Chairman, Departmental Committee on Graduate Students

HIGH PRESSURE PHASE EQUILIBRIUM STUDIES OF NEAR-PRIMARY PLANETARY BASALTS

by

Karen Susan Bartels

Submitted to the Department of Earth, Atmospheric and Planetary Sciences on 15 October 1990 in partial fulfillment of the requirements for the degree of Doctor of Philosophy

ABSTRACT

The high-pressure phase relations of primitive basalts from the earth and the eucrite parent body were determined using the techniques of experimental petrology. A high-MgO high-alumina basalt from Medicine Lake Volcano in northern California was chosen as an example of one type of primitive basalt from convergent margins on Earth. Magnesian eucrite clasts from howardites were chosen as the most primitive examples available of the howardite-eucrite-diogenite achondrite meteorite association.

Anhydrous phase relations were determined at 1 atm and 10 to 15 kbar for one sample of primitive high-alumina basalt (79-35g) from Giant Crater at Medicine Lake Volcano. This composition was found to be multiply saturated with olivine + augite + plagioclase + spinel near its liquidus at about 11 kbar. Additional experiments were conducted on mixtures of this sample with orthopyroxene and olivine to determine the location of the multiple saturation boundaries where the liquid coexists with the assemblage olivine + augite + orthopyroxene + plagioclase at 10 kbar and olivine + augite + orthopyroxene + spinel at 15 kbar. This information led to further experiments on another primitive high-alumina basalt from Medicine Lake (82-72f) at 10 to 12 kbar. This sample was also saturated with olivine + augite + plagioclase + spinel near its liquidus at 11 kbar. Orthopyroxene was only observed on the liquidus in one experiment. The primitive high-alumina basalt from Medicine Lake is low in K_2O (0.07 wt.%) and high in MgO (>10 wt.%) and Ni (231 ppm), with a light-REE depleted REE pattern. The high pressure phase equilibria and the geochemical characteristics of this basalt support a model whereby primary high-alumina basalt is formed by partial melting of a spinel-lherzolite assemblage just below the base of the crust at depths equivalent to 11 kbar pressure.

Melting experiments were conducted on synthetic analogs of two magnesian eucrite clasts from howardites, Kapoeta clast rho and Yamato 7308 pigeonite - eucrite clast 1, at 1 atm and 1 kbar pressure at oxygen fugacities in the range of IW (iron-wüstite) to IQF (iron-quartz-fayalite). The compositions of liquids and coexisting minerals (olivine - low-Ca pyroxene - plagioclase - spinel) were used to constrain possible melting and crystallization processes in the parent bodies of eucrite basalts. Our experimental results at 1 atm indicate that the olivine - low-Ca pyroxene - plagioclase - spinel - liquid and olivine - low-Ca pyroxene - spinel - liquid boundaries are reaction boundaries involving

olivine, in agreement with previous studies. At 1 kbar, however, the olivine primary phase volume shrinks, and the reaction relationship involving olivine disappears for both boundaries. The maximum pressure attained in a Vesta-sized eucrite parent body (EPB) is about 1 kbar, and these results provide important constraints on models relating the Howardite-Eucrite-Diogenite (HED) meteorite association through melting and differentiation processes.

Thesis Supervisor: Dr. Timothy L. Grove
Professor of Geology

TABLE OF CONTENTS

ACKNOWLEDGEMENTS

I would like to thank my advisor, Tim Grove, for his guidance and support and for introducing me to the joys and frustrations of experimental petrology. Roger Burns helped me gain confidence in my research abilities when I first came to M.I.T. and has been a friendly source of support ever since. I'm grateful to Fred Frey for trying to keep me honest in my discussion of trace elements; his trace element class did much toward my development as a critical scientific thinker. John Longhi and Mike Perfit provided much appreciated detailed reviews of parts of this thesis. My education at M.I.T. was enhanced through my interactions with Michael Geisler and Claire Kramsch, who helped me learn German, as well as bits of literature, philosophy, psychology and linguistics.

I'm grateful to Tom Juster, Ro Kinzler and Tom Sisson for "showing me the ropes" around the lab and for engaging in lively intellectual discussions, scientific and otherwise. Michael Baker, Karin Ehlers, Andrea Foster, Tanya Furman, Philippe Gurriet, Bill Jones, Sarah Kruse, Steve Recca, Tom Wagner and Deb Zervas provided encouragement, friendship and support during my years at M.I.T.

Special thanks to my friend and teacher Richard Worm, who has shared my love of geology and the outdoors for the past 13 years. Professors Donald Biggs, Steve Richardson, Karl Seifert and Ken Windom at Iowa State University further encouraged my interest in mineralogy and petrology.

My family, Cathy, Roger, Kim, Dale, David and Marilynn Bartels, was a constant source of love and support during the ups and downs of this long, strange, and always interesting journey. Thanks, love, and remembrance also

to my grandmother, Mary Bartels. My in-laws, Ann, David, Bob and Margaret Guell, also stood by me through thick and thin.

Finally, innumerable thanks to my husband, David Guell, for his steadfast love, faith and friendship as we shared this adventure called graduate school.

INTRODUCTION

The work presented in the two chapters of this thesis was undertaken to investigate the phase relations of primitive basalts from two terrestrial planetary bodies. The purpose of the studies was to understand the processes that led to the formation of these magmas and the implications of these processes on the evolutionary history of the planet. Chapter One describes melting experiments carried out using a near-primary magma from a convergent margin setting, a high-alumina basalt from Medicine Lake Volcano in northern California. These experiments were designed to provide information on the process of melt generation in the mantle wedge above a subduction zone. The second chapter describes the results of melting experiments conducted from 1 atmosphere to 1 kilobar on compositions of magnesian eucrite clasts from howardite meteorites. These experiments were designed to set limits on the size of the eucrite parent body and to explore melting and differentiation processes that occurred during the formation of the eucrite parent body.

Both experimental studies are concerned with the way in which magmas are generated by the partial melting of chondritic mantle sources. In the case of the Cascades the melting event is recent (Quaternary) and the mantle reservoir has experienced a long and complex history of differentiation. However, in the case of the eucrite parent body, the mantle melting event was confined to a brief period of time shortly after the accretion of the eucrite parent body, and the melts investigated may be primary magmas of that melting event.

Each chapter of this thesis begins with an introduction providing background information and setting forth the problem of interest. A section on experimental and analytical techniques is next, followed by a description and explanation of the experimental results. Finally, the significance of these results to the problem at hand is discussed.

CHAPTER ONE

HIGH PRESSURE PHASE RELATIONS OF A PRIMITIVE HIGH-ALUMINA BASALT FROM MEDICINE LAKE VOLCANO, CALIFORNIA

INTRODUCTION

The volcanics erupted in subduction zone settings show a wide variation in chemistry. Materials contributed by the subducted slab, the mantle wedge above the subduction zone, and the overlying continental or arc crust influence the end product erupted at a subduction zone volcano. Basalts are an important component of the volcanic suites in continental and island arcs. In many continental and island arc settings basalts can be found in association with the more evolved eruptive products (andesites and derivative lavas) and the basalt can be shown to be parental to these more evolved magmas. Basalt provides the most direct information about the melt generation processes involving subducted slab and overlying mantle wedge, because compared to derivative andesitic lava, basalt has been less affected by processes of fractional crystallization and assimilation of continental crust.

Early experimental studies (Yoder and Tilley, 1962; Kushiro, 1972; Mysen et al., 1974; Nicholls and Ringwood, 1973) focused on the problem of whether andesite associated with subduction zone volcanism was a direct partial melt of the subducted oceanic crust or overlying hydrated mantle. The results of these investigations were that melts produced by melting of hydrous mantle were most similar to basalt. In the case of eclogite melting the trace and rare earth element abundances in andesites (or arc basalts) are inconsistent with the presence of garnet or clinopyroxene as the likely residues of eclogite melting.

The high pressure phase relations of a small number of basaltic magmas from subduction zone environments have been studied using the methods of experimental petrology. The goal of these studies has been to determine the mantle source material, the depth and temperature of melting and the type of melting processes involved in producing these basalts. Tatsumi et al. (1983)

assumed that three basalt types found in the Japan arc were primary magmas, determined their melting relations at high pressure, and inferred mantle depths and temperatures of melt generation. (In this paper the term *primary magma* is used to mean a liquid that has been separated from its source region at depth and delivered to the surface without experiencing subsequent modification). Johnston (1986) chose a basalt from the South Sandwich Islands arc and found that it was not saturated on its liquidus with peridotite mantle residue phases at any pressure. Instead he found an interval of pressure where garnet and clinopyroxene were near liquidus phases and postulated an eclogite source. Gust and Perfit (1987) studied the phase relation of a high MgO, low Al_2O_3 basalt from the Aleutian arc and found that its high pressure phase equilibria were similar to those of primitive MORB (mid-ocean ridge basalt), and postulated a peridotite source. The present study determines the high pressure phase relations of another type of basalt from a subduction zone environment, primitive high-alumina basalt (HAB) from Medicine Lake Volcano, CA.

<u>High-alumina basalt</u>

One of the basalt types found in convergent margin settings is high alumina basalt. Powers (1932) described aphyric MgO- and Al_2O_3- rich basalts from the vicinity of Medicine Lake volcano, and Tilley (1950) recognized this basalt type as high alumina basalt (HAB) and noted its occurrence in a variety of igneous provinces including intraplate settings, mid-ocean ridges, and island arcs. Kuno (1960) first recognized the volumetric importance of HAB in convergent margin environments and included HAB as a major primary magma type in his classification of the aphyric basalts of central Honsyu and the Izu Islands, Japan, in addition to the previous categories of tholeiite and alkali basalt. Kuno defined HAB as basalt with higher Al_2O_3 (generally > 17 wt.%) than tholeiite for similar SiO_2 and alkali contents (K_2O + Na_2O) and

with lower alkali content than alkali basalt, and pointed out that these factors hold only as long as aphyric rocks are compared, since tholeiitic rocks rich in plagioclase phenocrysts will also be high in Al_2O_3. Kuno proposed that HAB is a very common basalt type in orogenic belts; in addition to the Japanese HAB, the basalts from the Kuriles, Kamchatka, Aleutian Islands, High Cascades, Nicaragua, New Zealand, Taiwan and Sumatra fall within the field of HAB on Kuno's Al_2O_3 vs (Na_2O + K_2O) discrimination diagrams.

Primitive HAB from Medicine Lake Volcano

HAB is an abundant rock type in the Cascades and in the northern part of the Basin and Range province (Waters, 1962). Several HAB localities from the Cascades (Crater Lake, Lassen Peak, Modoc Lava-Bed Quadrangle) are mentioned in Kuno's (1960) paper, and analyses of aphyric Modoc HAB from Powers (1932) and Yoder and Tilley (1957) are cited as other examples of the HAB lava type.

The Cascade range, characterized by its impressive andesite stratovolcanoes, also consists of large volumes of HAB contained in lava fields, cinder cones, and small shield volcanos. Medicine Lake Volcano is a Quaternary shield volcano covering about 2500 km^2 with an estimated volume of 600 km^3 (Donnelly-Nolan, 1988). It is part of a belt of shield volcanoes formed in an extensional tectonic environment parallel and to the east of the composite volcanoes of the High Cascades, and it is located about 50 km ENE of Mt. Shasta (Figure 1-1). Powers (1932), Anderson (1941) and Donnelly-Nolan (1988) have mapped and described the geology of the volcano. The shield consists mainly of high-alumina basalt and basaltic andesite, and the summit is topped by andesite erupted from an elliptical arrangement of vents. Its highest point is Mt. Hoffman at 2398 m above sea level, and Medicine Lake lies within the summit rim. Other eruptions of lavas ranging from andesite to

rhyolite occurred at the volcano, and basalt flows originating at vents on the flanks of the volcano extend outward up to 40 km. Primitive HAB has erupted at this volcano throughout its history and has been demonstrated to be parental to the calc-alkaline rock suite, consisting of basaltic andesite, andesite and rhyolite, produced at the volcano through processes of fractional crystallization, assimilation and magma mixing (Gerlach and Grove, 1982; Grove et al., 1982; Grove et al., 1988). The samples chosen for this study, 79-35g and 82-72f, are HAB's erupted about 10,500 years ago from Giant Crater, a vent 9 km SSW of Medicine Lake (Grove et al., 1982; Donnelly-Nolan et al., 1991, submitted JGR), and are among the most primitive lavas at Medicine Lake Volcano (MgO = 9.9 - 10.5 wt.%, Mg # = 67 - 69). These lavas are high Al_2O_3 (18.5 wt.%) olivine basalts with low TiO_2 (0.6 wt.%), K_2O (0.07 wt.%), and P_2O_5 (0.05 wt.%) (See Table 1-1). They are aphanitic and microporphyritic, containing only 2 vol.% microphenocrysts of olivine (Fo_{89}) and plagioclase (An_{86}), and hence are considered to represent liquid compositions. Samples 79-35g and 82-72f are compositionally similar to Warner and Modoc basalts, also from Medicine Lake Volcano, described and analyzed by Powers (1932) and Anderson (1941) and given as an illustrative example of HAB by Tilley (1950) and Kuno (1960).

The primitive Medicine Lake HAB contrasts with the more abundant lower-MgO HAB found in island arc settings. The Medicine Lake HAB is a primitive, aphyric lava with high MgO (>10%) and Ni (231 ppm) contents. The Ni content of 82-72f is sufficiently high for it to have been derived by partial melting of a mantle peridotite, assuming an initial Ni concentration of 3000 ppm in mantle olivine (Hart and Davis, 1978) and a partition coefficient ($D_{Ni}^{ol/liq}$) of 13 (Kinzler et al., 1990). Therefore, this basalt is a strong candidate as a primary magma. In contrast, many island arc HABs are

strongly porphyritic, containing 30-60 modal % plagioclase with low MgO contents (< 7 %) and low Ni contents (< 150 ppm). The formation of these common arc HABs will be discussed further after the description of the results of the high pressure experiments on the primitive Medicine Lake HAB.

Melting experiments were conducted on sample 79-35g at 10, 12 and 15 kbar to quantify the liquid line of descent, the order of phase appearance, and phase proportions expected for crystallization under anhydrous conditions. Additional melting experiments were conducted on mixes of 79-35g plus orthopyroxene and 79-35g plus olivine to determine compositions of liquids saturated with a plagioclase lherzolite mineral assemblage at 10 kbar, and a spinel lherzolite mineral assemblage at 15 kbar. The results of these experiments lead to further experiments at 10 to 12 kbar on sample 82-72f. The results of melting experiments from this study will be compared to the results of previous experimental studies on other high-alumina basalts (Tatsumi et al., 1983; Johnston, 1986; Gust and Perfit, 1987; Baker and Eggler, 1987). Our results will then be used to infer a model for the origin of primitive, near-primary magmas at Medicine Lake Highland and in similar volcanic environments.

EXPERIMENTAL METHODS

Experimental procedures

Small rock chips from 79-35g, a fresh, fine-grained, equi-granular, distinctly non-porphyritic, diktytaxitic lava, were reduced to a homogeneous powder by grinding in a SPEX WC shatterbox, and this powder was used as starting material for the first set of experiments. A second set of experiments was conducted using mixtures of 79-35g with orthopyroxene and 79-35g with

olivine. These mixes were prepared by grinding powdered 79-35g with either hand picked, clean, crushed Kragero orthopyroxene or hand picked, clean, crushed San Carlos olivine in an automatic agate mortar and pestle for 3 hours. The final set of experiments was performed using sample 82-72f, prepared in the same way as 79-35g. Table 1-1 provides the starting compositions used in this study. Melting experiments were carried out on sample 79-35g at 1 atm by Grove et al. (1982) and on sample 82-72f in this study. The experimental conditions and proportions of phases observed in experiments on 79-35g at 10, 12 and 15 kbar are reported in Table 1-2. Experimental conditions and proportions of phases observed in experiments at 10 and 15 kbar on the mix compositions (Table 1-1) are reported in Table 1-4, and the results of experiments on 82-72f at 1 atm and 10, 11, and 12 kbar are reported in Table 1-6.

The 1-atm experiments were conducted in Deltech quenching furnaces in an atmosphere of CO_2/H_2 gas. Pellets of powdered rock starting material were sintered to 0.008" diameter Pt-Fe alloy loops custom made to minimize Fe loss from the experimental charge (Grove, 1981). Temperature was monitored using Pt-$Pt_{90}Rh_{10}$ thermocouples calibrated against the melting points of gold, lithium metasilicate and diopside on the IPTS 1968 temperature scale (Biggar, 1972). Oxygen fugacity was monitored using ZrO_2-CaO electrolyte cells calibrated at the Fe-FeO buffer.

High pressure experiments were conducted using a 1/2" solid-medium piston cylinder apparatus (Boyd and England, 1960). The temperature was monitored and controlled using Pt-$Pt_{90}Rh_{10}$ thermocouples, and reported temperatures are estimated to be accurate to within +/- 15°C based upon the reproducibility of experimental results. Experiments were performed using the piston-in method (Johannes et al., 1971). The pressure medium consisted of an

outer cell of NaCl and an inner cell of Pyrex, and the reported pressure assumes no friction correction. Pressure was calibrated at 10 kbar by the gold melting technique (Akella and Kennedy, 1971), and the observed pressure correction was 0-1 kbar. This lies within the uncertainty of the calibration, so the pressures reported here do not include a friction correction.

Approximately 10 mg of starting material was packed into a graphite capsule and dried in an oven at 175°C for 2 hours. The graphite capsule was then welded into a platinum capsule and placed in a ceramic sleeve. This 0.125" sample assembly was centered in the hot spot of a graphite furnace using crushable alumina (An900) spacers. The thermocouple was located 0.125" above the center of the hot spot, or 0.0625" above the top of the sample capsule, and was separated from the capsule by a 0.0625" wafer of An900. The temperature gradient between the thermocouple position and the center of the sample was measured to be 45°C. Temperatures reported in Table 1-2 are corrected for this temperature difference. The oxygen fugacity of the experimental assemblage is estimated to be between Fe-FeO (IW) and Fe_2SiO_4-Fe_3O_4-SiO_2 (FMQ) (M.B.Baker, personal communication).

Duration of Experiments

Experiments ranged in duration from one to six hours for high-temperature, near-liquidus experiments to 24 hours or longer for low-temperature, highly-crystalline experiments. Iron loss was estimated by materials balance calculations in which the measured compositions of all the phases in the experiment were balanced against the starting composition. Iron loss ranged from undetectable to 6.4 % of the total FeO present (i.e., for sample 79-35g, 8.53 wt.% FeO minus 0.0 to 0.51 wt.%). Experiments which lost more than this amount of iron are not reported here. No blebs of Fe were noted in the experiments, indicating that smelting of iron by the graphite

capsule was not a complication of these experiments. The amount of Fe loss depends on the integrity of the graphite capsule during the experiment, and is not simply correlated with experiment duration. Brittle failure of the graphite capsule results in "rivers" of liquid forming a connection between the silicate part of the sample and the outer Pt capsule, and the access of liquid to Pt causes Fe loss.

At 12 kbar several experiments were conducted under identical conditions but for varying lengths of time, in order to investigate the effect of experiment duration on phase assemblages and compositions. Results of experiments conducted at 1270°C for 3 hours (H96) and 19 hours (H132) indicate that 3 hours is not long enough to allow re-equilibration of the starting material at this temperature and pressure. Olivine occurred in H96, the shorter experiment, but not in the longer experiment H132 (see Table 1-2). Figure 1-2 shows backscattered electron images of H96 and H132. The olivine grains in H96 are rounded and the margins appear to have dissolved. In addition, the olivine grains are zoned; some have Mg-rich cores and Fe-rich rims, and some have Fe-rich cores and Mg-rich rims. The pyroxene grains in H96 contain large unreacted cores and thin (10 micron) reaction rims. The pyroxene grains in H132, in contrast, have reacted to a greater extent and have thicker (30 to 50 micron) rims. The plagioclase rims are also thicker in H132 than in H96 (10 vs. 3 microns), although this is not visible in the photograph.

The difference in phase assemblage between these two experiments appears to be due to different extents of melting and reaction. In H96, there is a larger amount of pyroxene and plagioclase stored in unreacted cores. As melting proceeds, addition of these components to the liquid moves it off of the olivine-plagioclase-augite saturation boundary. The longer experiment is

considered to be more representative of the actual phase assemblage at this temperature, and olivine is thus not considered a stable phase in these experiments at 12 kbar. Experiments conducted at 1280°C for 6, 14 and 28 hours (H204, H131, H201) have identical phase assemblages with similar phase proportions (Table 1-2). These results suggest that, especially for experiments containing less than 80 % liquid, minimum experiment times of > 6 hours are desirable.

Analytical methods

Experimental products were analyzed with the MIT 4-spectrometer JEOL 733 Superprobe and reduced using Bence and Albee (1968) matrix corrections with modifications of Albee and Ray (1970). Standardization of the MIT JEOL superprobe was checked for each analytical session against a natural MORB glass working standard from the East Pacific Rise. This glass has been analyzed at our facility more than 1500 times over a range of 18 months, including the duration of this experimental study. The compositions of minerals and glasses from experiments are summarized in Tables 1-3, 1-5, and 1-7. Compositions of phases in each experiment were used to compute the phase proportions (provided in Tables 1-2, 1-4, and 1-6) by materials balance (Bryan et al., 1969).

Samples 79-35g and 82-72f were analyzed for major and selected trace elements by x-ray fluorescence (XRF) at the laboratory of M. Rhodes, University of Massachusetts, Amherst, and for REE and other selected trace elements by neutron activation analysis (INAA) at M.I.T.(see Tables 1-1 and 1-9).

EXPERIMENTAL RESULTS

Liquid line of descent at 1 atm and 10, 12 and 15 kbar

The results of melting experiments on 79-35g from 1 atm (Grove et al., 1982) to 15 kbar are shown in Figure 1-3. Each symbol represents an experiment and indicates which phases are present at that temperature and pressure, and the lines drawn are the interpretation of this data. At 1 atm 79-35g is saturated on its liquidus at 1230°C with plagioclase and olivine, and is multiply saturated with plagioclase + olivine + augite at 1170°C. At 10 kbar the order of phase appearance remains the same, with olivine + plagioclase on the liquidus at 1285°C, followed by olivine + plagioclase + augite at 1275°C. The slope of the olivine + plagioclase liquidus curve up to 10 kbar is 5.5°C per kbar. At 12 and 15 kbar, however, augite is the liquidus phase, and the liquidus curve above about 11 kbar is considerably steeper, with a slope of 30°C per kbar. At 12 kbar, augite is on the liquidus at 1305°C, followed by augite + spinel + plagioclase at 1290°C. Augite and spinel are the first phases observed at 1345°C in the 15 kbar experiments, with augite + spinel + plagioclase at 1295°C. The liquidus temperature is estimated to be 1365°C and there may exist a small interval of augite crystallization. Olivine is no longer a stable phase in experiments at 12 and 15 kbar. The dashed line indicates the reaction relation olivine + liquid = augite + spinel which terminates the coexistence of liquid and olivine for this bulk composition. The intersection of this reaction boundary with the olivine + plagioclase + liquid line and the augite + liquid line at approximately 11 kbar and 1290°C, point A on Figure 1-3, marks the equilibrium liquid + olivine + plagioclase + augite + spinel (see Presnall et al., 1978 and Kushiro and Yoder, 1966, for details on the analog reactions in CMAS). This intersection marks the point at which the olivine +

plagioclase + augite + liquid and the augite + spinel + plagioclase + liquid boundaries merge. Composition 79-35g is multiply saturated with olivine, augite and plagioclase within 10° to 20°C of its liquidus temperature at 10 kbar, and multiply saturated augite, plagioclase and spinel within 15° to 20°C of its liquidus temperature at 12 kbar, and it is estimated that olivine, augite, plagioclase and spinel occur on the liquidus at about 11 kbar.

Multiple saturation experiments on mix compositions

The phase diagram depicted in Figure 1-3 shows that liquids in melting experiments on sample 79-35g are not saturated with low-Ca pyroxene over the pressure range of 1 atm to 15 kbar. In order to locate the olivine-orthopyroxene-augite-plagioclase/spinel multiple saturation boundaries at 10 and 15 kbar, experiments were conducted on mixtures of 79-35g plus orthopyroxene and 79-35g plus olivine, respectively. These phases were added solely for the purpose of changing the bulk composition so that the location of the olivine-orthopyroxene-augite-plagioclase/spinel multiple saturation boundaries could be determined by melting experiments. The results of these experiments are shown in Figure 1-4A in the Olivine-Cpx-Quartz pseudoternary projection and in Figure 1-4B in Plagioclase-Cpx-Quartz pseudoternary projection.

Multiple saturation at 10 kbar

At 10 kbar, an 84:16 (by weight) mixture of 79-35g and orthopyroxene (#2 in Figure 1-4A) crystallized olivine + orthopyroxene first, followed by olivine + augite + orthopyroxene + plagioclase (Table 1-4). Figure 1-4 shows this 10 kbar olivine + orthopyroxene + augite + plagioclase + liquid boundary (indicated by a star) along with the olivine + plagioclase + augite boundary determined from the 10 kbar experiments on 79-35g alone. Also shown on Figure 1-4A are the projected positions of the compositions of augite

and orthopyroxene coexisting with liquids on the 10 kbar orthopyroxene + liquid = olivine + augite + plagioclase reaction boundary. The liquids saturated with only olivine + orthopyroxene from the 10 kbar experiments on the 84:16 mix cannot be used to constrain the liquid + olivine + orthopyroxene + plagioclase boundary since they are not saturated with plagioclase. The dashed lines emanating from the projected positions of the liquids on the 10 kbar olivine + augite + orthopyroxene + plagioclase + liquid reaction boundary are the inferred olivine + orthopyroxene + plagioclase + liquid and the inferred orthopyroxene + augite + plagioclase + liquid boundaries.

At 10 kbar, a liquid saturated with the assemblage olivine + augite + plagioclase moves away from a plane which joins augite (solid circles), olivine, and plagioclase (which forms the fourth apex of the pseudoquaternary and plots above the plane of the page), along the olivine + augite + plagioclase + liquid boundary towards decreasing normative silica. Thus, the down temperature direction along the olivine + augite + plagioclase + liquid boundary at 10 kbar is away from the Quartz apex in the pseudoternary. This path of liquid evolution with olivine + augite + plagioclase crystallization is the opposite of the down temperature direction along the same boundary at 1 atm (Grove et al., 1982).

The nature of the reaction at the 10 kbar liquid + orthopyroxene + olivine + augite + plagioclase multiple saturation boundary depends on the compositions of the liquid and pyroxenes. The tie line between orthopyroxene (triangles) and the 10 kbar, multiply saturated liquids (star) pierces the plane defined by olivine, augite (circles) and plagioclase. This piercing relationship requires the multiple saturation boundary to be a reaction boundary, along which orthopyroxene + liquid = olivine + augite + plagioclase. In a down

temperature direction, this reaction is terminal to the coexistence of orthopyroxene + liquid.

Also shown in Figure 1-4A are the starting compositions, 79-35g (#1) and the 84:16 79-35g/orthopyroxene mixture (#2). Note that the 79-35g bulk composition is in the olivine primary phase volume relative to the 10 kbar boundaries. During fractional crystallization at 10 kbar, a liquid with the bulk composition of 79-35g crystallizes olivine + plagioclase, moving away from the olivine apex to the olivine + plagioclase + augite boundary. Further crystallization involves olivine + plagioclase + augite and liquids evolve along the olivine + plagioclase + augite boundary towards nepheline normative compositions. Liquids evolving by fractional crystallization of 79-35g at 10 kbar, therefore, will never reach the liquid + olivine + plagioclase + augite + orthopyroxene reaction boundary.

Multiple saturation at 15 kbar

Three melting experiments conducted at 15 kbar on the 80:20 mix (by weight) of 79-35g plus olivine (#3 in Figure 1-4A) over a temperature range 1355°C to 1325°C produced liquids saturated with olivine, augite, orthopyroxene and spinel (Table 1-4). Figure 1-4A shows the compositions of the two higher temperature liquids (Table 1-5) and the projected positions of the pyroxenes with which all three experiments were saturated and the starting mix composition. The third, lowest temperature, 15 kbar experiment projects to a strongly silica undersaturated position and is not shown in Figure 1-4.

The 15 kbar multiply saturated liquid compositions trend off to strongly nepheline normative projected positions. Plagioclase is not stable for this starting composition at 15 kbar, and thus the liquids are enriched in an Na_2O-rich plagioclase component. The liquids project close to the plagioclase apex,

at slightly silica undersaturated positions relative to the pseudoquaternary volume (Figure 1-4B).

The effect of increasing pressure from 10 to 15 kbar changes the saturating aluminous phase from plagioclase to spinel and shifts the position of the multiple saturation boundary towards higher normative olivine, and lower normative quartz contents. This shift is consistent with that observed in numerous previous studies in simple and natural systems (e.g. Presnall et al.., 1978; Stolper, 1980). Increasing pressure also changes the reaction relationship along the melting boundary from liquid + orthopyroxene = olivine + augite + plagioclase, at 10 kbar, to liquid + olivine = augite + orthopyroxene + spinel, at 15 kbar.

The effect of pressure on pyroxene composition

Augite composition depends upon experimental pressure, temperature, and whether or not orthopyroxene is a coexisting phase. Compared to the augite grown in the 1 atm experiments, the augites produced in 10 to 15 kbar experiments have lower wollastonite content (Wo, $CaSiO_3$) and higher Ca-Tschermak content (CaTs, $CaAlSiAlO_6$). Over the pressure range 10 to 15 kbar, Wo decreases and CaTs increases with increasing pressure. At a given pressure, augites coexisting with orthopyroxene have lower Wo than those that do not. Grove et al. (1989) used experiments on this HAB and several primitive MORB compositions (Kinzler and Grove, 1991, submitted JGR) to develop a geobarometer based on the variation of Al^{VI} in augites from experiments saturated with augite + plagioclase +/- olivine +/- orthopyroxene +/- spinel. The expression recovers pressure to within +/- 1 kbar for experiments up to 12 kbar for MORB and HAB compositions, but is not as useful for undersaturated magmas. Coexisting augite and orthopyroxene in the high pressure experiments contain a high percentage of non-quadrilateral

components [other than $(Ca,Mg)SiO_3$, $(Ca,Fe)SiO_3$, $MgSiO_3$, and $FeSiO_3$; i.e. $R^{2+}Al^{VI}SiAl^{IV}O_6$, $R^{2+}TiAl_2O_6$]. This high proportion of others components exceeds the limits of geothermometers based on the Wo and En contents of coexisting augite and orthopyroxene. Lindsley (1983) and Lindsley and Anderson (1983) caution against using their thermometer with augites containing more than 10% others, and the augites from these high pressure experiments contain about 10 % of these other components.

Experiments on 82-72f

Other primitive lavas from Medicine Lake Volcano are shown in Figure 1-5 on a portion of the pseudoternary Olivine - Clinopyroxene - Quartz phase diagram constructed based on the experiments described above. Lavas with more than 9 wt.% MgO were selected as primitive. Most of these lavas cluster between the 10 and 15 kbar multiple saturation boundaries. Lavas that are displaced to higher quartz normative compositions have probably experienced some crustal contamination (Grove et al., 1988). Most of these primitive lavas range in Mg# from 0.61-0.70 and CaO/Al_2O_3 ratio from 0.61-0.67 and have TiO_2 (0.70-0.84 wt.%), Na_2O (2.31-2.75 wt.%) and K_2O (0.08-0.35 wt.%) contents similar to 79-35g. One of the most primitive lavas is sample 82-72f, also collected from Giant Crater. The projected position of this lava is very near the 10 kbar orthopyroxene + liquid = olivine + augite + plagioclase reaction boundary and for this reason 82-72f was chosen for further experiments at 10 to 12 kbar and 1 atm. Experimental conditions and results for experiments on 82-72f are listed in Table 1-6.

At 1 atm, olivine alone is the liquidus phase at 1266°C, with plagioclase appearing 12°C lower at 1254°C. The aphyric texture of this rock, the existence of olivine alone on the liquidus and the fact that the liquidus temperature is predicted accurately by the Roeder and Emslie (1970) olivine-liquid equilibrium

formulation indicates that neither olivine nor plagioclase accumulation occurred with this sample (cf. Crawford et al., 1987). At 10 kbar olivine and plagioclase are the liquidus phases at about 1282°C, and at 12 kbar augite and spinel are liquidus phases at 1300°C. At 11 kbar, small amounts of olivine, augite and spinel are present in an experiment which is 99% liquid at 1290°C. By 1285°C, augite, plagioclase and spinel occur with olivine in an experiment which is 70% liquid (Figure 1-6A). The augite in this experiment is markedly sector-zoned, one zone with a composition like that of augite from the 10 kbar experiments saturated with orthopyroxene and the other with a composition like that of augite from experiments containing no orthopyroxene. One experiment at 1293°C contains orthopyroxene along with olivine and similarly sector-zoned augite, but this experiment lost a small amount of iron (Figure 1-6B). The Mg# of the glass ranges from 0.70 to 0.72, and the orthopyroxene grains are reverse zoned from $Wo_5En_{84.7}$ to Wo_5En_{87}. The cores of the orthopyroxene grains would be in equilibrium with a glass of Mg# 0.67 assuming a Mg-Fe exchange K_D of 0.28. Sample 82-72f is thus only slightly more Fe-rich than a liquid saturated with a plagioclase/spinel lherzolite mantle assemblage very near its liquidus at 11 kbar and is thus very close to a *primary* melt generated at this pressure.

DISCUSSION

Comparison of experimental results with previous studies

High pressure phase relations of arc basalts

For the primitive Medicine Lake HAB 79-35g, olivine and plagioclase are the liquidus phases from 1 atm to 10 kbar and augite is the liquidus phase from 10 to 15 kbar. These results differ from those of several recent studies on

other HAB and primitive arc compositions (Table 1-8). Two studies involving anhydrous high pressure experiments conducted on natural HAB from island arcs (Baker and Eggler, 1987; Johnston, 1986) found plagioclase as the liquidus phase from 1 atm to 17 kbar. Experiments conducted on natural and synthetic high-Mg, lower alumina basalts (Gust and Perfit, 1987; Tatsumi et al., 1983) show olivine as the liquidus phase until 10 kbar and 15 kbar, respectively.

The differences in results among these experimental studies are mainly due to differences in starting compositions. The term high-alumina basalt covers a wide range of basaltic compositions (Crawford et al., 1987). Baker and Eggler (1987) determined the phase relations for 3 HABs from the Aleutian island of Atka. These basalts have low Mg#s (0.43-0.54) and low CaO/Al_2O_3 ratios (0.43-0.60), with 18.7 to 19.7 % Al_2O_3. Johnston (1986) used a more primitive HAB from the South Sandwich Islands which has an Mg# of 0.63 and a CaO/Al_2O_3 ratio of 0.64, with 18.5 % Al_2O_3. The relatively low Mg#s, and, in the case of the Baker and Eggler study, the low CaO/Al_2O_3 ratios, result in plagioclase as the liquidus phase.

Experiments which used more primitive basaltic material as starting compositions have olivine as the liquidus phase. Tatsumi et al. (1983) calculated a primary "HAB" magma composition by adding olivine to a low-MgO HAB, and experiments were conducted on a synthetic mix of this composition. This synthetic basalt has a high Mg# (0.69) and a CaO/Al_2O_3 ratio of 0.60, but with only 15.7 % Al_2O_3. None of Tatsumi's high-pressure experiments were saturated with an aluminous phase. Gust and Perfit (1987) conducted experiments on a natural high-Mg basalt also containing 15.7 % Al_2O_3 from the Makushin volcanic field on Unalaska Island. The Aleutian basalt has a relatively high Mg# (0.65) and a high CaO/Al_2O_3 ratio (0.64), and is therefore more comparable (except for Al_2O_3 content) to the HAB used in

this study, sample 79-35g (Mg# = 0.67 and CaO/Al_2O_3 = 0.64). Their results are similar to the results reported here, with olivine as the liquidus phase up to 10 kbar (here olivine plus plagioclase), and augite as the liquidus phase at P > 10 kbar. The results of these experiments, which used primitive basalts as starting materials, are probably the most appropriate for understanding the sources of primary magmas.

Anhydrous partial melting experiments on mantle peridotite at 10 kbar

Crawford et al. (1987) recognized that liquids produced in 10 kbar anhydrous melting experiments on mantle peridotite have the composition of high-Mg HAB (see their Table 5). Table 1-8 lists the compositions of 10-kbar melts saturated with a spinel-lherzolite assemblage from the studies of Fujii and Scarfe (1985), Falloon and Green (1987), and Takahashi (1986). These compositions are plotted in Figure 1-7 in the Olivine-Cpx-Quartz and Olivine-Plagioclase-Quartz pseudoternary projections along with the field of high-Mg HAB from Giant Crater and the compositions of HAB used in other high pressure melting studies. The 10 kbar mantle melts have high Mg#s (0.69 - 0.72) and high Al_2O_3 contents (17.1 - 19.2 wt.%), and are very similar to the high-Mg HAB from Giant Crater, which have Mg# from 0.67 - 0.70 and Al_2O_3 of 18.5 wt.%.

Geochemical characteristics of high-Mg HAB from Giant Crater

Perfit et al. (1980) have noted that major-element compositions of primitive IAB (island arc basalt) are similar to primitive MORB (mid-ocean ridge basalt), overlapping in terms of Al_2O_3 (15 - 18 wt.%), TiO_2 (0.4 - 1.2 wt.%), and CaO and FeO contents but with slightly higher K_2O. The primitive HAB from Giant Crater at Medicine Lake also has major-element characteristics similar to primitive MORB (high Mg#, low TiO_2, low K_2O) except for their distinctively higher Al_2O_3 contents. Only a few primitive

MORBs contain > 18 wt.% Al_2O_3. For the 114 primitive MORBs tabulated by Elthon (1990), the average Al_2O_3 is 16.3 wt.% with only three samples containing over 18 wt.% Al_2O_3. The Ni contents of IAB are typically lower than those for MORB at equivalent Mg#s; few IAB have Ni > 150 ppm. Sample 82-72f h!s a Ni content of 231 ppm (Table 1-9), which is higher than most IAB but within the range of Ni contents for primitive, aphyric MORB (200-300 ppm) (Basaltic Volcanism Study Project, 1981).

The chondrite-normalized REE pattern for the Giant Crater HAB is light-REE depleted with a slight positive Eu anomaly; the ratio $(La/Sm)_{CH}$ is about 0.5 and heavy-REE contents are at 7 to 8 times chondritic values. Figure 1-8A shows the REE pattern for 82-72f compared to the pattern for a primitive MORB from the Kane Fracture Zone, AII78-3-103 (Bryan et al., 1981). The pattern for 82-72f is similar to that for MORB, but with lower abundances, suggesting either a more depleted source or higher degrees of melting involved in forming 82-72f. The slight positive Eu anomaly is not a result of plagioclase accumulation; the sample is aphyric (not plagioclase porphyritic) and its liquidus temperature is predicted accurately by the Roeder and Emslie (1970) olivine-liquid equilibrium formulation, which would not be the case if significant plagioclase accumulation had occurred (cf. Crawford et al., 1987). The positive Eu anomaly could result from clinopyroxene remaining in the source (Johnson and Kinzler, 1989) and constrains the oxygen fugacity of the source as more reducing than the QFM (quartz-fayalite-magnetite) buffer (Sun et al., 1974). Most IAB have flat to light-REE enriched patterns (Basaltic Volcanism Study Project, 1981), although Davidson (1987) has noted a subset of IAB from the Lesser Antilles that are light-REE depleted. The ratio (Ba/La) ranges from 4-10 for N-type MORB (Sun et al., 1979) with depleted LREE patterns, whereas IAB with flat or LREE enriched REE patterns generally have

(Ba/La) ranging from 18-110 (Hickey et al., 1982). The (Ba/La) ratio of 20 for 82-72f is within this range of arc-like signatures. Other trace element signatures generally considered characteristic of arc basalts are enrichments in large-ion lithophile elements (LILE; Ba, Sr, Rb, K, Th) and depletions in high field-strength elements (HFSE; Ta, Nb, Zr, Hf) relative to REE. Alkali abundances are correlated with continental crustal age and thickness; in areas with young crust the K and Rb contents are relatively low compared to other LILE. The Giant Crater HAB has Ba and Sr enrichments characteristic of basalts formed at active continental margins in areas of young crust. Figure 1-8B is a diagram of chondrite-normalized trace element abundances showing the enrichment in Ba and Sr relative to REE for 82-72f compared to the primitive MORB AII78-103. Relative depletions in HFSE are greater in magnitude in arc lavas with higher overall incompatible element contents; the primitive HAB from Medicine Lake has generally low incompatible element contents and no appreciable depletions in HFSE (Figure 1-8b). This pattern of Ba and Sr enrichment with no relative depletion of HFSE is observed in other HAB from the Cascades. Bacon (1990) has reported HAB (high-alumina olivine tholeiites in his terminology) from Crater Lake, OR, that have similar trace element patterns to 82-72f (Figure 1-8b), and Leeman et al. (1989) also find that most basalts from the Southern Washington Cascades lack HFSE depletions.

Relation of high-Mg HAB from Giant Crater to other lavas

Medicine Lake Volcano

The lavas series at Medicine Lake follows a calc-alkaline differentiation trend, ranging from high-Mg HAB through basaltic andesite, andesite, dacite and rhyolite. Samples 79-35g and 82-72f are among the most primitive lavas erupted at Giant Crater and are similar to other primitive HAB erupted at Medicine Lake throughout its history (Donnelly-Nolan, 1988). The Giant

Crater lava flow is compositionally zoned from primitive HAB to more evolved basaltic andesites. The geology and geochemistry of this flow is described by Donnelly-Nolan et al. (JGR 1991, submitted) and the origin of the compositional zoning is discussed by Baker et al. (JGR 1991, submitted), who show that primitive HAB is parental to the more evolved compositions through processes of fractional crystallization, assimilation of crustal material and magma mixing.

Cascades and other subduction zone environments

The basalts and related calc-alkaline derivative lavas at Medicine Lake are similar in major element chemistry to other lavas from the southern Cascades (Smith and Carmichael, 1968; Donnelly-Nolan et al., 1991, submitted JGR). Table 1-10 lists compositions of HAB and other primitive rock compositions from the Cascades and other subduction zone settings. These compositions are plotted in the Olivine-Cpx-Quartz and Olivine-Plagioclase-Quartz pseudoternary projections in Figure 1-9. Also shown is the field for HAB compositions from Medicine Lake Volcano and the field for the most primitive HAB from Giant Crater. Most of the HAB compositions overlap with the field of Medicine Lake HAB, which range in SiO_2 47.3-51.4, Al_2O_3 16.6-21.8, MgO 5.7-10.5, CaO 9.1-11.9, Na_2O 2.3-3.4, K_2O 0.1-0.9 and TiO_2 0.5-1.8 wt.%. Only one other HAB from the Cascades (Bear Creek, OR) is as primitive as the high-Mg HAB from Medicine Lake. The other HAB listed are more typical arc HAB and range in Mg# from 0.48 to 0.62. Among the low-Al_2O_3 compositions are the Aleutian high-MgO basalt MK-15, an Aleutian picrite, and a basaltic andesite from Mt. Shasta.

Model for the genesis of primitive HAB

There has been much debate about whether HAB represents primary melt. Crawford et al. (1987) point out that "while Tilley (1950) and Kuno

(1960) defined HAB on the basis of aphyric (i.e., liquid) compositions, the great majority of arc lavas subsequently classified as HAB are strongly porphyritic, often with 30-60 modal% of phenocrysts, of which plagioclase is usually dominant (Ewart, 1982)." They define HAB as lavas with < 54 wt.% SiO_2, > 16.5 wt.% Al_2O_3, and usually < 7 wt.% MgO, and conclude that "typical" arc HAB compositions result from the accumulation of plagioclase into residual liquids produced by fractionation of a different type of primary magma. Some petrologists currently subscribe to a model whereby plagioclase-phyric low-MgO HAB is produced via fractionation of mafic phases from a primitive high-MgO "low-alumina" (< 16 wt.% Al_2O_3) basalt derived from partial melting of the mantle wedge above the descending slab (Perfit et al., 1980; Kay, 1980). Although others (Brophy and Marsh, 1986) have argued that low-MgO HAB represents primary magma formed from melting the eclogite slab, geochemical and petrologic objections have been raised against this hypothesis (Crawford et al., 1987), and Brophy (1989) has concluded that the ability to produce low-MgO HAB from high-MgO LAB (low-alumina basalt) eliminates many of the arguments supporting the eclogite-derived model.

The compositions from Table 1-10 are plotted in Figure 1-10 in an Mg# vs. Al_2O_3 diagram. The field of arc basalts shown is from Gust and Perfit (1987). The area of the field above 17 wt.% Al_2O_3 is labeled "HAB" although some rocks falling within this field could be alkali basalts by Kuno's (1960) definition. Also shown are the fields for the Aleutian high-MgO low-Al_2O_3 basalts and the Giant Crater high-MgO high-Al_2O_3 basalts. The curves labeled 10, 12 and 15 are the experimentally determined crystallization paths for 79-35g at 10, 12 and 15 kbar.

Gust and Perfit (1987) proposed that low-MgO HAB could be derived from a high-MgO low-Al_2O_3 basalt such as MK-15 via high pressure olivine +

clinopyroxene fractionation at the base of the arc crust. Crawford et al. (1987) suggested an alternative explanation for the genesis of HAB in arcs; they noted the similarity of experimentally produced partial melts of mantle peridotite material at 10 kbar (Fujii and Scarfe, 1985; Takahashi, 1986; Falloon and Green, 1987) to high-MgO, high Al_2O_3 basalts and proposed that these could be parental to lower MgO HAB. Our experimental results lend support to this model. Alternatively, lower-MgO HAB could be produced by accumulation of plagioclase into or crustal contamination of a lava derived by olivine + plagioclase +/- augite fractionation from a high-MgO parent at 10 kbar or lower pressures (the 1 atm crystallization path is parallel to the 10 kbar path). Grove et al. (1982) developed a model based on low-pressure assimilation and fractional crystallization processes to relate the primitive HAB to the more evolved compositions at Medicine Lake Volcano.

High-MgO HAB represents one type of primary magma produced by partial melting of the mantle wedge overlying the downgoing slab in subduction zones. The high pressure phase relations indicate that the primitive HAB from Giant Crater are saturated with olivine, augite, plagioclase and spinel on the liquidus at about 11 kbar. These liquids are close to orthopyroxene saturation at this pressure as well; the liquids plot very near the reaction boundary involving orthopyroxene at 10 kbar. This pressure range corresponds to the pressure expected at the crust-upper mantle contact beneath Medicine Lake Volcano (Zucca et al., 1986). Medicine Lake Volcano is located in an area dominated by extensional tectonics which would favor rapid ascent of primitive HAB from its source in the mantle just beneath the base of the crust, through the crust and to the volcano at the surface. Thus, these lavas are close to unmodified partial melts of a plagioclase/spinel-lherzolite mantle source. The high Ni content is a further line of support for a primary

mantle origin, and the light-REE depleted REE pattern suggests that the mantle source is as depleted or more so than the source for MORB. Magmas similar to the primitive HAB from Medicine Lake Volcano could be parental to the more evolved Cascade calc-alkaline lavas. High-Mg HAB has been demonstrated to be parental to the calc-alkaline association at Medicine Lake Volcano, and these lavas are similar to other Cascade lavas. All of the above lends support to the hypothesis that primitive high-alumina basalt like that from Giant Crater represents an input of primary magma to the Cascades.

REFERENCES FOR CHAPTER ONE

Akella J. and Kennedy G.C. (1971) Melting of gold, silver and copper: proposal for a new high pressure calibration scale. *J. Geophys. Res., 76,* 4969-4977.

Albee A. L. and Ray L. (1970) Correction factors for electron microprobe microanalysis of silicates, oxides, carbonates, phosphates and sulfates. *Anal. Chem., 42,* 1408-1414.

Anders E. and Grevesse N. (1989) Abundances of the elements: Meteoritic and solar. *Geochim. Cosmochim. Acta, 53,* 197-214.

Anderson C.A. (1941) Volcanoes of the Medicine Lake Highland, California. *Univ. Calif. Publ. Bull. Dep. Geol. Sci, 25,* 347-422.

Bacon C.R. (1990) Calc-alkaline, shoshonitic, and primitive tholeiitic lavas from monogenetic volcanoes near Crater Lake, Oregon. *J. Petrol., 31,* 135-166.

Baker D.R. and Eggler D.H. (1987) Compositions of anhydrous and hydrous melts coexisting with plagioclase, augite, and olivine or low-Ca pyroxene from 1 atm to 8 kbar: Application to the Aleutian volcanic center of Atka. *Am. Mineral., 72,* 12-28.

Baker M.B (1988) Evolution of lavas at Mt. Shasta volcano, N. California: An experimental and petrologic study. Ph.D. thesis, M.I.T.

Baker M.B., Grove T.L., Kinzler R.J., Donnelly-Nolan J.M. and Wandless G.A., submitted, *J. Geophys. Res.,* Origin of compositional zonation (high alumina basalt - basaltic andesite) in the Giant Crater lava field, Medicine Lake volcano, northern California.

Basaltic Volcanism Study Project (1981) *Basaltic Volcanism on the Terrestrial Planets.* Pergamon Press, New York.

Bence A. E. and Albee A. L. (1968) Empirical correction factors for the electron microanalysis of silicates and oxides. *J. Geol., 76,* 382-403.

Biggar G.M. (1972) Diopside, lithium metasilicate, and the 1968 temperature scale. *Mineral. Mag., 38,* 768-770.

Boyd F.R. and England J.L. (1960) Apparatus for phase equilibrium studies at pressures up to 50 kbars and temperatures up to 1750 ^{o}C. *J. Geophys. Res., 65,* 741-748.

Brandon A.D. (1989) Constraints on magma genesis behind the Neogene Cascade arc: evidence from major and trace element variation of high alumina and tholeiitic volcanoes of the Bear Creek area. *J. Geophys. Res., 94,* 7775-7798.

Brophy J.G. (1989) Can high-alunina arc basalt be derived from low-alumina arc basalt? Evidence from Kanaga Island, Aleutian Arc, Alaska. *Geology, 17,* 333-336.

Brophy J.G. and Marsh B.D. (1986) On the origin of high-alumina arc basalt and the mechanics of melt extraction. *J. Petrol., 27,* 763-789.

Bryan W.B., Finger L.W. and Chayes F (1969). Estimating proportions in petrographic mixing equations by least squares approximation. *Science, 163,* 926-927.

Bryan W.B., Thompson G. and Ludden J.N. (1981) Compositional variation in Normal MORB from 22°-25°N; Mid-Atlantic Ridge and Kane Fracture Zone. *J. Geophys. Res., 86,* 11815-11836.

Crawford A.J., Falloon T.J. and Eggins S. (1987) The origin of island arc high-alumina basalts. *Contrib. Mineral. Petrol., 97,* 417-430.

Davidson J.P. (1987) Crustal contamination vs. subduction zone enrichment: Examples from the lesser Antilles and implications for mantle source compositions of island arc volcanic rocks. *Geochim. Cosmochim. Acta, 51,* 2185-2198.

Donnelly-Nolan J.M. (1988) A magmatic model of Medicine Lake Volcano, California. *J. Geophys. Res., 93-B5,* 4412-4420.

Donnelly-Nolan J.M., Champion D.E., Grove T.L., Baker M.B., Taggart J.E. and Bruggman P.E., submitted, *J. Geophys. Res.,* The Giant Crater lava field: Geology and geochemistry of a compositionally zoned tholeiitic to calc-alkaline basaltic eruption at Medicine Lake volcano, California, and implications for the origin of arc basalt.

Elthon D. (1990) The petrogenesis of primary mid-ocean ridge basalts. *Aquatic Sciences, 2,* 27-53.

Ewart A. (1982) The mineralogy and petrology of Tertiary-Recent orogenic volcanic rocks with special reference to the andesitic-basaltic compositional range. In: *Andesite* (Thorpe R.S., ed.), pp 22-95. Wiley, New York.

Falloon T.J. and Green D.H. (1987) Anhydrous partial melting of MORB pyrolite and other peridiotite compositions at 10 kbar: Implications for the origin of primitive MORB glasses. *Mineral. Petrol., 37,* 181-219.

Fujii T. and Scarfe C.M. (1985) Compositions of liquids coexisting with spinel lherzolite at 10 kbar and the genesis of MORBs. *Contrib. Mineral. Petrol., 90,* 18-28.

Gerlach D.C.and Grove T.L. (1982) Petrology of Medicine Lake Highland volcanics: characterization of end-members of magma mixing. *Contrib. Mineral. Petrol., 80,* 147-159.

Gorshkov G.S. (1970) Volcanism and the Upper Mantle. Plenum Press, New York.

Grove T.L. (1981) Use of Fe/Pt alloys to eliminate the iron loss problem in 1-atm gas mixing experiments: theoretical and practical considerations. *Contrib. Mineral. Petrol., 78,* 298-304.

Grove T.L., Gerlach D.C., Sando T.W. and Baker M.B. (1982) Origin of calc-alkaline series lavas at Medicine Lake volcano by fractionation, assimilation and mixing: corrections and clarifications. *Contrib. Mineral. Petrol., 82,* 407-408.

Grove T.L., Kinzler R.J., Baker M.B., Donnelly-Nolan J.M. and Lesher C.E. (1988) Assimilation of granitic crust by basaltic magma at Burnt Lava flow, Medicine Lake volcano, northern California. *Contrib. Mineral. Petrol., 99,* 320-343.

Grove T.L., Kinzler R.J. and Bartels K.S. (1989) Effects of pressure on alumina substitution in igneous augite: an empirical barometer (abstract). *Eos, Trans. Am. Geophys. Union, 70(43),* 1401-1402.

Gust DA and Perfit MR (1987) Phase relations of a high-Mg basalt from the Aleutian Island Arc: Implications for primary island arc basalts and high-Al basalts. Contrib Mineral Petrol 97:7-18.

Hart S.R. and Davis K.E. (1978) Nickel partitioning between olivine and silicate melt. *Earth Planet. Sci. Lett., 40,* 203-219.

Hart W.K., Aronson J.L. and Mertzman S.A. (1984) Areal distribution and age of low-K, high-alumina olivine tholeiite magmatism in the northwestern Great Basin. *Geol Soc Am Bull 95,* 186-195, Suppl Data 84-3.

Hickey R.L., Gerlach D.C. and Frey F.A. (1982) Geochemical variations in volcanic rocks from central-South Chile (33-42°S). In: *Andean Magmatism:*

Chemical and Isotopic Constraints (Harman R.S. and Barreiro B.A., eds.), pp.72-95. Shiva Publishing, Nantwich.

Johannes W., Bell P.M., Mao H.K., Boettcher A.L., Chipman D.W., Hays J.F., Newton R.S. and Siefert F. (1971) An interlaboratory comparison of piston-cylinder pressure calibration using the albite breakdown reaction. *Contrib Mineral Petrol 32,* 24-38.

Johnson K.T.M. and Kinzler R.J. (1989) Partitioning of REE, Ti, Zr, Hf and Nb between clinopyroxene and basaltic liquid: an ion microprobe study (abstract). *Eos, Trans. Am. Geophys. Union, 70(43),* 1388.

Johnston A.D. (1986) Anhydrous P-T phase relations of near-primary high-alumina basalt from the South Sandwich Islands. *Contrib Mineral Petrol 92,* 368-382.

Kay R.W. (1980) Volcanic arc magmas: implications of a melting-mixing model for element recycling in the crust-upper mantle system. *J. Geol., 88,* 497-522.

Kinzler R.J., Grove T.L. and Recca S.I. (1990) An experimental study on the effect of temperature and melt composition on the partitioning of nickel between olivine and silicate melt. *Geochim. Cosmochim. Acta, 54,* 1255-1265.

Kinzler R.J. and Grove T.L., submitted to *J. Geophys. Res.*, Primary magmas of mid-ocean ridge basalts.

Kuno H (1960) High-alumina basalt. *J. Petrol., 1,* 12-145.

Kuno H (1968) Origin of andesite and its bearing on the island arc structure. *Bull. Volcanol., 32,* 141-174.

Kushiro I. (1972) Effect of water on the composition of magmas formed at high pressures. *J. Petrol., 13,* 311-334.

Kushiro I. and Yoder H.S., Jr. (1966) Anorthite-forsterite and anorthite-enstatite reactions and their bearing on the basalt-eclogite transformation. *J. Petrol., 7,* 337-362.

Leeman W.P., Smith D.R., Hildreth W., Palacz Z. and Rogers N. (1989) Compositional diversity in late Cenozoic basalts in a transect across the Southern Washington Cascades: Implications for subduction zone magmatism. *U.S. Geological Survey Open File Report 89-178,* pp.318-350.

Lindsley D.H. (1983) Pyroxene thermometry. *Am. Min., 68,* 477-493.

Lindsley D.H. and Anderson D.J. (1983) A two-pyroxene thermometer. *Proceedings of the Thirteenth Lunar and Planetary Science Conference, J. Geophys. Res., 88, Suppl.,* A887-A906.

Mysen B.O., Kushiro I., Nicholls I.A. and Ringwood A.E. (1974) A possible mantle origin for andesite magmas: Discussion and replies. *Earth Planet. Sci. Lett., 21,* 221-229.

Nicholls I.A. and Ringwood A.E. (1973) Effect of water on olivine stability in tholeiites and production of SiO_2-saturated magmas in the island-arc environment. *J. Geol., 81,* 285-300.

Nye C.J. and Reid M.R. (1986) Geochemistry of primary and least fractionated lavas from Okmok volcano, central Aleutians: implications for arc magma genesis. *J. Geophys. Res., 91,* 271-287.

Perfit M.R., Gust D.A., Bence A.E., Arculus R.J. and Taylor S.R. (1980) Chemical characteristics of island arc basalts: Implications for mantle sources. *Chemical Geology, 30,* 227-256.

Powers H.A. (1932) The lavas of the Modoc Lava-Bed Quadrangle, California. *Am. Min., 17,* 253-294.

Presnall D.C., Dixon S.A., Dixon J.R., O'Donnell T.H,. Brenner N.L., Schrock R.L. and Dyeus D.W. (1978) Liquidus phase relations on the join diopside-forsterite-anorthite from 1 atm to 20 kbar: Their bearing on the generation and crystallization of basaltic magma. *Contrib. Mineral. Petrol., 66,* 203-220.

Roeder P.L and Emslie R.F. (1970) Olivine-liquid equilibrium. *Contrib. Mineral. Petrol., 29,* 275-289.

Smith A.L. and Carmichael I.S.E. (1968) Quaternary lavas from the southern Cascades, Western U.S.A. *Contrib. Mineral. Petrol., 19,* 212-238.

Stolper E. (1980) Phase diagram for mid-ocean ridge basalts: Preliminary results and implications for petrogenesis. *Contrib. Mineral. Petrol., 74,* 13-27.

Sun C-O., Williams R.J. and Sun S-S. (1974) Distribution coefficients of Eu and Sr for plagioclase-liquid and clinopyroxene-liquid equilibria in oceanic ridge basalt: an experimental study. *Geochim. Cosmochim. Acta, 38,* 1415-1433.

Sun S.S., Nesbitt R.W. and Sharaskin A.Y. (1979) Geochemical characteristics of mid-ocean ridge basalts. *Earth Planet. Sci. Lett., 44,* 119-138.

Takahashi E. (1986) Melting of a dry peridotite KLB-1 up to 20 GPa: implications on the origin of peridotite upper mantle. *J. Geophys. Res., 91,* 9367-9382.

Tatsumi Y., Sakuyama M., Fukuyama H. and Kushiro I. (1983) Generation of arc basalt magmas and thermal structure of the mantle wedge in subduction zones. *J. Geophys. Res., 88-B7,* 5815-5825.

Tilley C.E. (1950) Some aspects of magmatic evolution. *Quat. J. Geol. Soc. London, 106,* 37-50.

Tormey D.R., Grove T.L. and Bryan W.B. (1987) Experimental petrology of normal MORB near the Kane Fracture Zone: 22°-25°N, mid-Atlantic ridge. *Contrib. Mineral. Petrol., 96,* 121-139.

Waters A.C. (1962) Basalt magma types and their tectonic associations: Pacific Northwest of the United States. In: *The Crust of the Pacific Basin,* American Geophysical Union Monograph 6, pp. 158-170.

Westerveld J. (1962) Quaternary volcanism on Sumatra. *Bull. Geol. Soc. Amer., 63,* 561-594.

Whitford D.J., Nicholls I.A. and Taylor S.R. (1979) Spatial variations in the geochemistry of Quaternary lavas across the Sunda arc in Java and Bali. *Contrib. Mineral. Petrol., 70,* 341-356.

Yoder H.S. and Tilley C.E. (1957) Basalt magmas. *Carnegie Inst. Washington Yearb., 56,* 156-161.

Yoder H.S., Jr. and Tilley C.E. (1962) Origin of basalt magmas: An experimental study of natural and synthetic rock systems. *J. Petrol., 3,* 342-532.

Zucca J.J., Fuis G.S., Milkereit B., Mooney W.D. and Catchings R.D. (1986) Crustal structure of northeastern California. *J. Geophys. Res., 91,* 7359-7382.

Table 1-1 Starting compositions used in melting experiments

	79-35g[a]	82-72f[a]	Kragero[b] opx	San Carlos[b] olivine
SiO_2	47.7	47.7	57.3	39.9
TiO_2	0.65	0.59	0.06	-
Al_2O_3	18.6	18.5	0.10	-
FeO*	8.53	8.20	9.49	11.2
MgO	9.92	10.5	33.5	48.9
MnO	0.15	0.15	0.14	-
CaO	12.1	12.0	0.26	-
K_2O	0.07	0.07	n.d.[c]	n.d.
Na_2O	2.25	2.16	-[c]	n.d.
P_2O_5	0.05	0.06	n.d.	n.d.
total	100.02	99.93	100.9	100.0

[a] XRF analyses from University of Massachusetts, Amherst.
* All iron originally analyzed as Fe_2O_3 and recalculated to FeO.
[b] analyses from MIT microprobe.
[c] n.d. indicates element not determined; dash indicates element was analyzed but was below detectability limits.

Table 1-2 Run conditions and products for 79-35g experiments. See Table 1-3 for phase compositions.

Run #	T°C	Duration (hours)	Run products	Phase proportions	ΣR^2	Mg# (gl)
10 kbar						
H89	1290	3	gl	100		
H75	1280	3	gl,ol,pl	99:1:tr	0.25	0.68
H81	1260	6	gl,ol,pl,cpx	61:8:21:10	0.45	0.58
H83	1245	9	gl,ol,pl,cpx	52:10:28:9	1.12	0.56
H88	1240	5	gl,ol,pl,cpx	43:10:33:14	1.12	0.51
12 kbar						
H105	1325	3	gl	100		
H98	1310	2.75	gl,cpx	100:tr	0.24	0.68
H95	1290	3.33	gl,cpx	93:7	0.26	0.66
H202	1290	8	gl,cpx,pl,sp	92:11:-4:1	0.23	0.65
H97	1285	4	gl,cpx,pl,sp	89:10:tr:1	0.02	0.64
H201	1280	28	gl,cpx,pl,sp	78:18:2:2	0.89	0.64
H131	1280	14	gl,cpx,pl,sp	77:19.5:2:1.6	0.08	0.62
H204	1280	6	gl,cpx,pl,sp	77:19:3:2	0.31	0.62
H132	1270	19	gl,cpx,pl,sp	69:24:6:1	0.23	0.60
H96*	1270	3	gl,cpx,ol,pl,sp	66:31:-4:4:2	0.03	0.59
H94*	1265	5	gl,cpx,ol,pl,sp	51:32:tr:14:3	0.10	0.56
15 kbar						
H107	1370	1.2	gl	100		
H100	1345	3	gl,cpx,sp	90:9:1	0.20	0.66
H101	1315	3	gl,cpx,sp	81:18:1	0.36	0.64
H134	1305	2	gl,cpx,sp	76:23:1	0.52	0.61
H135	1290	11.5	gl,cpx,sp,pl	61:36:2:1.5	0.10	0.57
H136	1275	23	gl,cpx,sp,pl	11:58:5:26	1.24	0.42

* See text for discussion of 12 kbar experiments containing olivine

abbreviations used throughout Tables: gl=glass, ol=olivine, pl=plagioclase, cpx=augite, sp=spinel, opx=low-Ca pyroxene.

Table 1-3A Microprobe analyses of phases from 10 kbar melting experiments on 79-35g.

Run	**H89**	**H75**	**H75**	**H75**	**H81**	**H81**	**H81**	**H81**
Phase	gl[7][1]	gl[7]	ol[5]	pl[3]	gl[7]	ol[4]	pl[5]	cpx[8]
SiO_2	47.5(2)[2]	48.3(2)	40.2(5)	48.7(3)	48.1(5)	39.6(6)	51.2(5)	51.3(8)
TiO_2	0.59(4)	0.57(3)	-[3]	n.d.[3]	0.89(6)	0.02(0)	n.d.	0.51(9)
Al_2O_3	17.9(1)	18.2(2)	0.07(2)	32.7(2)	17.4(1)	0.09(3)	31.2(3)	7.1(11)
Cr_2O_3	0.08(3)	0.06(2)	-	n.d.	0.04(3)	-	n.d.	0.18(3)
FeO	8.45(6)	8.44(7)	14.2(23)	0.58(7)	10.7(2)	18.1(12)	0.46(3)	5.97(30)
MgO	10.0(1)	9.90(9)	46.2(19)	0.19(8)	8.33(22)	42.6(12)	0.20(3)	18.0(11)
MnO	0.13(3)	0.16(5)	0.24(7)	n.d.	0.19(3)	0.28(3)	n.d.	0.20(3)
CaO	11.8(1)	11.8(1)	0.43(5)	16.2(1)	10.7(1)	0.43(6)	14.4(3)	17.2(10)
K_2O	0.12(1)	0.09(1)	n.d.	0.03(1)	0.15(2)	n.d.	0.05(1)	n.d.
Na_2O	2.40(3)	2.52(15)	n.d.	2.38(9)	3.12(9)	n.d.	3.53(23)	0.43(4)
P_2O_5	0.17(6)	0.01(1)	n.d.	n.d.	0.07(3)	n.d.	n.d.	n.d.
total	99.2	100.0	101.4	100.8	99.7	101.1	101.0	100.9
Run	**H83**	**H83**	**H83**	**H83**	**H88**	**H88**	**H88**	**H88**
Phase	gl[7]	ol[4]	pl[4]	cpx[7]	gl[7]	ol[4]	pl[3]	cpx[7]
SiO_2	48.3(4)	39.4(4)	52.2(3)	52.5(4)	47.0(2)	38.4(3)	51.7(4)	50.7(9)
TiO_2	1.03(5)	0.02(1)	n.d.	0.50(4)	1.24(7)	0.03(1)	n.d.	0.54(12)
Al_2O_3	16.7(1)	0.08(2)	30.8(3)	5.50(46)	16.3(1)	0.07(1)	29.7(4)	6.4(11)
Cr_2O_3	0.03(3)	-	n.d.	0.17(2)	0.03(2)	-	n.d.	0.14(3)
FeO	11.4(2)	18.6(7)	0.55(9)	6.29(24)	12.7(1)	19.0(6)	0.48(10)	6.66(42)
MgO	8.08(22)	42.7(5)	0.23(7)	18.0(4)	7.46(16)	41.9(5)	0.30(13)	17.6(6)
MnO	0.22(4)	0.29(1)	n.d.	0.20(3)	0.23(3)	0.29(8)	n.d.	0.22(4)
CaO	10.6(1)	0.41(3)	13.8(1)	17.8(4)	10.0(1)	0.44(5)	13.0(3)	17.0(5)
K_2O	0.17(1)	n.d.	0.06(1)	n.d.	0.19(2)	n.d.	0.06(2)	n.d.
Na_2O	3.35(14)	n.d.	3.82(7)	0.41(3)	3.42(9)	n.d.	4.07(14)	0.45(6)
P_2O_5	0.09(4)	n.d.	n.d.	n.d.	0.13(1)	n.d.	n.d.	n.d.
total	100.0	101.5	101.5	101.4	98.7	100.1	99.3	99.6

1. Number in brackets indicates number of microprobe analyses. 2. Oxides are reported in weight percent. Number in parentheses is 1 standard deviation of the mean in terms of least units reported. Thus, 47.5(2) indicates 47.5 +/- 0.2 wt.%. 3. n.d. indicates element not determined; dash indicates element was analyzed but was below detectability limits.

Table 1-3B Microprobe analyses of phases from 12 kbar melting experiments on 79-35g.

Run	**H105**	**H98**	**H98**	**H95**	**H95**	**H202**	**H202**	**H202**
Phase	gl[7]	gl[7]	cpx[4]	gl[7]	cpx[8]	gl[6]	cpx[17]	pl[7]
SiO_2	48.5(4)	47.8(2)	51.4(11)	48.1(2)	50.5(17)	47.9(0)	49.3(2)	47.0(6)
TiO_2	0.58(2)	0.60(4)	0.38(19)	0.63(4)	0.36(12)	0.68(2)	0.35(1)	n.d.
Al_2O_3	18.2(1)	17.9(1)	9.4(35)	18.6(1)	9.4(27)	18.8(1)	10.2(3)	31.2(5)
Cr_2O_3	0.05(4)	0.04(2)	0.17(10)	-	0.20(7)	-	0.10(1)	n.d.
FeO	8.34(7)	8.47(16)	5.7(11)	8.69(17)	5.6(14)	8.50(7)	5.67(9)	0.43(1)
MgO	10.3(1)	10.0(1)	17.9(27)	9.46(10)	18.6(16)	8.93(9)	17.4(2)	0.32(3)
MnO	0.16(3)	0.17(4)	0.15(4)	0.16(3)	0.17(6)	0.12(1)	0.15(1)	n.d.
CaO	11.9(1)	11.8(1)	14.6(39)	11.4(1)	15.7(14)	11.1(1)	15.8(3)	15.9(4)
K_2O	0.09(1)	0.09(1)	n.d.	0.10(1)	n.d.	0.11(1)	n.d.	0.02(0)
Na_2O	2.57(4)	2.45(10)	0.81(67)	2.66(11)	0.50(5)	2.80(4)	0.61(1)	2.19(25)
P_2O_5	0.02(1)	0.02(1)	n.d.	0.02(1)	n.d.	0.03(1)	n.d.	n.d.
total	100.7	99.3	100.5	99.9	101.0	99.0	99.6	97.1

Run	**H202**	**H97**	**H97**	**H97**	**H97**	**H201**	**H201**	**H201**
Phase	sp[4]	gl[7]	cpxr[15]	pl[4]	sp[4]	gl[8]	cpx[21]	pl[5]
SiO_2	0.18(1)	47.8(2)	50.4(6)	49.0(3)	0.00(1)	48.3(1)	50.0(1)	48.9(4)
TiO_2	0.09(0)	0.63(3)	0.39(6)	n.d.	0.08(1)	0.70(1)	0.43(3)	n.d.
Al_2O_3	65.9(2)	18.7(2)	9.3(11)	32.3(3)	67.0(4)	18.7(1)	9.53(23)	31.2(5)
Cr_2O_3	0.58(9)	-	0.11(4)	n.d.	0.63(14)	0.01(0)	0.08(1)	n.d.
FeO	10.2(1)	9.07(7)	5.99(57)	0.55(7)	10.1(2)	8.77(7)	6.61(14)	0.51(7)
MgO	21.4(1)	9.23(14)	18.6(8)	0.30(4)	21.7(1)	8.73(13)	17.9(2)	0.44(17)
MnO	0.09(1)	0.16(3)	0.19(5)	n.d.	0.10(2)	0.11(1)	0.16(1)	n.d.
CaO	0.11(1)	11.3(1)	15.4(13)	15.8(2)	0.09(2)	10.3(0)	14.6(3)	15.0(4)
K_2O	n.d.	0.10(2)	n.d.	-	n.d.	0.13(1)	n.d.	0.03(1)
Na_2O	n.d.	2.76(9)	0.51(5)	2.57(16)	n.d.	3.06(5)	0.65(1)	2.65(22)
P_2O_5	n.d.	0.03(1)	n.d.	n.d.	n.d.	0.06(1)	n.d.	n.d.
total	98.6	99.8	100.9	100.5	99.7	98.9	100.0	98.7

Table 1-3B, p.2 Microprobe analyses of phases from 12 kbar melting experiments on 79-35g.

Run	**H201**	**H131**	**H131**	**H131**	**H131**	**H204**	**H204**	**H204**
Phase	sp[4]	gl[7]	cpx[34]	pl[8]	sp[8]	gl[9]	cpx[19]	pl[6]
SiO_2	0.34(14)	48.2(1)	49.7(2)	48.9(10)	0.34(20)	48.4(1)	50.3(2)	49.5(4)
TiO_2	0.11(1)	0.70(1)	0.40(1)	n.d.	0.05(1)	0.72(2)	0.37(2)	n.d.
Al_2O_3	66.2(4)	18.6(1)	10.3(3)	31.7(6)	66.8(16)	18.8(1)	9.45(28)	30.8(6)
Cr_2O_3	0.33(4)	-	0.14(1)	n.d.	0.46(5)	0.01(0)	0.12(1)	n.d.
FeO	10.5(1)	9.64(4)	5.64(7)	0.48(12)	11.1(1)	9.41(4)	6.25(9)	0.64(8)
MgO	21.2(0)	8.94(2)	17.9(2)	0.42(10)	21.0(5)	8.63(2)	18.2(2)	0.71(13)
MnO	0.09(1)	0.21(1)	0.13(1)	n.d.	0.10(1)	0.14(1)	0.16(1)	n.d.
CaO	0.14(2)	10.5(0)	15.8(1)	15.3(7)	0.11(4)	10.5(0)	14.9(2)	14.8(4)
K_2O	n.d.	0.12(0)	n.d.	0.03(1)	n.d.	0.13(1)	n.d.	0.03(0)
Na_2O	n.d.	3.09(6)	0.53(1)	2.59(40)	n.d.	3.07(4)	0.57(3)	2.78(19)
P_2O_5	n.d.	0.04(1)	n.d.	n.d.	n.d.	0.06(0)	n.d.	n.d.
total	98.9	100.1	100.5	99.4	100.0	99.9	100.3	99.3

Run	**H204**	**H132**	**H132**	**H132**	**H132**	**H96**	**H96**	**H96**
Phase	sp[4]	gl[7]	cpx[31]	pl[8]	sp[7]	gl[7]	cpx[15]	ol[4]
SiO_2	0.22(1)	48.3(1)	49.9(1)	49.4(11)	0.56(27)	47.1(7)	50.2(9)	39.0(2)
TiO_2	0.10(0)	0.76(3)	0.38(1)	n.d.	0.06(0)	0.80(5)	0.39(8)	-
Al_2O_3	66.4(1)	18.8(0)	10.2(2)	30.9(11)	66.6(4)	18.4(4)	9.6(15)	0.09(0)
Cr_2O_3	0.41(9)	-	0.10(1)	n.d.	0.30(7)	0.02(2)	0.10(5)	0.03(2)
FeO	10.8(1)	9.96(14)	6.68(12)	0.65(34)	11.4(1)	10.7(2)	6.58(75)	17.8(9)
MgO	21.1(0)	8.44(7)	17.9(2)	0.64(47)	20.9(2)	8.53(21)	18.7(13)	41.3(6)
MnO	0.06(2)	0.18(1)	0.20(1)	n.d.	0.08(1)	0.17(5)	0.18(3)	0.28(5)
CaO	0.10(2)	10.2(1)	14.6(3)	14.7(9)	0.13(4)	9.90(7)	14.6(14)	0.45(2)
K_2O	n.d.	0.12(1)	n.d.	0.04(1)	n.d.	0.14(1)	n.d.	n.d.
Na_2O	n.d.	3.25(5)	0.62(1)	2.85(57)	n.d.	3.36(22)	0.53(6)	n.d.
P_2O_5	n.d.	0.04(1)	n.d.	n.d.	n.d.	0.05(2)	n.d.	n.d.
total	99.2	100.1	100.6	99.2	100.0	99.2	100.9	99.0

Table 1-3B, p.3 Microprobe analyses of phases from 12 kbar melting experiments on 79-35g.

Run	**H96**	**H96**	**H94**	**H94**	**H94**	**H94**	**H94**
Phase	pl[3]	sp[4]	gl[7]	cpx[8]	ol[3]	pl[3]	sp[4]
SiO_2	51.6(3)	-	48.0(4)	50.6(9)	39.8(5)	52.3(4)	-
TiO_2	n.d.	0.15(2)	0.90(6)	0.67(25)	0.01(0)	n.d.	0.16(3)
Al_2O_3	30.6(3)	66.7(4)	18.2(5)	7.9(20)	0.11(1)	29.9(2)	66.3(4)
Cr_2O_3	n.d.	0.20(9)	0.04(2)	0.11(7)	0.04(1)	n.d.	0.23(9)
FeO	0.46(9)	13.0(7)	11.3(7)	8.0(13)	17.2(14)	0.50(9)	13.1(8)
MgO	0.25(14)	19.5(6)	7.91(28)	17.9(11)	43.0(16)	0.32(18)	19.6(5)
MnO	n.d.	0.12(3)	0.18(4)	0.23(4)	0.25(1)	n.d.	0.11(3)
CaO	13.8(2)	0.09(2)	9.13(14)	14.7(15)	0.38(0)	12.9(3)	0.08(2)
K_2O	0.05(2)	n.d.	0.18(1)	n.d.	n.d.	0.05(1)	n.d.
Na_2O	3.82(5)	n.d.	3.85(18)	0.59(8)	n.d.	4.29(12)	n.d.
P_2O_5	n.d.	n.d.	0.07(2)	n.d.	n.d.	n.d.-	n.d.
total	100.6	99.8	99.8	100.7	100.8	100.3	99.6

Table 1-3C Microprobe analyses of phases from 15 kbar melting experiments on 79-35g.

Run	**H107**	**H100**	**H100**	**H100**	**H101**	**H101**	**H101**	**H134**	**H134**
Phase	gl[7]	gl[7]	cpx[20]	sp[3]	gl[7]	cpx[21]	sp[3]	gl[7]	cpx[11]
SiO_2	48.2(2)	48.6(3)	48.7(8)	-	48.4(1)	49.2(7)	0.24(27)	48.6(1)	48.7(2)
TiO_2	0.61(3)	0.63(4)	0.37(6)	0.12(1)	0.66(3)	0.31(5)	0.08(1)	0.66(1)	0.36(1)
Al_2O_3	18.1(2)	18.8(4)	11.8(15)	66.5(5)	19.3(1)	11.4(10)	67.7(1)	19.7(0)	12.9(3)
Cr_2O_3	0.05(3)	0.03(2)	0.08(4)	0.65(1)	0.03(3)	0.12(4)	0.80(7)	-	0.10(1)
FeO	8.45(13)	8.76(17)	6.31(72)	10.4(4)	8.93(8)	5.64(57)	10.5(1)	9.21(5)	5.61(12)
MgO	10.1(2)	9.69(32)	15.9(11)	21.3(1)	8.78(38)	16.8(9)	21.4(2)	8.24(2)	15.7(2)
MnO	0.15(2)	0.16(2)	0.11(5)	0.12(2)	0.18(5)	0.11(4)	0.13(1)	0.13(1)	0.15(1)
CaO	11.8(1)	11.5(2)	15.4(11)	0.23(20)	10.9(1	15.3(12)	0.15(5)	10.7(0)	16.9(3)
K_2O	0.09(1)	0.10(1)	n.d.	n.d.	0.10(1)	n.d.	n.d.	0.11(1)	n.d.
Na_2O	2.53(6)	2.73(14)	0.75(12)	n.d.	2.93(12)	0.62(6)	n.d.	2.93(4)	0.86(3)
P_2O_5	0.02(1)	0.03(1)	n.d.	n.d.	0.03(2)	n.d.	n.d.	0.03(1)	n.d.
total	100.1	101.0	99.4	99.9	100.2	99.5	101.0	100.3	101.3

Run	**H134**	**H135**	**H135**	**H135**	**H135**	**H136**	**H136**	**H136**	**H136**
Phase	sp[4]	gl[7]	cpx[10]	pl[5]	sp[2]	gl[6]	cpx[11]	pl[6]	sp[3]
SiO_2	0.53(20)	49.0(1)	49.1(2)	50.0(4)	0.20(11)	47.9(8)	49.2(4)	55.5(19)	0.24(5)
TiO_2	0.38(20)	0.73(2)	0.45(2)	n.d.	0.01(1)	1.53(10)	0.66(3)	n.d.	0.17(0)
Al_2O_3	67.5(10)	19.7(1)	12.3(2)	31.5(14)	67.4(3)	18.1(10)	9.80(82)	27.9(13)	64.4(2)
Cr_2O_3	-	-	0.04(1)	n.d.	0.29(4)	-	0.02(1)	n.d.	0.12(2)
FeO	11.3(2)	9.80(8)	7.12(20)	0.56(8)	12.4(2)	13.8(9)	10.6(3)	0.39(13)	18.8(3)
MgO	20.6(1)	7.24(15)	15.8(1)	0.36(12)	20.0(1)	5.31(69)	16.3(4)	0.16(7)	16.5(0)
MnO	0.10(3)	0.13(1)	0.16(1)	n.d.	0.11(5)	0.16(4)	0.23(1)	n.d.	0.10(1)
CaO	0.23(5)	9.62(6)	15.5(2)	14.9(7)	0.17(1)	7.04(32)	12.7(8)	10.4(13)	0.16(2)
K_2O	n.d.	0.17(1)	n.d.	0.05(1)	n.d.	0.47(5)	n.d.	0.15(4)	n.d.
Na_2O	n.d.	3.72(10)	0.99(2)	2.95(31)	n.d.	5.65(21)	1.01(1)	5.70(81)	n.d.
P_2O_5	n.d.	0.03(1)	n.d.	n.d.	n.d.	0.24(6)	n.d.	n.d.	n.d.
total	100.6	100.1	101.5	100.3	100.6	100.2	100.5	100.2	100.5

Table 1-4 Run conditions and products for mix experiments. See Table 1-5 for phase compositions.

Run #	T°C	Duration (hours)	Run products	Phase proportions	ΣR^2	Mg# (gl)
10 kbar						
H152	1290	7	gl,opx,ol	90:4:6	0.16	0.70
H141	1280	7	gl,opx,ol,cpx,pl	51:12:8:12:16	0.003	0.58
H142	1270	12.5	gl,opx,ol,cpx,pl	51:14:6:15:14	0.009	0.58
15 kbar						
H203	1355	20	gl,opx,ol,cpx,sp	39:-8:52:15:3	0.08	0.62
H192	1340	24	gl,opx,ol,cpx,sp	58:-5:28:16:3	0.004	0.65
H197	1325	24	gl,opx,ol,cpx,sp	37:-6:53:11:5	0.07	0.51

Table 1-5A Microprobe analyses of phases in 10 kbar mix experiments. See Table 1-4 for experimental details.

Run	**H152**	**H152**	**H152**	**H141**	**H141**	**H141**	**H141**	**H141**
Phase	gl[7]	opx[31]	ol[7]	gl[7]	opx[6]	cpx[7]	ol[3]	pl[5]
SiO_2	49.8(1)	55.7(2)	41.1(2)	49.0(9)	53.7(3)	51.0(2)	39.7(1)	51.1(4)
TiO_2	0.59(1)	0.12(1)	0.01(0)	0.88(1)	0.21(2)	0.43(2)	0.04(1)	n.d.
Al_2O_3	16.8(1)	3.31(34)	0.10(2)	17.4(7)	4.64(44)	7.02(20)	0.09(1)	30.7(3)
Cr_2O_3	-	0.08(1)	-	-	0.06(1)	0.07(1)	0.03(0)	n.d.
FeO	8.55(9)	7.82(11)	11.7(1)	11.0(1)	8.31(53)	6.56(41)	17.4(83)	0.44(2)
MgO	11.2(3)	31.7(3)	48.4(2)	8.34(13)	29.8(6)	19.8(2)	43.3(96)	0.23(2)
MnO	0.16(1)	0.14(1)	0.15(1)	0.10(2)	0.12(1)	0.15(2)	0.15(4)	n.d.
CaO	10.9(5)	2.27(16)	0.36(1)	10.6(3)	3.29(50)	14.8(4)	0.39(2)	13.7(2)
K_2O	0.08(1)	n.d.	n.d.	0.16(1)	n.d.	n.d.	n.d.	0.06(0)
Na_2O	2.49(2)	0.00(0)	n.d.	2.89(2)	0.10(3)	0.38(2)	n.d.	3.51(13)
P_2O_5	0.01(0)	n.d.	n.d.	-	n.d.	n.d.	n.d.	n.d.
total	100.6	101.1	101.9	100.4	100.2	100.2	101.1	99.7

Run	**H142**	**H142**	**H142**	**H142**	**H142**
Phase	gl[7]	opx[2]	cpx[4]	ol[5]	pl[3]
SiO_2	48.9(1)	53.1(3)	51.7(1)	39.3(1)	48.8(1)
TiO_2	0.81(5)	0.23(2)	0.35(2)	0.03(1)	n.d.
Al_2O_3	17.5(16)	6.16(31)	6.30(19)	0.15(1)	31.5(3)
Cr_2O_3	-	0.06(1)	0.11(2)	0.15(1)	n.d.
FeO	10.8(3)	9.40(44)	7.56(51)	16.1(7)	0.54(6)
MgO	8.52(12)	27.6(4)	20.7(2)	43.6(8)	0.47(13)
MnO	0.11(2)	0.08(1)	0.15(1)	0.13(2)	n.d.
CaO	10.5(1)	2.91(43)	12.4(4)	0.39(5)	15.7(3)
K_2O	0.15(1)	n.d.	n.d.	n.d.	0.04(0)
Na_2O	2.99(10)	0.23(2)	0.40(3)	n.d.	2.42(2)
P_2O_5	-	n.d.	n.d.	n.d.	n.d.
total	100.3	99.8	99.7	99.9	99.5

Table 1-5B Microprobe analyses of phases in 15 kbar mix experiments. See Table 1-4 for experimental details.

Run	**H203**	**H203**	**H203**	**H203**	**H203**	**H192**	**H192**	**H192**
Phase	gl[8]	opx[14]	cpx[17]	ol[5]	sp[5]	gl[9]	opx[10]	cpx[9]
SiO_2	47.4(3)	52.6(5)	50.0(9)	39.8(2)	0.62(4)	48.0(1)	53.2(15)	51.5(7)
TiO_2	0.80(4)	0.21(4)	0.41(6)	0.03(1)	0.14(2)	0.64(3)	0.20(6)	0.45(5)
Al_2O_3	17.8(1)	8.42(81)	12.(3)	0.14(1)	66.0(6)	17.9(2)	7.4(21)	8.1(11)
Cr_2O_3	0.02(1)	0.05(3)	-	-	0.20(9)	0.03(1)	0.02(2)	0.09(2)
FeO	9.99(13)	8.77(27)	6.79(55)	14.8(2)	10.4(1)	9.07(1)	8.80(22)	6.96(36)
MgO	9.32(15)	28.5(4)	18.0(4.8)	45.1(1)	21.2(1)	9.49(3)	29.2(9)	20.3(8)
MnO	0.16(2)	0.07(4)	0.18(3)	0.18(3)	0.00(0)	0.16(3)	0.13(3)	0.17(1)
CaO	8.61(11)	2.25(17)	11.7(9)	0.29(1)	0.14(6)	10.1(1)	2.37(30)	12.6(0)
K_2O	0.21(1)	n.d.	n.d.	n.d.	n.d.	0.14(2)	n.d.	n.d.
Na_2O	4.44(18)	0.20(2)	0.89(17)	n.d.	n.d.	2.99(14)	0.14(3)	0.56(9)
P_2O_5	0.13(2)	n.d.	n.d.	n.d.	n.d.	0.04(2)	n.d.	n.d.
total	98.9	101.1	99.9	100.3	98.8	98.6	101.5	100.8

Run	**H192**	**H192**	**H197**	**H197**	**H197**	**H197**	**H197**
Phase	ol[4]	sp[2]	gl[10]	opx[6]	cpx[8]	ol[5]	sp[3]
SiO_2	40.3(2)	0.15(2)	47.2(7)	52.7(8)	51.7(2)	39.8(22)	0.40(11)
TiO_2	0.04(1)	0.10(1)	0.84(5)	0.15(3)	0.28(9)	0.03(1)	0.14(0)
Al_2O_3	0.31(26)	67.2(1)	19.3(4)	8.1(12)	8.38(87)	0.12(3)	66.6(3)
Cr_2O_3	0.03(1)	0.24(21)	-	-	0.05(3)	0.02(1)	0.33(1)
FeO	14.1(1)	10.1(2)	10.8(4)	8.48(2)	6.69(48)	14.8(2)	10.6(1)
MgO	46.8(3)	22.0(8)	6.28(7)	29.4(4)	21.4(1.0)	45.0(5)	21.4(3)
MnO	0.16(1)	0.10(1)	0.16(3)	0.14(3)	0.15(5)	0.19(2)	0.08(1)
CaO	0.36(6)	0.08(1)	8.61(5)	2.14(5)	11.7(1.9)	0.31(1)	0.11(2)
K_2O	n.d.	n.d.	0.23(2)	n.d.	n.d.	n.d.	n.d.
Na_2O	n.d.	n.d.	4.98(4)	0.14(2)	0.64(4)	n.d.	n.d.
P_2O_5	n.d.	n.d.	0.11(1)	n.d.	n.d.	n.d.	n.d.
total	102.0	99.8	98.5	101.3	100.9	100.3	99.7

Table 1-6 Run conditions and products for 82-72f experiments. See Table 1-7 for phase compositions.

Run #	T°C	Duration (hours)	Run products	Phase proportions	ΣR^2	Mg# (gl)
1 atm						
F5	1270	15	gl	100		0.70
F2	1264	21	gl,ol	100:tr		0.70
F1	1244	22	gl,ol,pl	98:1:1	0.16	0.69
F4	1238	50	gl,ol,pl	83:5:11	0.18	0.67
F3	1229	24	gl,ol,pl	75:7:17	0.80	0.65
10 kbar						
B3	1287	4	gl	100		0.70
B6	1277	4	gl,ol,pl	89:4:7	0.24	0.67
11 kbar						
H219	1300	4	gl	100		0.70
H235	1293	15	gl,ol,cpx,opx	*		0.71
B14	1290	4	gl,ol,cpx,sp	99:tr:1:tr	0.11	0.70
H225	1285	20	gl,ol,cpx,pl,sp	70:tr:20:8:2	0.07	0.64
12 kbar						
B16	1305	2	gl	100		0.70
B10	1290	2	gl,cpx,sp	91:9:tr	0.33	0.68
B12	1285	3	gl,cpx,pl,sp	86:11:2:1	0.28	0.67

* Phases markedly zoned in composition; mass balance calculation not performed.

Table 1-7A Microprobe analyses of phases in 1 atm melting experiments on 82-72f. See Table 1-6 for experimental details.

Run	**F5**	**F2**	**F1**	**F1**	**F1**	**F4**
Phase	gl[10]	gl[10]	gl[21]	ol[3]	pl[6]	gl[10]
SiO_2	48.0(2)	48.0(2)	47.8(2)	40.1(2)	48.0(2)	48.6(2)
TiO_2	0.56(4)	0.55(6)	0.55(3)	-	n.d.	0.65(3)
Al_2O_3	18.7(1)	18.7(1)	18.6(1)	0.08(1)	32.2(2)	17.6(1)
Cr_2O_3	0.08(4)	0.07(3)	0.09(4)	0.03(1)	n.d.	0.09(4)
FeO	8.10(17)	7.98(13)	8.40(15)	11.3(2)	0.56(6)	8.83(13)
MgO	10.6(1)	10.8(1)	10.4(1)	47.2(3)	0.33(16)	9.89(9)
MnO	0.15(3)	0.16(4)	0.15(3)	0.16(2)	n.d.	0.17(5)
CaO	11.8(1)	11.7(1)	11.7(1)	0.34(1)	16.2(1)	11.7(1)
K_2O	0.09(1)	0.09(1)	0.09(1)	n.d.	0.01(1)	0.10(1)
Na_2O	2.24(12)	2.19(13)	2.29(10)	n.d.	1.83(6)	2.32(11)
P_2O_5	0.13(2)	0.13(2)	0.14(3)	n.d.	n.d.	0.13(3)
total	100.5	100.4	100.2	99.4	99.2	100.1

Run	**F4**	**F4**	**F3**	**F3**	**F3**
Phase	ol[4]	pl[5]	gl[10]	ol[4]	pl[4]
SiO_2	39.9(1)	47.2(5)	48.9(2)	39.8(2)	49.8(3)
TiO_2	0.04(3)	n.d.	0.68(7)	-	n.d.
Al_2O_3	0.04(2)	32.4(2)	17.2(2)	0.10(7)	31.2(2)
Cr_2O_3	0.07(3)	n.d.	0.09(4)	0.13(5)	n.d.
FeO	11.9(2)	0.56(10)	8.93(28)	12.8(4)	0.54(4)
MgO	46.7(3)	0.33(9)	9.39(14)	45.9(3)	0.33(10)
MnO	0.19(9)	n.d.	0.19(4)	0.20(2)	n.d.
CaO	0.37(2)	16.5(4)	11.7(1)	0.38(1)	15.5(3)
K_2O	n.d.	-	0.12(1)	n.d.	0.04(1)
Na_2O	n.d.	1.90(26)	2.54(14)	n.d.	2.44(16)
P_2O_5	n.d.	n.d.	0.14(4)	n.d.	n.d.
total	99.2	98.9	99.9	99.3	99.9

Table 1-7B Microprobe analyses of phases in 10 kbar melting experiments on 82-72f. See Table 1-6 for experimental details.

Run	**B3**	**B6**	**B6**	**B6**
Phase	gl[10]	gl[17]	ol[10]	pl[7]
SiO_2	48.3(2)	48.8(1)	40.0(1)	49.8(4)
TiO_2	0.57(4)	0.64(3)	0.02(2)	n.d.
Al_2O_3	18.7(1)	18.3(1)	0.09(1)	32.1(2)
Cr_2O_3	0.05(4)	0.05(3)	0.04(1)	n.d.
FeO	8.05(15)	8.56(13)	12.7(2)	0.35(5)
MgO	10.8(1)	9.92(9)	47.4(4)	0.27(4)
MnO	0.16(4)	0.20(5)	0.18(4)	n.d.
CaO	11.9(1)	12.1(1)	0.35(2)	15.7(3)
K_2O	0.07(1)	0.09(1)	n.d.	0.04(1)
Na_2O	2.45(10)	2.56(8)	n.d.	2.83(19)
P_2O_5	0.15(3)	0.16(3)	n.d.	n.d.
total	101.2	101.4	100.8	101.1

Table 1-7C Microprobe analyses of phases in 11 kbar melting experiments on 82-72f. See Table 1-6 for experimental details.

Run	**H219**	**H235**	**H235**	**H235**	**H235**	**H235**	**H235**	**H235**
Phase	gl[7]	gl1[6]	gl2[5]	opxc[4]	opxr[3]	cpx1[13]	cpx2[11]	ol[7]
SiO_2	48.1(2)	49.9(4)	50.8(2)	53.5(6)	54.0(7)	53.1(6)	49.1(6)	39.8(3)
TiO_2	0.56(3)	0.65(3)	0.60(2)	0.15(2)	0.14(1)	0.19(3)	0.41(3)	0.01(1)
Al_2O_3	18.7(1)	17.4(1)	17.1(1)	7.01(35)	5.80(51)	6.22(61)	11.9(9)	0.10(1)
Cr_2O_3	0.07(4)	0.01(2)	0.01(2)	0.08(1)	0.06(2)	0.06(3)	0.13(6)	0.01(1)
FeO	8.11(17)	7.90(2)	7.53(15)	7.73(10)	7.13(15)	6.43(78)	5.00(37)	11.6(1)
MgO	10.7(1)	10.8(1)	11.0(1)	30.3(1)	30.8(4)	23.2(21)	17.6(5)	47.9(5)
MnO	0.16(4)	0.10(2)	0.10(3)	0.12(1)	0.13(2)	0.14(5)	0.14(3)	0.17(3)
CaO	11.9(1)	11.5(1)	11.3(1)	2.56(20)	2.58(22)	11.4(28)	16.3(5)	0.31(2)
K_2O	0.09(1)	0.11(1)	0.12(1)	n.d.	n.d.	n.d.	n.d.	n.d.
Na_2O	2.40(12)	2.30(9)	2.38(7)	0.05(2)	0.08(2)	0.29(9)	0.45(2)	n.d.
P_2O_5	0.13(2)	0.15(1)	0.15(1)	n.d.	n.d.	n.d.	n.d.	n.d.
total	100.9	100.8	101.1	101.5	100.7	101.0	101.0	99.9

Run	**B14**	**B14**	**B14**	**H225**	**H225**	**H225**	**H225**	**H225**
Phase	gl[9]	cpx[9]	ol[6]	gl[7]	ol[5]	cpx1[6]	cpx2[11]	pl[7]
SiO_2	48.1(1)	50.2(10)	40.1(3)	47.6(3)	40.0)2)	53.0(4)	49.9(3)	50.5(1)
TiO_2	0.57(4)	0.35(5)	0.02(1)	0.80(4)	0.00	0.21(3)	0.41(5)	n.d.
Al_2O_3	18.7(1)	9.8(16)	0.11(1)	18.3(1)	0.15(3)	5.68(11)	10.3(2)	31.0(2)
Cr_2O_3	0.06(4)	0.13(3)	0.01(1)	-	0.00	0.05(1)	0.08(2)	n.d.
FeO	8.14(10)	4.7(3)	11.7(1)	9.43(16)	14.4(4)	6.36(35)	5.79(64)	0.27(5)
MgO	10.5(1)	18.8(12)	47.4(4)	9.31(21)	45.2(3)	21.3(5)	18.0(2)	0.22(2)
MnO	0.21(6)	0.14(2)	0.14(2)	0.14(4)	0.19(1)	0.16(2)	0.15(4)	n.d.
CaO	11.9(1)	16.0(9)	0.36(3)	11.1(1)	0.33(2)	13.5(6)	15.1(9)	14.3(1)
K_2O	0.08(1)	n.d.	n.d.	0.11(2)	n.d.	n.d.	n.d.	0.04(1)
Na_2O	2.41(16)	0.45(4)	n.d.	2.70(6)	n.d.	0.41(2)	0.51(9)	3.3(1)
P_2O_5	0.13(3)	n.d.	n.d.	0.06(3)	n.d.	n.d.	n.d.	n.d.
total	100.8	100.6	99.8	99.6	100.3	100.7	100.2	99.6

Table 1-7D Microprobe analyses of phases in 12 kbar melting experiments on 82-72f. See Table 1-6 for experimental details.

Run	**B16**	**B10**	**B10**	**B10**	**B12**	**B12**	**B12**	**B12**
Phase	gl[20]	gl[10]	cpx[14]	sp[4]	gl[10]	cpx[14]	sp[5]	pl[2]
SiO_2	48.0(2)	48.8(2)	49.3(2)	0.15(0)	48.8(2)	50.4(9)	0.14(2)	51.1(5)
TiO_2	0.56(3)	0.58(2)	0.37(3)	0.07(2)	0.58(2)	0.32(6)	0.08(1)	n.d.
Al_2O_3	18.7(1)	19.2(1)	11.8(5)	67.0(1)	19.3(1)	10.2(12)	67.3(5)	31.2(3)
Cr_2O_3	0.09(4)	0.02(2)	0.17(5)	1.42(14)	0.03(3)	0.08(3)	1.00(25)	n.d.
FeO	8.17(19)	8.49(9)	5.11(16)	9.21(32)	8.63(16)	5.38(36)	9.16(13)	0.40(2)
MgO	10.7(1)	10.1(1)	18.2(5)	22.8(3)	9.83(17)	19.1(12)	22.7(2)	0.32(9)
MnO	0.15(5)	0.20(3)	0.14(2)	0.09(2)	0.17(3)	0.15(3)	0.07(2)	n.d.
CaO	11.8(1)	11.6(1)	15.5(6)	0.10(1)	11.5(1	14.9(11)	0.07(2)	14.6(1)
K_2O	0.10(1)	0.08(2)	n.d.	n.d.	0.09(2)	n.d.	n.d.	0.05(0)
Na_2O	2.34(13)	2.74(9)	0.50(3)	n.d.	2.77(9)	0.48(3)	n.d.	3.28(9)
P_2O_5	0.11(2)	0.16(3)	n.d.	n.d.	0.17(3)	n.d.	n.d.	n.d.
total	100.7	102.0	101.1	100.8	101.9	101.0	100.5	101.0

Table 8 Compositions pertaining to other experimental studies

	1	2	3	4	5	6	7	8	9	10	11	12
	Melts coexisting with spinel lherzolite at 10 kbar						Starting compositions for other HAB studies					
SiO_2	48.8	50.9	50.2	50.36	50.37	49.2	50.4	49.0	54.7	50.3	49.4	51.2
TiO_2	0.88	0.81	0.65	0.77	0.65	0.60	1.29	1.02	0.79	0.54	0.85	0.75
Al_2O_3	17.5	19.16	17.21	17.05	17.11	17.7	19.7	19.0	18.7	18.5	15.7	15.7
FeO	7.77	6.82	7.68	7.51	7.54	6.7	9.08	9.47	7.90	7.61	9.76	9.21
MgO	9.82	8.52	10.5	10.37	10.41	9.5	5.05	6.18	3.29	7.32	12.05	9.64
MnO	0.26	-	-	-	-	-	0.28	0.21	0.31	0.21	0.15	0.16
CaO	10.8	10.48	11.6	11.53	11.74	11.4	9.59	11.4	7.96	11.8	9.43	10.2
K_2O	0.16	-	-	-	-	-	0.79	0.65	0.99	0.25	0.34	0.92
Na_2O	3.11	3.31	2.18	2.18	2.17	2.9	3.42	2.56	4.10	1.80	2.33	2.77
P_2O_5	0.13	-	0.32	-	0.06	0.12	0.31	0.11	0.25	-	-	0.21
Total	99.23	100.0	100.34	99.77	100.05	98.12	99.91	99.60	98.99	98.33	100.01	100.76
Mg#	0.69	0.69	0.71	0.71	0.71	0.72	0.50	0.54	0.43	0.63	0.69	0.65

1. Fujii and Scarfe (1985) 10 kb 1250°C PMM-1
2. Falloon and Green (1987) 10 kb 1310°C MPuY-87; 3. Falloon and Green (1987) 10 kb 1350°C MPY-87); 4. Falloon and Green (1987) 10 kb 1350°C MPY-87; 5. Falloon and Green (1987) 10 kb 1350°C MPY-87)
6. Takahashi (1986) 10 kb 1325°C KLB-1 7. Baker and Eggler (1987) AT-1; 8. Baker and Eggler (1987) AT-112; 9. Baker and Eggler (1987) AT-41
10. Johnston (1986) SSS1.4; 11. Tatsumi et al. (1983) HAB mix; 12. Gust and Perfit (1987) MK-15

Table 9 Trace element data for 82-72f in ppm.

Ni	Cr	Sc	V	Co	Zn	Sr	Ba	Zr	Nb	Hf	Ta	Th
231	*193*	*34*	*154*	*50*	53	183	26	39	1.37	*0.90*	*	*

La	Ce	Nd	Sm	Eu	Tb	Yb	Lu
1.32	*4.58*	*4.09*	*1.34*	*0.624*	*0.329*	*1.75*	*0.273*

XRF data from University of Massachusetts. INAA data from MIT in italics.
* Concentrations below detection limit

Table 10 High-alumina basalts and primitive arc basalts

	1	2	3	4	5	6	7	8	9	10	11	12	13	14
SiO_2	48.90	48.90	50.8	51.81	48.62	50.10	52.5	48.84	49.51	47.26	47.66	47.10	50.87	51.2
TiO_2	0.97	0.90	1.27	0.93	0.49	0.83	0.72	0.64	0.64	0.88	1.00	0.90	0.74	0.94
Al_2O_3	17.58	19.1	18.7	18.48	13.44	17.39	15.30	16.92	18.19	18.56	16.91	18.52	15.58	21.0
FeO	10.22	10.15	9.7	9.29	8.28	8.97	7.07	8.12	10.26	9.24	9.85	7.91	9.15	7.39
MgO	7.79	5.9	5.0	5.97	15.99	7.10	10.17	10.27	7.07	9.62	9.06	10.89	9.57	5.21
MnO	0.16	0.1	0.12	0.21	0.17	0.17	0.14	0.16	0.28	0.08	0.17	-	0.16	0.13
CaO	10.82	11.3	9.5	9.05	10.57	12.1	9.61	12.01	9.83	11.54	11.20	11.98	10.05	10.7
K_2O	0.27	0.8	1.44	1.07	0.47	0.57	0.58	0.15	0.48	0.20	0.23	-	0.91	0.39
a Q	2.32	2.4	3.3	2.97	1.82	2.54	3.01	1.81	2.49	2.24	2.53	2.33	2.75	2.91
P_2O_5	0.09	-	0.32	-	0.06	0.12	0.22	0.08	0.17	0.08	0.13	0.09	0.21	0.16
Total	99.12	99.55	100.15	99.78	99.91	99.89	99.32	99.0	99.64	99.7	98.74	99.72	99.99	100.0
Mg#	0.58	0.51	0.48	0.53	0.77	0.58	0.72	0.69	0.55	0.65	0.62	0.71	0.65	0.56

1. Porphyritic HAB, Higashi-Izu region, Japan (Kuno, 1968); 2. HAB, Kuriles (Gorshkov, 1970); 3. HAB, Java and Bali (Whitford et al., 1979); 4. HAB, Anak, Krakatau (Westerveld, 1962); 5. Porphyritic picrite, Okmok, Aleutians (Nye and Reid, 1986); 6. Plagioclase porphyritic HAB, Okmok, Aleutians (Nye and Reid, 1986); 7. Basaltic andesite, Mt. Shasta, CA, Cascades (Baker, 1988); 8. HAB, Bear Creek, OR, Cascades (Brandon, 1989); 9. Aphyric HAB, Amagi, Japan (Kuno, 1960); 10. HAB, Modoc Lava-Bed Quadrangle, CA (Powers, 1932); 11. High-alumina olivine tholeiite, average of 50 analyses from northwestern Great Basin, USA (Hart et al., 1984); 12. HAB, Warner basalt, Modoc Lava-Bed Quadrangle, CA (Powers, 1932); 13. High-Mg basalt MK-15, Makushin volcano, Unalaska Island, Aleutians (Gust and Perfit, 1987); 14. plagioclase porphyritic HAB (Lake HAB) Medicine Lake, CA *(Grove unpubl. data)*

FIGURES FOR CHAPTER ONE

Figure 1-1

Location map for Medicine Lake Volcano. Giant Crater flow mapped by Donnelly-Nolan.

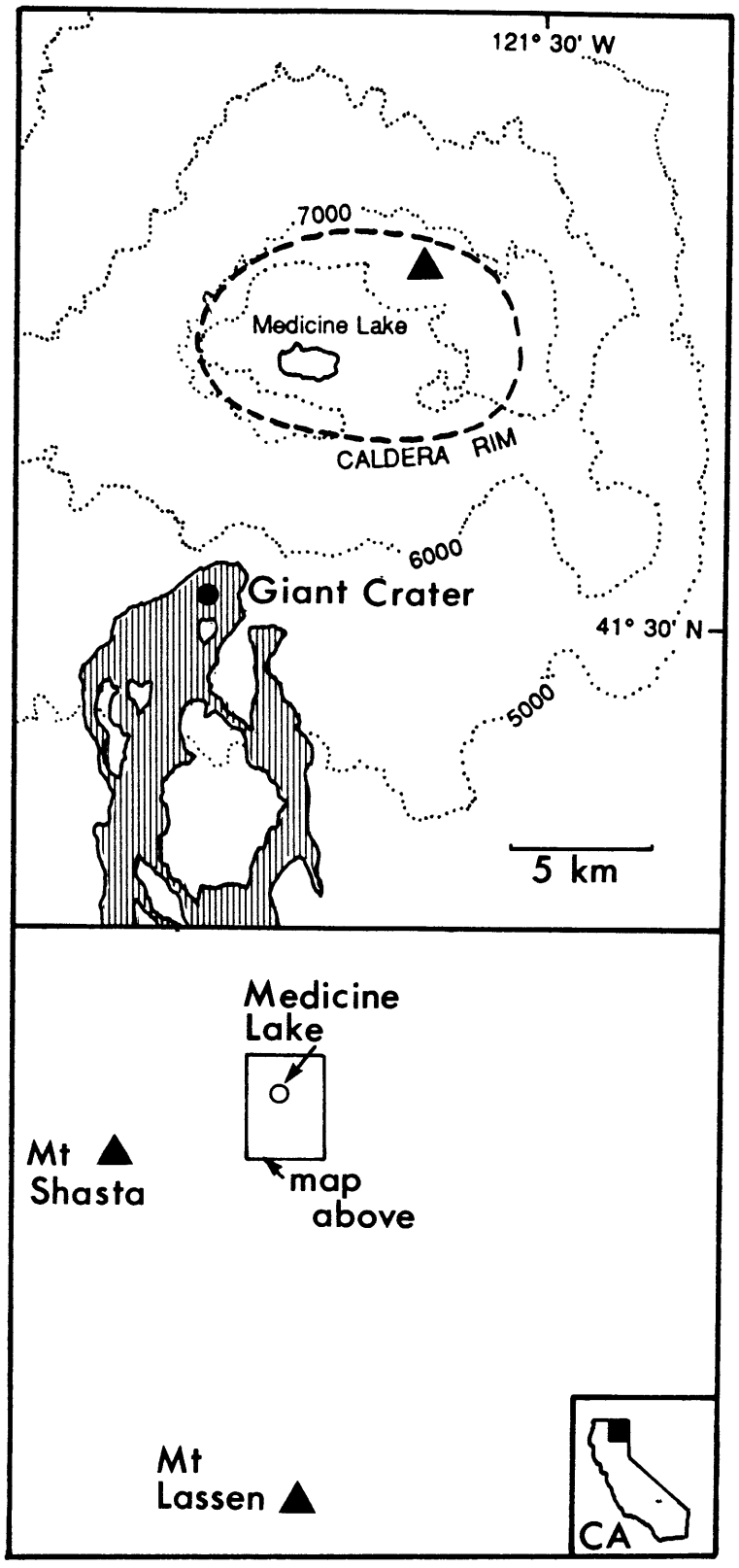
121° 30' W
7000
Medicine Lake
CALDERA RIM
6000
Giant Crater
41° 30' N
5000
5 km
Medicine Lake
Mt Shasta
map above
Mt Lassen
CA

Figure 1-2

Backscattered electron images of phase produced during short vs. longer experiments at the same temperature at 12 kbar. A) Photo of H96 which was run for 3 hours. Phases present are glass (gl), augite (aug), olivine (ol), plagioclase (pl), and spinel (not shown in photo). B) Photo of H132 which was run for 19 hours. Phases present are glass (gl), augite (aug), spinel (sp) and plagioclase (not shown in photo). Note the higher proportion of glass and the thicker overgrowth rims on the augite in this photo compared to A. Scale is the same in each photo; scale bar in lower left corner of A is 100 microns.

A

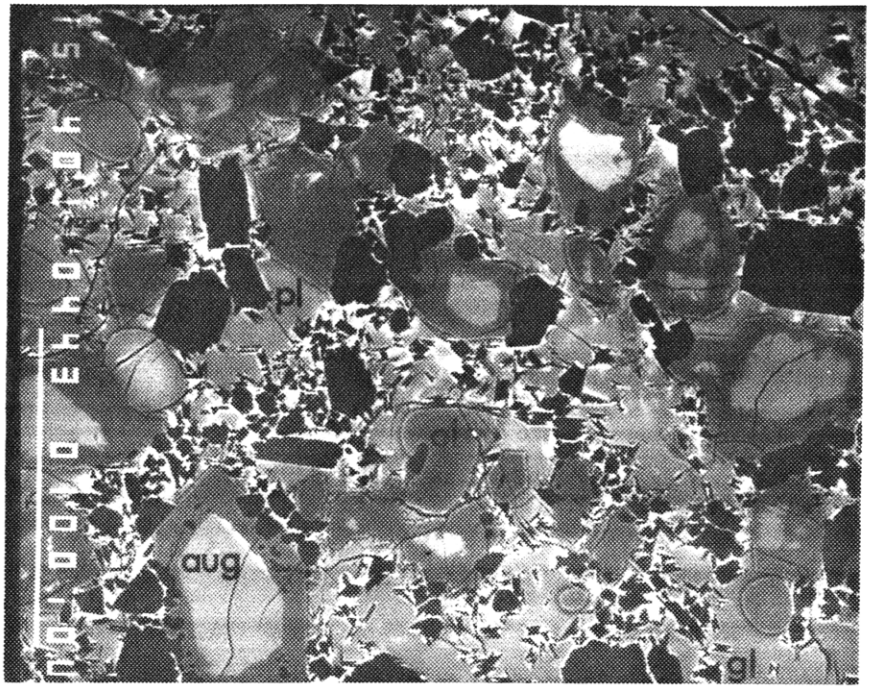

B

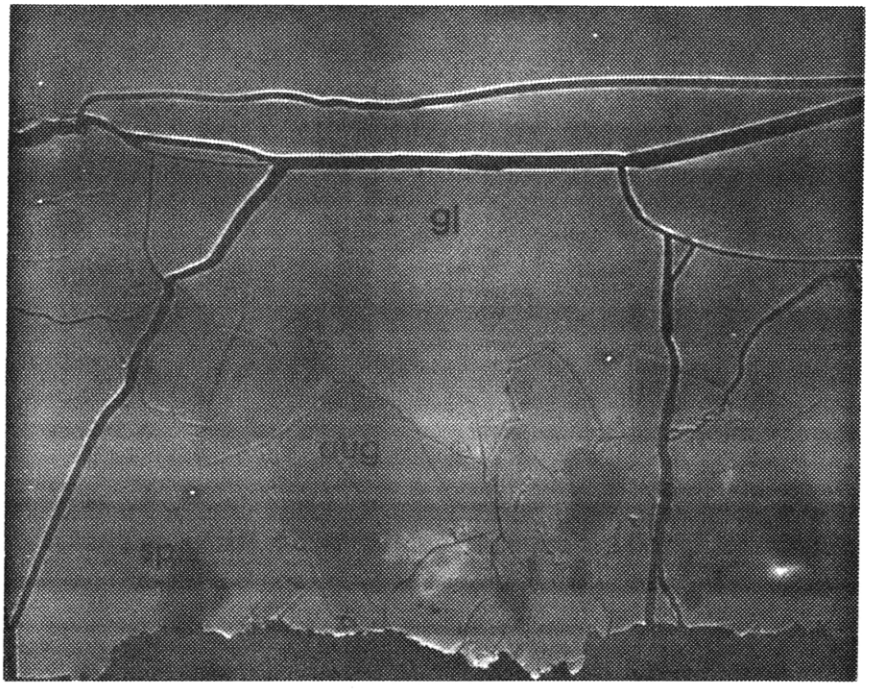

Figure 1-3

Pressure - temperature diagram showing results of melting experiments from 1 atm to 15 kbar on 79-35g. Symbols indicate which phases coexist with glass (l=glass, ol=olivine, pl=plagioclase, cpx=augite, sp=spinel) and lines drawn are the interpretation of this data. The symbol at 1290°C and 12 kbar represents two experiments, one containing plagioclase and the other not. The dashed line indicates the reaction olivine + liquid = augite + spinel. Point A marks the equilibrium liquid + olivine + plagioclase + augite + spinel.

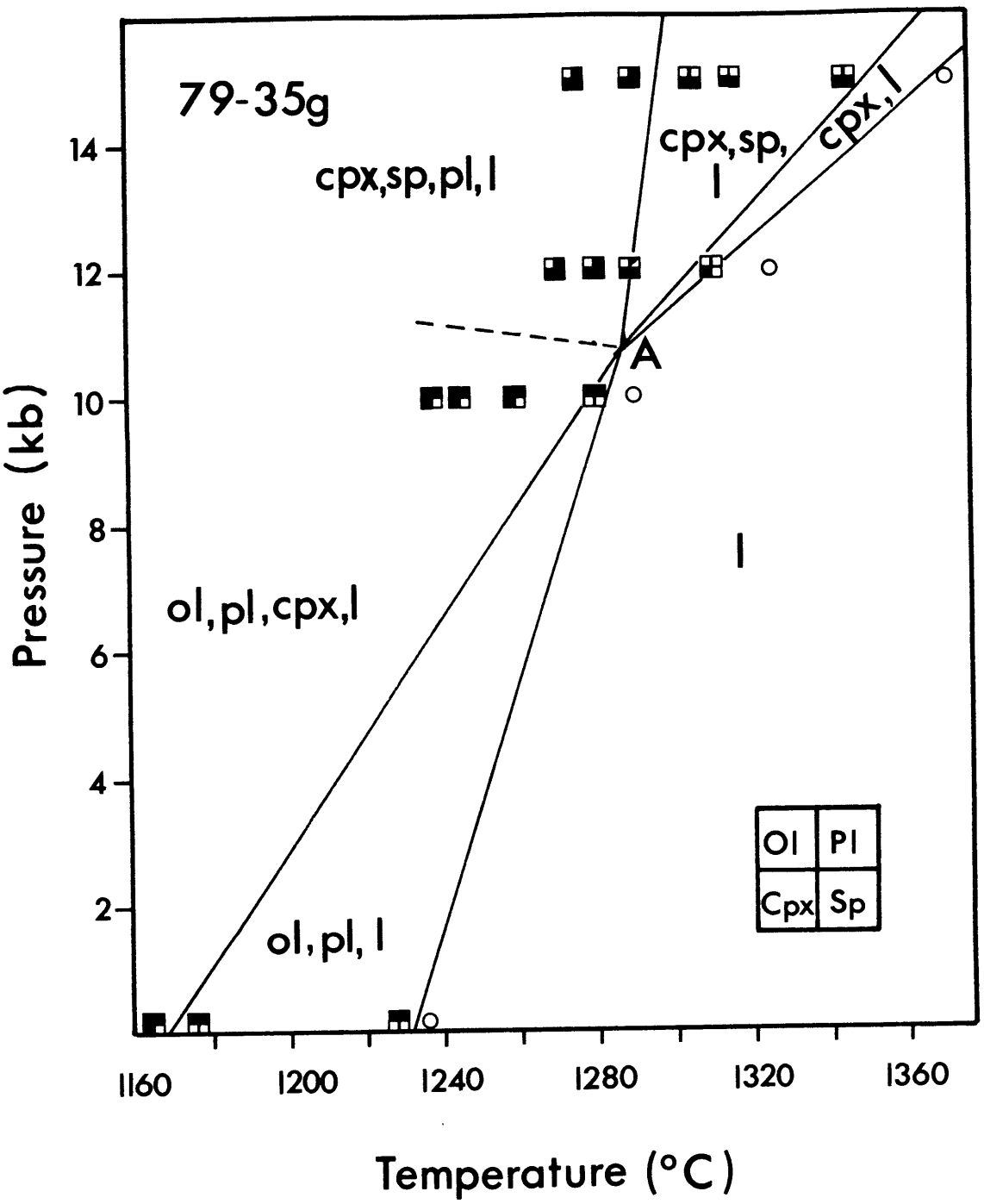
79-35g
cpx,sp,pl,l
cpx,sp,
l
cpx,l
A
l
ol,pl,cpx,l
ol,pl,l
Ol
Pl
Cpx
Sp
Pressure (kb)
14
12
10
8
6
4
2
1160
1200
1240
1280
1320
1360
Temperature (°C)

Figure 1-4

A. Results of melting experiments projected into the Olivine-Cpx-Quartz pseudoternary. Compositions are recalculated into the Olivine-Cpx-Plagioclase-Quartz pseudoquaternary using the mineral component scheme of Tormey et al. (1987) (with oxygen units), and then projected through plagioclase onto the Olivine-Cpx-Quartz pseudoternary. Number 1 indicates the projected position of 79-35g. The star indicates two liquid compositions saturated with olivine + orthopyroxene + augite + plagioclase at 10 kbar on a mix of 79-35g with orthopyroxene. The projected position of this bulk composition is indicated by #2. The x symbol represents liquids saturated with olivine + plagioclase + augite at 10 kbar. The positions of the plagioclase saturated olivine-orthopyroxene and augite-orthopyroxene liquid boundaries at 10 kbar are estimated as dashed lines. The olivine + orthopyroxene + augite + spinel saturated liquids produced from the mixture of 79-35g plus olivine (indicated by #3) at 15 kbar are shown as circled stars. Pyroxene compositions from the experiments are also plotted in this figure. The symbol key for pyroxenes is indicated on the figure.

B. Results of melting experiments projected into the Plagioclase-Cpx-Quartz pseudoternary using the mineral component scheme of Tormey et al. (1987). Symbols are the same as in Figure 1-4A.

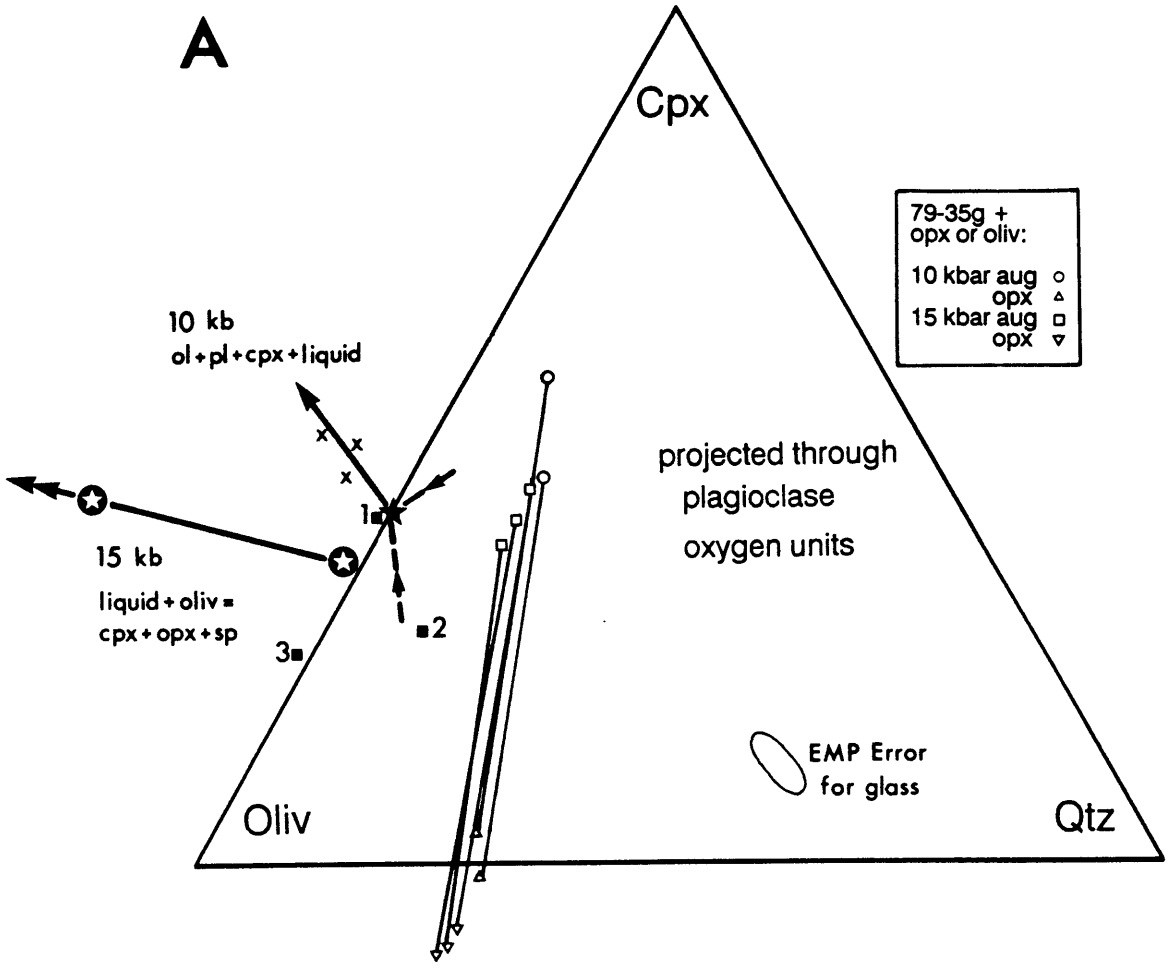
A
Cpx
79-35g +
opx or oliv:
10 kbar aug
opx
15 kbar aug
opx
10 kb
ol + pl + cpx + liquid
projected through
plagioclase
oxygen units
15 kb
liquid + oliv =
cpx + opx + sp
1
2
3
EMP Error
for glass
Oliv
Qtz

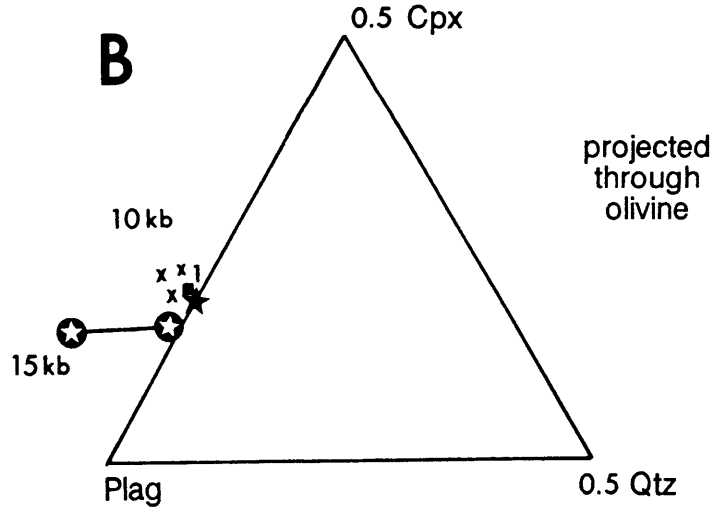
B
0.5 Cpx
projected
through
olivine
10 kb
1
15 kb
Plag
0.5 Qtz

Figure 1-5

Other primitive lavas from Medicine Lake projected into the Olivine-Cpx-Quartz and Olivine-Plagioclase-Quartz pseudoternaries. See the caption for Figure 1-4 for a description of the projection scheme. The 10 and 15 kbar boundaries from Figure 1-4 are indicated, and the ellipse represents the error associated with the XRF analyses of these rocks in this projection scheme. The open circle is the position of 82-72f.

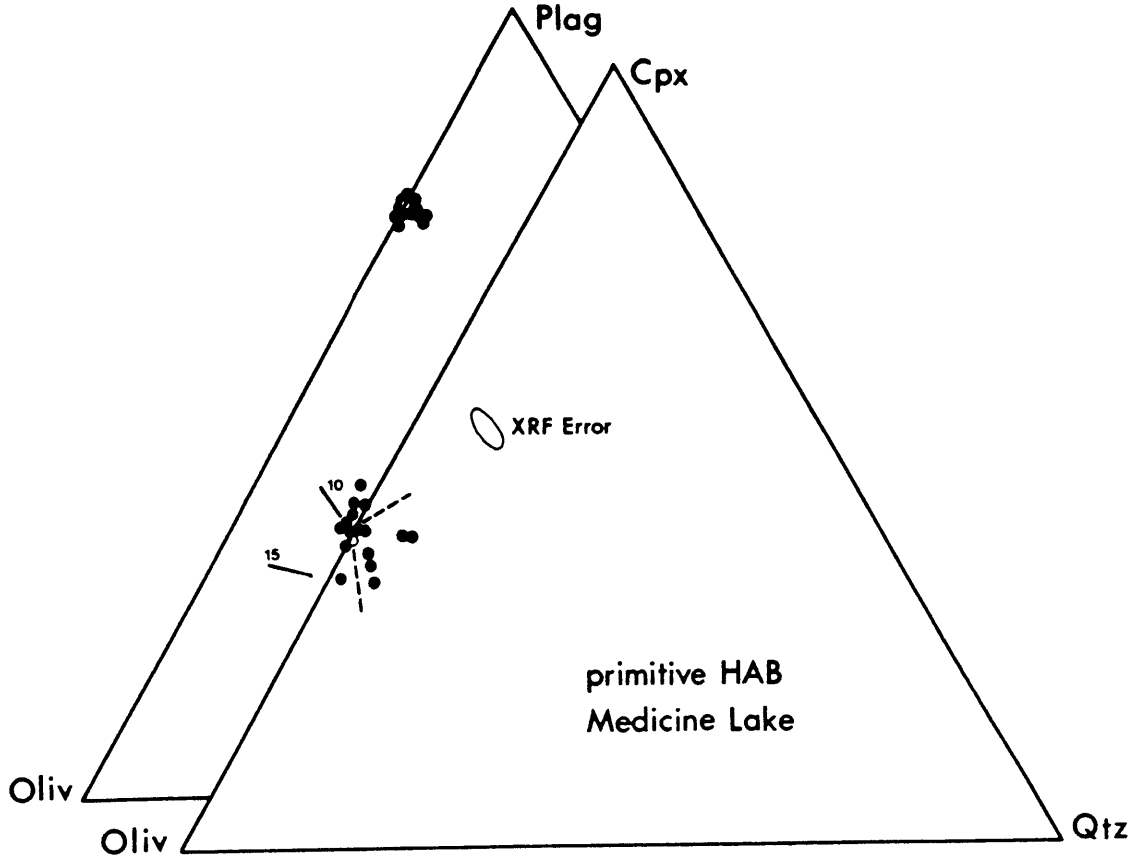
Plag
Cpx
XRF Error
10
15
primitive HAB
Medicine Lake
Oliv
Oliv
Qtz

Figure 1-6

Backscattered electron images of 11 kbar experiments on 82-72f. A) H225 was conducted at 11 kbar and 1285°C. Phases present are glass (gl), augite (aug), olivine (ol), plagioclase (pl), and spinel (sp). B) H235 was conducted at 11 kbar and 1293°C. Phases present are glass (gl), augite (aug), olivine (ol), and orthopyroxene (opx). This experiment lost a small amount of iron and the orthopyroxene is zoned with more Mg-rich rims. Scale is the same in each photo and the scale bar is 600 microns.

A

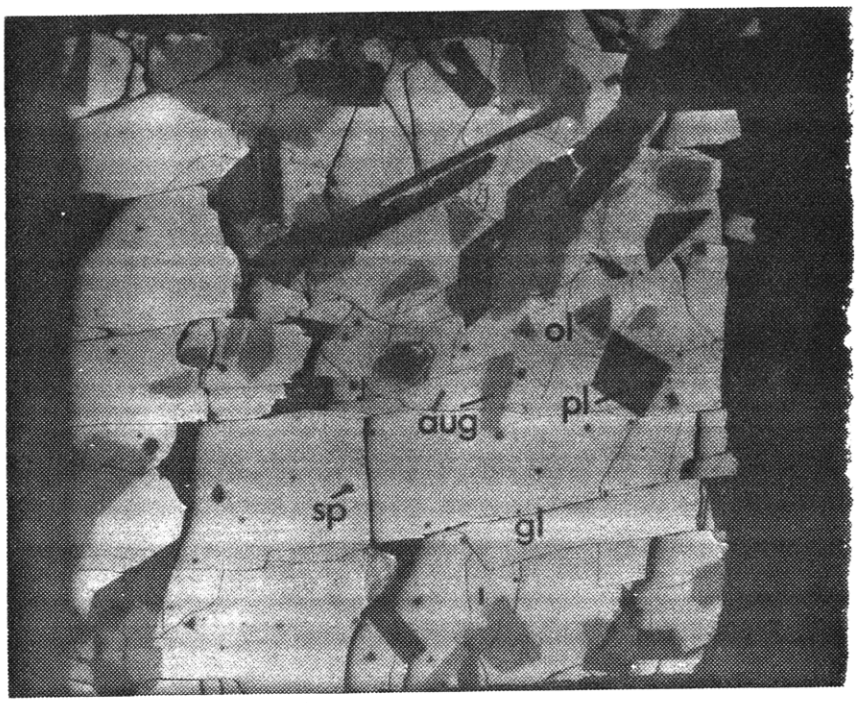

B

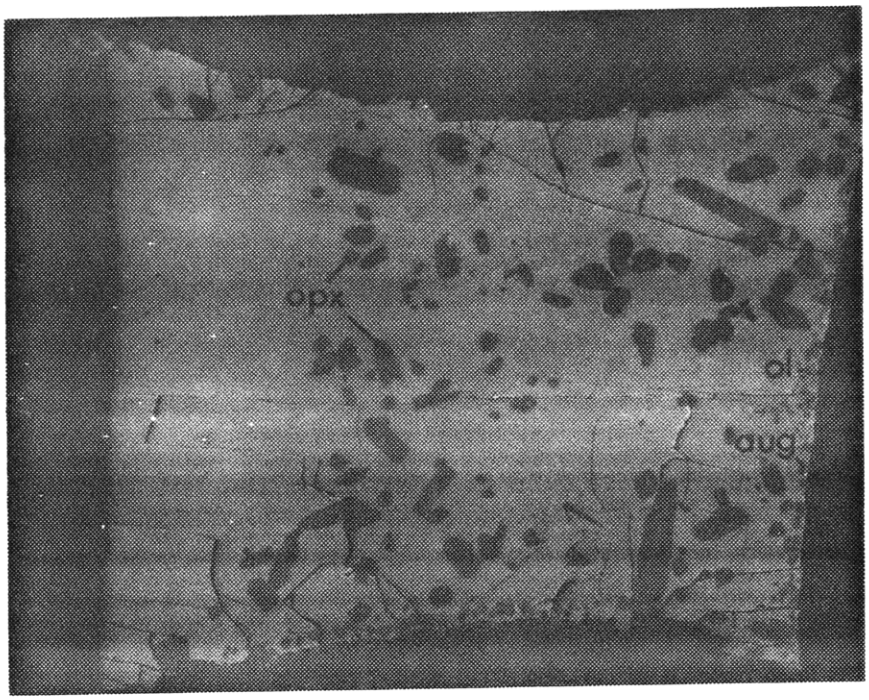

Figure 1-7

Compositions of other high-alumina basalt used in high-pressure phase equilibria studies (dots) and compositions of liquids coexisting with a spinel lherzolite assemblage at 10 kbar (squares) projected into the Olivine-Cpx-Quartz and Olivine-Plagioclase-Quartz pseudoternaries. See caption for Figure 1-4 for description of projection scheme. Numbers next to symbols correspond to numbered entry in Table 1-8. The shaded field is the field for primitive HAB from Giant Crater.

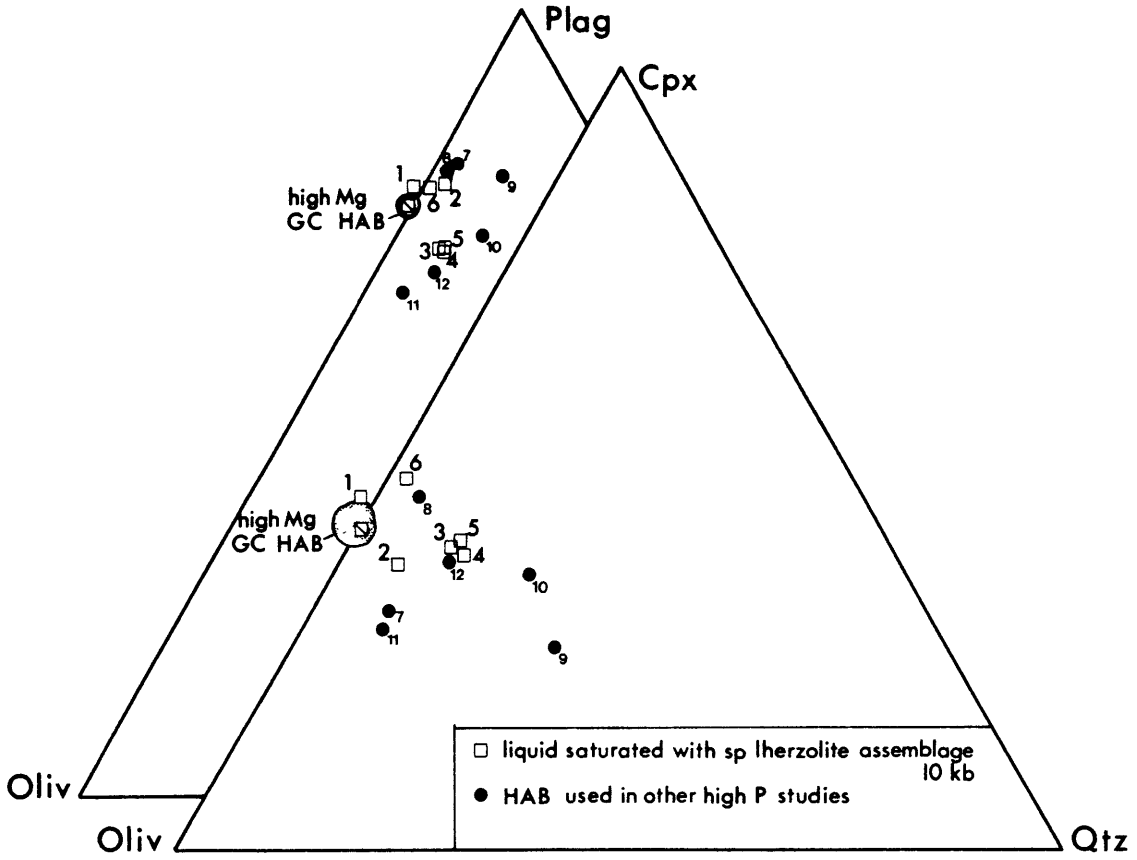
Plag
Cpx
Oliv
Oliv
Qtz
high Mg
GC HAB
high Mg
GC HAB
□ liquid saturated with sp lherzolite assemblage
10 kb
● HAB used in other high P studies

Figure 1-8

Trace element patterns for 82-72f compared to MORB. A)REE pattern of 82-72f compared to primitive MORB AII78-3-103 (from Bryan et al., 1981). B) Spider diagram comparing trace element abundances of 82-72f with another high-alumina basalt from the Cascades and to the primitive MORB AII78-3-103. See Table 1-9 for trace element concentrations for 82-72f. Normalizing values from Anders and Grevesse (1989), except for K (100 ppm), Rb (0.22 ppm) and Sr (7.4 ppm) (Stan Hart, personal communication).

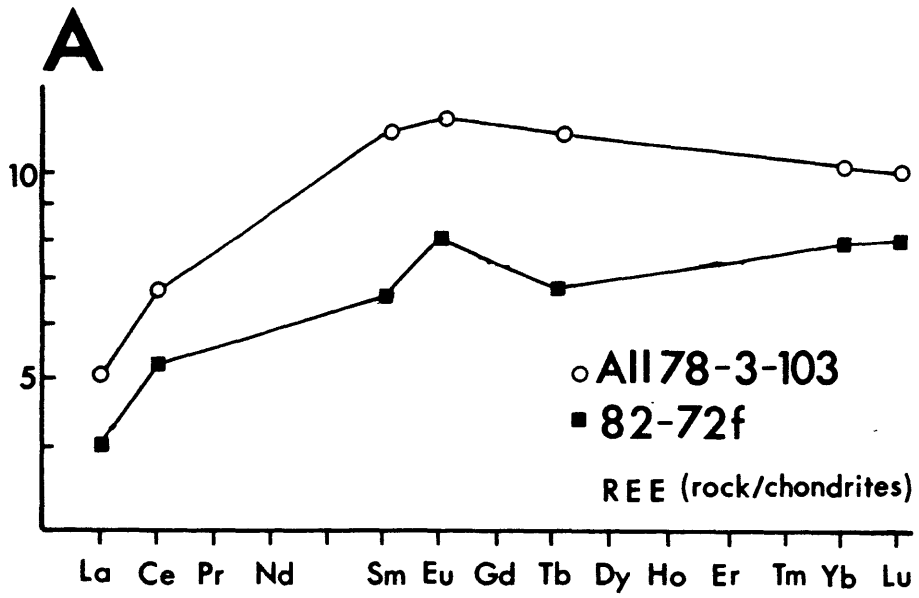
A
10
5
All78-3-103
82-72f
REE (rock/chondrites)
La Ce Pr Nd Sm Eu Gd Tb Dy Ho Er Tm Yb Lu

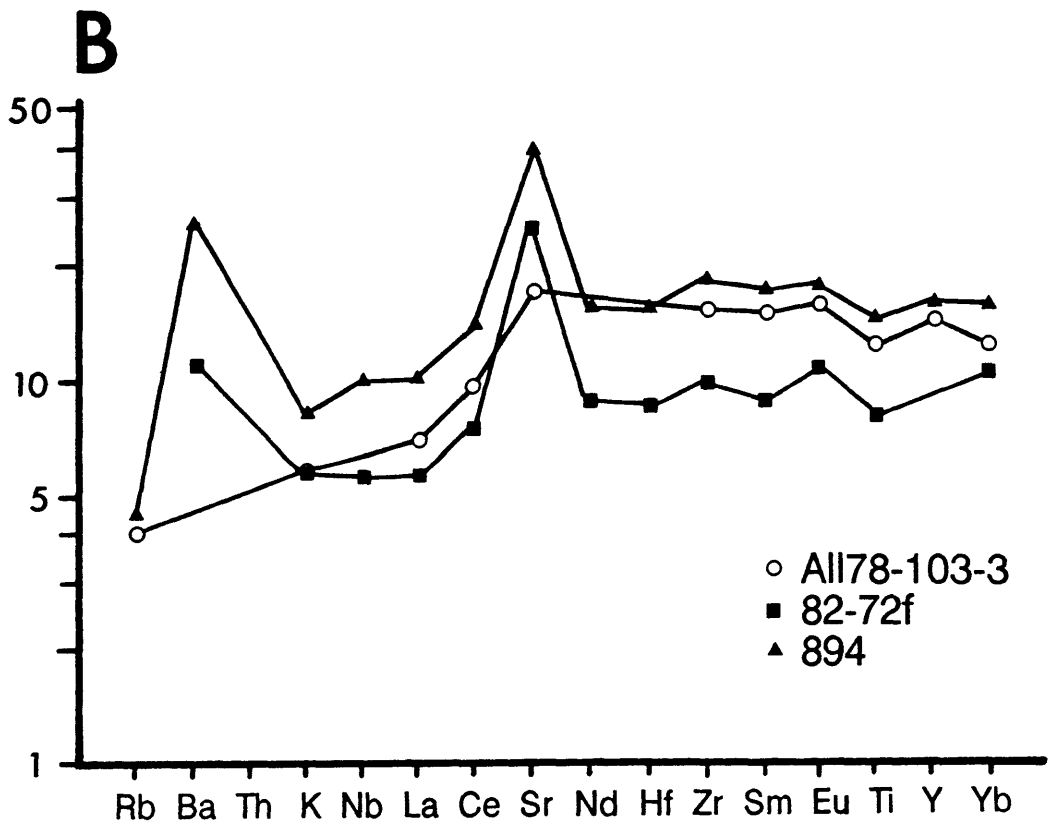
B
50
10
5
1
All78-103-3
82-72f
894
Rb Ba Th K Nb La Ce Sr Nd Hf Zr Sm Eu Ti Y Yb

Figure 1-9

Compositions of other high-alumina basalt and primitive arc lavas projected into the Olivine-Cpx-Quartz and Olivine-Plagioclase-Quartz pseudoternaries. See caption for Figure 1-4 for description of projection scheme. Numbers correspond to numbered entry in Table 1-10. The shaded field is the field for primitive HAB from Giant Crater, and the dotted field is the field for all HAB from Medicine Lake.

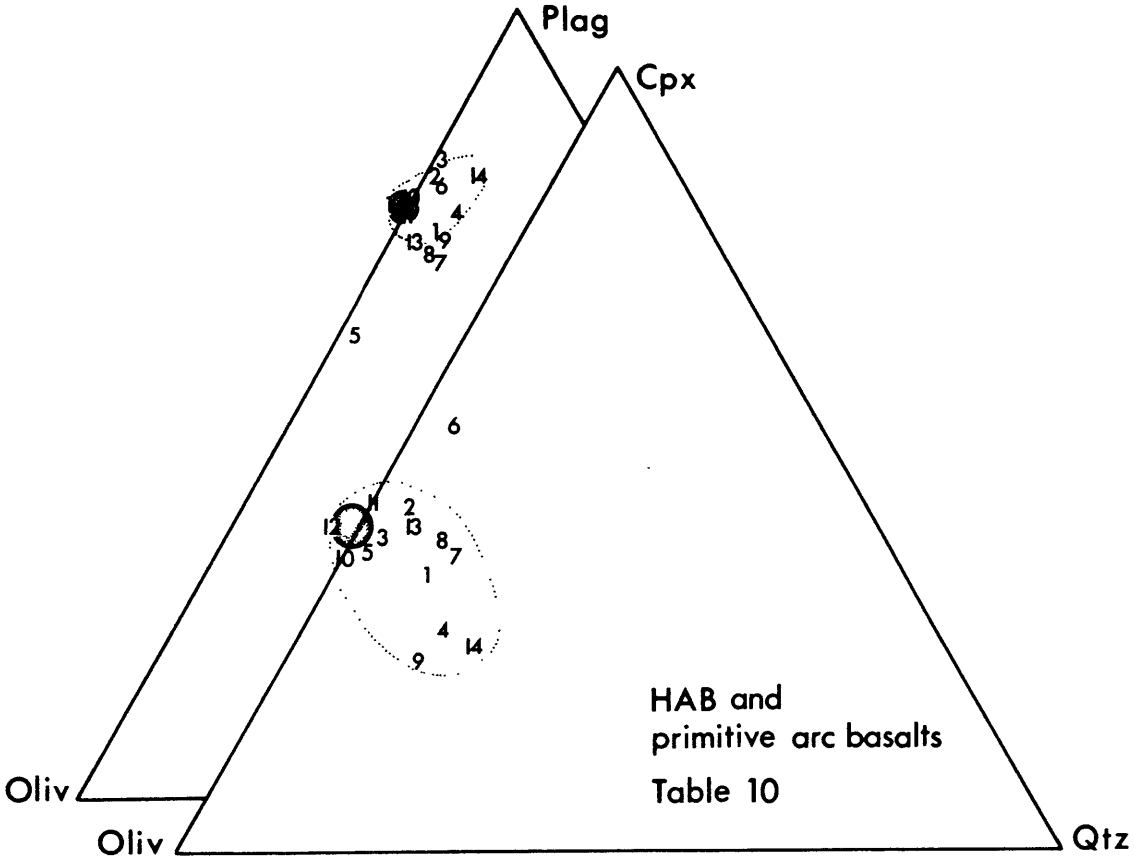
Plag
Cpx
Oliv
Oliv
Qtz
HAB and
primitive arc basalts
Table 10

Figure 1-10

Mg# vs. Al_2O_3 for arc basalts. Field for arc basalts is from Gust and Perfit (1987). Mg# is calculated as Mg/[Mg + 0.9 Fe] (and not as Mg/[Mg + Fe] as in the rest of this paper) to match Gust and Perfit's calculations. The area of the field above 17 wt.% Al_2O_3 is labeled "HAB" although some rocks falling within this field could be alkali basalts by Kuno's (1960) definition. Also shown are the fields for the Aleutian high-MgO low-Al_2O_3 basalts and the Giant Crater high-MgO high-Al_2O_3 basalts. The curves labeled 10, 12 and 15 are the experimentally determined crystallization paths for 79-35g at 10, 12 and 15 kbar.

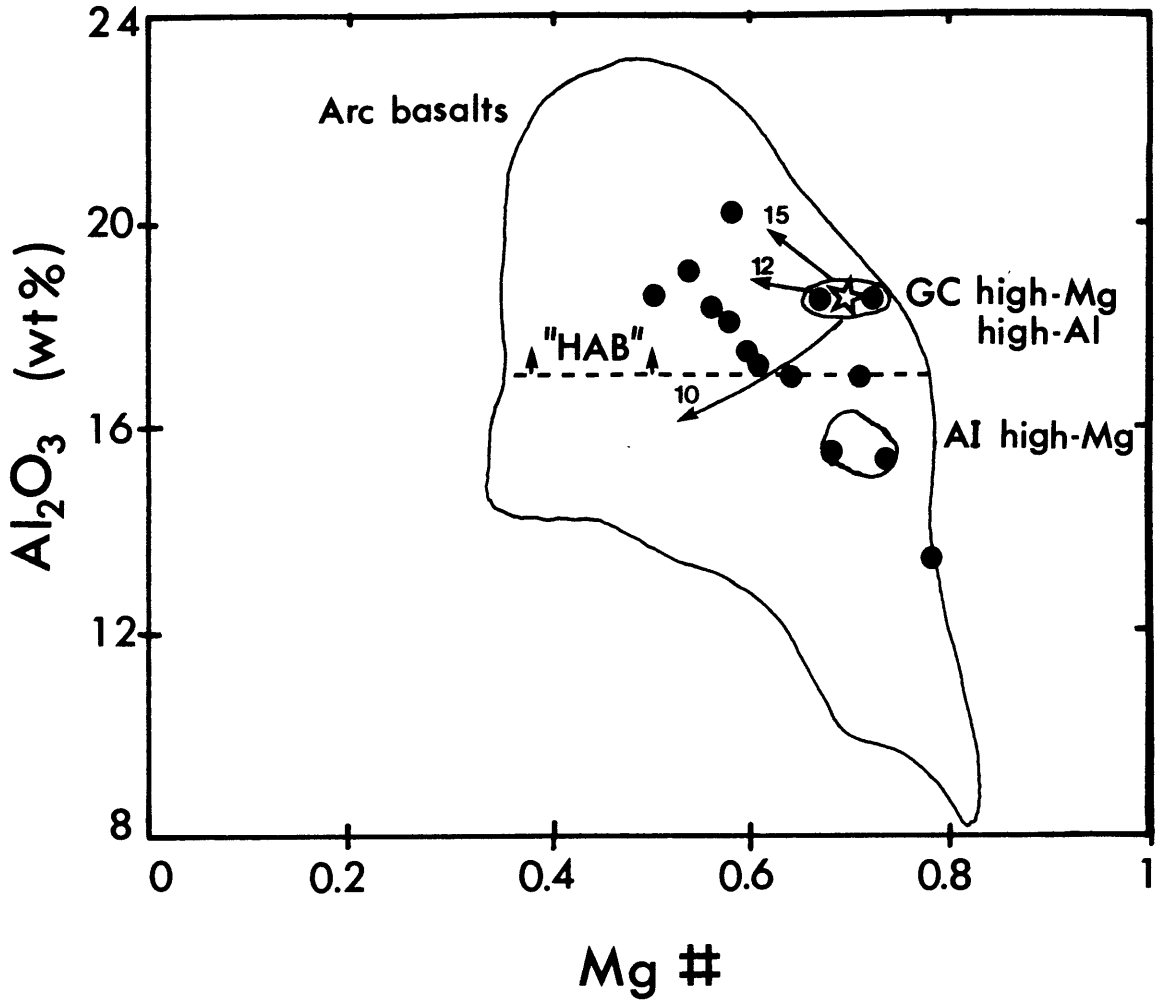
24
20
16
12
8
0
0.2
0.4
0.6
0.8
1
Al_2O_3 (wt%)
Mg #
Arc basalts
15
12
10
"HAB"
GC high-Mg
high-Al
Al high-Mg

CHAPTER TWO

HIGH PRESSURE EXPERIMENTS ON MAGNESIAN EUCRITE COMPOSITIONS: CONSTRAINTS ON MAGMATIC PROCESSES IN THE EUCRITE PARENT BODY

INTRODUCTION

Eucrites are the most abundant type of basaltic achondrite meteorites. There is strong geochemical evidence that eucrites are genetically related to diogenites (pyroxene cumulate) and howardites (polymict breccias of eucrite and diogenite clasts) but the igneous processes that relate the Howardite-Eucrite-Diogenite (HED) meteorite group are debated. The models proposed to explain the origin of the eucrites fall into two groups: partial melting of a chondritic source and fractional crystallization of olivine and pyroxene from a mafic basaltic magma. The challenge in interpreting the HED meteorite association lies in explaining the processes linking the main-group non-cumulate iron-rich eucrites and the more magnesian silicate minerals in diogenites and the cumulate portions of howardites. (See Hewins and Newsom, 1988, for a review of these models).

Stolper (1977) and Consolmagno and Drake (1977) viewed eucrites as primary magmas derived by varying degrees of partial melting of a single source. Liquids produced by partial melting remain at the liquid - olivine - low-Ca pyroxene - plagioclase - metal reaction boundary (determined experimentally at 1 atm by Stolper, 1977), producing eucritic liquids, until plagioclase is exhausted from the source. Thereafter, continued melting moves liquids up along the olivine - pyroxene reaction boundary. These melts crystallize only pyroxene when separated from their residue, and this process could produce the cumulus minerals of diogenites. A weakness of this model is that the class of liquids residual from the crystallization which produced the diogenite cumulates has not been identified.

A fractionation model for the origin of eucrites (Mason, 1962) requires that a differentiating magma follows the olivine - low-Ca pyroxene boundary during fractional crystallization and that this boundary be a cotectic or a reaction curve which remains tangential to pyroxene so that liquids will follow it to the reaction point. Other models have proposed that the boundary shifts with changing Mg# during fractionation so that the olivine - low-Ca pyroxene boundary remains cotectic or tangential (Ikeda and Takeda, 1985; Warren, 1985; Longhi and Pan, 1987; Beckett and Stolper, 1987; Hewins, 1987). Longhi and Pan (1987) and Beckett and Stolper (1987) determined that at 1 atm the olivine - pyroxene boundary is a reaction boundary that is not tangential to pyroxene and that fractionation of proposed mafic parent magmas (e.g. Ikeda and Takeda, 1985), although capable of producing pyroxenes with compositions similar to those in diogenites, would not produce eucritic liquids at low pressures.

Potential parental magmas for derivative eucrites and diogenite cumulates have been identified as clasts in howardite meteorites. Yamato 7308 pigeonite-eucrite clast 1 (PE1) and Kapoeta clast rho have been proposed (Delaney et al. 1981, 1984; Ikeda and Takeda, 1985) as parent magmas for the two distinct geochemical trends (incompatible element-poor and incompatible element-rich, respectively). Delaney et al. (1981,1984) suggested that these two magmas were produced by differing degrees of partial melting and Ikeda and Takeda (1985) proposed a model in which the incompatible element-poor parent formed at the top of a magma ocean and experienced volatile loss.

The proposed parent magmas can produce derivative eucrites and cumulate diogenites only by high pressure fractional crystallization. At elevated pressure conditions, the relevant phase boundaries move toward olivine and are no longer reaction boundaries (Longhi and Pan, 1987; Warren

and Wasson, 1979). Based on existing phase equilibrium data, Longhi and Pan (1988a) estimated that 2 kbar is the minimum pressure necessary to cause this change in the olivine - pyroxene - plagioclase boundary and the olivine - pyroxene boundary. Polybaric fractionation of pyroxene and minor olivine from a mafic parent during ascent in the parent body could produce both diogenites and eucrites. The principal objection to the elevated pressure fractionation model is the presumed small size of the parent body. The maximum pressure which would be attained in the interior of a eucrite parent body is inferred to be about 1 kbar.

The effect of pressure on the phase boundaries relevant to eucrite petrogenesis is an important constraint which has been estimated but never experimentally determined. If the olivine - pyroxene - liquid boundary changes from a peritectic to a cotectic reaction at a pressure of 1 kbar, then a fractionation model can explain the HED group associations. Therefore, the compositions of Kapoeta rho and Yamato PE1 were used as starting materials for this experimental study and the position and nature of the olivine - pyroxene - plagioclase - spinel - metal and olivine - pyroxene - spinel boundaries were determined at 1 atm and 1 kbar.

EXPERIMENTAL METHODS

Synthetic analogs of two magnesian eucrite clasts from howardites, Kapoeta clast rho and Yamato 7308 PE clast 1, were made from reagent grade oxides and high purity iron metal following the method of Grove and Bence (1977). Table 2-1 lists the compositions of the eucrite clasts as determined by Dymek et al. (1976) and Ikeda and Takeda (1985). Also shown are microprobe

analyses of glasses produced by fusion of the powdered oxide starting material in high purity iron capsules sealed in evacuated silica glass tubes.

Melting experiments were conducted on both compositions at 1 atm and 1 kbar using iron-wüstite (IW) and iron-quartz-fayalite (IQF) oxygen fugacity buffers. Run conditions and the phase appearance sequence are listed in Table 2-2. The 1 atm experiments were carried out in Deltech vertical quench furnaces. Runs were terminated by quenching into water. For one set of experiments, pressed pellets of starting material were sintered onto Pt-Fe alloy wire loops (custom made to minimize iron exchange between silicate charge and loop; Grove, 1981) and hung in the hot spot of the furnace with the oxygen fugacity controlled at IW using a CO_2-H_2 gas mixture. Starting material for a second set of experiments was packed into high purity iron capsules, which were then sealed along with a buffer packet in evacuated silica glass tubes. The solid buffering assemblage consisted of either a fine powdered mixture of synthetic fayalite and reagent grade SiO_2 wrapped in iron foil or powdered wüstite in iron foil. The solid IW buffer was used only at temperatures greater than 1180°C, where the IQF assemblage melts.

The same solid buffering techniques were used in the 1 kbar experiments. Capsules measuring 0.188" long by 0.063" diameter were made of 0.001" thick high purity iron foil and were used for both the buffer packets and as containers for the starting material. For each run, two capsules of starting material and a buffer packet were welded into a capsule made of 0.001" thick Pt tubing. The 0.001" foil was used in the experimental design to ensure that the gas pressure was transmitted efficiently to the silicate sample. Melting experiments at 1 kbar total pressure were conducted in Titanium-Zirconium-Molybdenum (TZM) alloy pressure vessels using argon as the pressure medium. The design of the vessel is similar to that pictured in

Williams (1968). Briefly, the vessel is 1" in outer diameter by 12" in length with a 1/4" inner diameter by 11" deep hole, bored smooth and rounded at its base. The vessel is enclosed in an inconel 600 sheath and bathed in Ar gas at a small positive pressure. The end of the pressure vessel containing the charge was positioned in a Deltech furnace so that a temperature gradient of less than 2°C was present over the experimental charge. The cold seal at the top of the pressure vessel was cooled by a recirculating water bath. Temperature was monitored by a Pt-Rh thermocouple placed at the position of the sample on the outside of the pressure vessel. The temperature difference between the inside and outside of the vessel was determined by direct measurement during calibration runs, and experimental run temperatures were corrected for this difference. Runs were terminated by removing the pressure vessel from the furnace and inverting it so that the experimental charge fell to the water-cooled end of the vessel, minimizing crystal growth during quench.

Analytical methods

Experiments were quenched, the contents of the buffer packets examined optically, and silicate experimental products mounted in epoxy, polished and carbon-coated for analysis by electron microprobe. Compositions of experimentally produced phases listed in Table 2-3 were obtained with the MIT 4-spectrometer JEOL 733 Superprobe using the on-line data reduction and matrix correction procedures of Bence and Albee (1968) with modifications of Albee and Ray (1970). An experiment was judged successful if materials balance calculations resulted in a value of wt.% FeO for the model bulk composition which differed by less than 2.5 % relative from the starting composition (Table 2-4). Experiments not analyzed in this manner were accepted if the glass fell in the same chemical trend in terms of SiO_2, Mg#, and CaO/Al_2O_3 as the glasses from those which were mass balanced. In

several experiments at 1 kbar, iron loss resulted from the reduction of the charge due to exhaustion of the buffer or exposure to the highly reducing argon atmosphere of the pressure vessel through a hole in the Pt capsule, and these experiments are not reported here.

EXPERIMENTAL RESULTS

The phase appearance sequence for experiments at 1 atm and 1 kbar is shown in Figure 2-1 and listed in Table 2-2. At 1 atm, Cr-spinel is on the liquidus at 1350°C, followed by olivine, pigeonite, and finally plagioclase. The experiments reported here were conducted at a range of temperatures (1210° - 1140°C) from just below the onset of pigeonite crystallization through about 20°C of the plagioclase interval in order to locate the olivine - low-Ca pyroxene and olivine - low-Ca pyroxene - plagioclase saturated liquid boundaries. The assemblage olivine - low-Ca pyroxene - spinel persists in the highest temperature well-characterized experiments at 1210°C. Plagioclase appears at 1160°C at 1 atm and at 1167°C at 1 kbar.

Glasses from experiments defining the olivine - low-Ca pyroxene - plagioclase - spinel - metal (five-phase) and olivine - low-Ca pyroxene - spinel - metal (4-phase) boundaries are plotted in Figure 2-2 in the Olivine - Anorthite - SiO_2 molar projection of Stolper (1977). The olivine - low-Ca pyroxene - plagioclase - spinel saturated 1 atm liquids produced at IW are nearly identical to those produced at IQF, and both plot near the projected position of Stolper's 1 atm five-phase boundary (indicated by point A in Figure 2-2) based on his experiments on Juvinas and Sioux County. The liquids saturated with olivine - low-Ca pyroxene - spinel at 1 atm define a reaction curve in agreement with Longhi and Pan (1987) and Beckett and Stolper

(1987). At 1 kbar the boundaries move to lower SiO_2 values and shift slightly toward olivine with respect to a line of constant Olivine - Anorthite proportions, plotting just below the Pyroxene - Anorthite join. Olivine is in reaction with liquid along the 1 atm boundaries, but this reaction relationship disappears at 1 kbar. The change from a reaction to a precipitation relation for olivine is reflected in the textures of the olivine crystals; at 1 atm olivine is subhedral to anhedral, whereas at 1 kbar the crystals are euhedral (Figure 2-3).

Table 2-5 lists stoichiometric coefficients of phases involved in the melting and crystallization reactions that occur along these boundaries. The reaction coefficients were calculated by multiple linear regression using techniques similar to those employed by Juster et al. (1989). The compositions of liquid and mineral phases from pairs of experiments saturated with the same assemblage were used to calculate the proportions of mineral phases required to produce the lower temperature liquid from the higher temperature liquid. At 1 atm, both the olivine - low-Ca pyroxene - plagioclase - spinel and olivine - low-Ca pyroxene - spinel boundaries are reaction boundaries involving liquid + olivine +/- spinel. At 1 kbar, the reaction relationship involving olivine has disappeared for both boundaries. Note that the dominant phase in melting or crystallization along the olivine - low-Ca pyroxene - spinel boundary at 1 kbar is pyroxene. Under similar conditions, melting the Yamato composition involves less olivine, less pyroxene, and more plagioclase compared to the Kapoeta composition.

DISCUSSION

Phase boundaries

The experimentally determined 1 atm and 1 kbar olivine - low-Ca pyroxene - plagioclase - spinel - liquid and olivine - low-Ca pyroxene - spinel liquid boundaries are plotted using Stolper's Olivine - Anorthite - SiO_2 molar projection in Figure 2-4A along with the projected positions of pigeonite and plagioclase from 1 kbar experiments. Figure 2-4B depicts the same information in the oxygen unit Olivine - Plagioclase - SiO_2 projection scheme of Grove et al. (1983). The boundaries at 1 kbar lie in olivine normative space in the molar projection (Figure 2-4A), but they appear slightly SiO_2 normative in the oxygen unit projection (Figure 2-4B). Table 2-6 lists CIPW norms calculated for the liquids defining the 1 kbar boundaries. Although most have normative olivine, some contain normative quartz. Since the different projection schemes (including the CIPW norm, which makes simplifying assumptions about mineral chemistries) locate the boundaries in different places with respect to olivine saturation, other lines of evidence were used to evaluate the nature of these saturation boundaries. As mentioned previously in the description of the results, textural evidence from the experiments suggests that olivine no longer reacts with liquid at 1 kbar. The olivine crystals grown in the 1 kbar experiments are euhedral whereas those from 1 atm experiments are subhedral and appear to have dissolved, suggesting that olivine reacts with liquid at 1 atm but not at 1 kbar (Figure 2-3). Furthermore, the algebraic signs of the stoichiometric coefficients calculated for melting and crystallization along these boundaries (Table 2-5) are consistent with the interpretation that olivine no longer reacts with liquid at 1 kbar: pigeonite (*plus* plagioclase) *minus* olivine *minus* spinel = liquid at 1 atm but pigeonite (*plus* plagioclase) *plus* olivine

plus spinel = liquid at 1 kbar. The calculated reaction coefficients for the olivine - low-Ca pyroxene - spinel - liquid boundary at 1 kbar indicate that the boundary is nearly tangential to pyroxene. Based on a linear interpolation of reaction stoichiometries from Table 2-5, the pressure at which the reaction relationship disappears is 0.9 kbar.

Longhi and Pan (1988a) estimated that pressures in excess of 2 kbar are necessary to saturate magnesian eucritic liquids with olivine (plus low-Ca pyroxene and plagioclase). Their calculations are based on a parameterization of the olivine - low-Ca pyroxene boundary as a function of pressure determined from experiments on lunar basalts at pressures up to 18 kbar. Longhi and Pan (1988a) cite an uncertainty of +/- 2.9 kbar in the 8-20 kbar range and +/- 1 kbar at lower pressures. At a pressure of 2 kbar, their work predicts that a liquid saturated with olivine and low-Ca pyroxene will be marginally in reaction with olivine. The experiments reported here show that a magnesian eucrite liquid saturated with olivine and low-Ca pyroxene at 1 kbar is slightly olivine normative. This difference is at the limit of Longhi and Pan's stated error. A potential difficulty with their estimate of the pressure dependence of the olivine - low-Ca pyroxene saturation boundary is that they included olivine - low-Ca pyroxene boundaries from above the stability field of plagioclase. The pressure dependence of the composition of 4-phase saturated liquids (olivine - low-Ca pyroxene - high-Ca pyroxene - aluminous-phase) is different in the spinel and plagioclase stability fields (Presnall et al. 1979). Therefore, one might expect a similar difference in the compositional dependence of the olivine - pyroxene boundaries associated with a lower variance plagioclase vs. spinel boundary.

Another major feature of the phase boundaries determined in this study is the shift of the olivine - low-Ca pyroxene - plagioclase - spinel - liquid

boundary away from the SiO_2 - Plagioclase join of the projection with increasing pressure. This is the opposite of the direction of movement of the enstatite-anorthite boundary determined by Sen and Presnall (1984) in the system Forsterite - Anorthite - Silica; in this subset of the CaO-MgO-Al_2O_3-SiO_2 (CMAS) system the pyroxene-plagioclase boundary shifts toward the SiO_2 - Plagioclase join [Olivine/(Olivine + Plagioclase) decreases] from 1 atm to 10 kbar, as shown in Figure 2-5. However, Figure 2-5 also shows the position of the forsterite + liquid = anorthite + enstatite + diopside reaction point determined by Presnall et al. (1979) in the system Forsterite-Diopside-Anorthite-Silica, another subset of CMAS, at 1 atm and 7 kbar. This boundary is more directly relevant to the eucrite five-phase boundary and moves in the same direction as the eucrite boundary, i.e. away from the SiO_2 - Plagioclase join with increasing pressure. Furthermore, a simple linear interpolation of the movement of the CMAS olivine - low-Ca pyx - high-Ca pyx - plagioclase - liquid boundary indicates that the shift of the liquid toward the Olivine - Plagioclase base is similar in magnitude to that observed in the eucrite experiments reported here. The offset of the boundaries determined for the eucrite compositions toward Olivine relative to the CMAS boundary is consistent with the observations of Longhi and Pan (1988b) and Grove and Juster (1989). Both predict that the effect of increasing Fe/[Fe+Mg] on olivine - low-Ca pyroxene - plagioclase saturation is to increase the olivine content and decrease the plagioclase content. This also means that iron gained by eucrite liquids from the iron capsule container during experiments could move the boundaries even further toward Olivine, but that is not a complication of these experiments. The Mg#s and the FeO contents are nearly equal for the five-phase saturated liquids from both 1 atm and 1 kbar experiments (Table 2-2), and iron gain or loss from the experiments reported here was minimal

(Table 2-4). The results of these experiments suggest that increasing Fe/[Fe+Mg] also slightly increases the magnitude of the pressure-induced shift of the olivine - low-Ca pyroxene - plagioclase boundaries away from the SiO_2 - Plagioclase join.

Eucrite parent body partial melting and fractional crystallization processes

Delaney et al. (1981, 1984) proposed that two distinct magnesian eucrite parents were produced by different degrees of partial melting at depth within the eucrite parent body. The asteroid 4 Vesta (radius 275 km) is commonly cited as a possible source for HED meteorites since it is the only known asteroid with a surface composition equivalent to that of a basaltic achondrite (Consolmagno and Drake, 1977; Gaffey, 1983). Infrared spectrophotometric observations by McCord et al. (1970) and Larson and Fink (1975) demonstrated that the surface of Vesta consists in part of pigeonite. For a planet of this size with a density appropriate for an EPB composition (3.5 g/cm^3) (Morrison, 1976), the pressure attained at the center is 1 kbar.

Partial melting.

The starting materials chosen for this study are magnesian eucrite clasts from howardites that belong to two distinct geochemical trends within the eucrite association. Yamato 7308 pigeonite-eucrite clast 1 (Y7308 PE1) is the most magnesian member of the incompatible element-poor trend, trend A, and Kapoeta clast rho is the most magnesian sample of the incompatible element-rich trend B (Ikeda and Takeda, 1985).

Figure 2-6 is a graph of Mg# vs. TiO_2 contents showing the paths followed by liquids during partial melting and fractional crystallization. The crystallization paths were constructed from the 1-atm experimental results and the partial melting paths were derived from the batch melting equation using bulk distribution coefficients calculated from 1-kbar mineral, melt, and phase

proportion data. Figure 2-6 resembles similar figures found in Hewins and Newsom (1988) and Longhi and Pan (1988a). Table 2-7 lists compositions of batch melts at the point of exhaustion of plagioclase from the source for EPB compositions Eu1 (Morgan et al., 1978) and Eu3 (Dreibus et al., 1977). Plagioclase is exhausted from Eu1 and Eu3 after about 10 wt.% melting. These melts were calculated using the composition of the 1-kbar five-phase saturation boundary and mineral/melt distribution coefficients (K_D's) for the major elements. The projected positions of the two magnesian eucrites, and the experimentally determined phase boundaries at 1 atm and 1 kbar are shown in Figure 2-7 in an enlarged portion of the Oliv - An - SiO_2 diagram used in Figure 2-2. The projected position of the two magnesian eucrite parents (Figure 2-7) indicates that these magmas could be produced by partial melting in the interior of an EPB at pressures of 1 kbar in which olivine, pigeonite and spinel were residual phases. If these two magnesian parents are produced by partial melting, a parent body that is at least the size of Vesta is necessary. An EPB source with an Mg# intermediate between that of Eu1 and Eu3 is also required for a parent body that would generate these two compositions as primary magmas by partial melting. The Mg# estimated using exchange $K_D^{Fe\text{-}Mg_s}$ ($FeO_{xtl}MgO_{liq}/MgO_{xtl}FeO_{liq}$) for olivine and pigeonite obtained from the 1 kbar experiments is approximately 0.75. The batch melting equation used to construct the partial melting curves in Figure 2-6 predicts that Kapoeta rho would be formed by 10 % and Yamato by 24 % (by weight) partial melting of such a source. If this were the case, the projected position of Kapoeta should lie very near the five-phase olivine - low-Ca pyroxene - plagioclase - spinel boundary in Figure 2-7. This is not the case. Kapoeta plots on the 1 kbar olivine - pigeonite - spinel boundary. The Yamato composition is produced by much higher amounts of melting and it should

plot along the 1 kbar olivine - pigeonite - spinel boundary. Therefore, objections may be raised against either Kapoeta or Yamato as primary magmas obtained by melting at pressure within the EPB. However, the existence of magnesian pyroxene and olivine indicate the presence of a group of more primitive eucrite magmas, and Kapoeta and Yamato may be the closest approximations to these compositions that are currently available in the meteorite collection.

Warren et al. (1990) and Jones (1987) have addressed the question of whether or not Kapoeta rho and Yamato 7308 PE1 are representative of liquid compositions. The presence of some relatively iron-rich cumulate pyroxene phenocrysts in Kapoeta, the relatively coarse texture of Yamato and the relatively high TiO_2 contents of the pyroxenes from both clasts indicate that these compositions might not represent uncontaminated melt compositions. The projected position of Kapoeta with respect to the 1 kbar boundaries on Figure 2-7 is consistent with the accumulation of pyroxene in the Kapoeta melt. However, Pomozdino (Warren et al., 1990) has textures representative of quenched liquid and is similar in Mg# and TiO_2 content to Kapoeta, thus requiring a similar higher-$Mg^{\#}$ source and suggesting the presence of primary magnesian eucrite liquid compositions. The average matrix composition for Pomozdino given by Warren et al. (1990) is located directly on the 1 atm five-phase boundary and could be a shallow-level partial melt of such a source. A parent body with an even higher Mg# (=80) (Warren and Jerde, 1987) is required to produce the most Mg-rich pyroxene and olivine in howardites. The partial melting path of Eu3 (Dreibus et al., 1977) is shown in Figure 2-6 and the composition of a 10 wt.% batch melt produced at plagioclase exhaustion is listed in Table 2-7. Partial melts produced along the dotted

portion of the Eu3 curve could be the primary magmas responsible for producing the diogenites and main group eucrites.

Other eucrite compositions have been proposed to be small degree partial melts of the EPB. The clustering of main group eucrites at the 1 atm olivine - low-Ca pyroxene - plagioclase - spinel - liquid - boundary (Figure 2-7) is one line of evidence supporting the model wherein these eucrites are produced by partial melting of a source similar to Eu1. Stolper (1977) pointed out that liquid compositions that cluster at a reaction boundary are most readily explained by partial melting. The main group eucrite cluster extends toward the 1 kbar five-phase boundary, suggesting higher pressure partial melting may also play a role in eucrite petrogenesis. Partial melts will remain at the reaction boundary until all the plagioclase is exhausted, and should show trace element evidence for the presence of plagioclase in the source residue. The REE patterns of Juvinas and Sioux County, which plot near the 1 atm five-phase boundary, are fairly flat, indicating that shallow-level partial melting of a Eu1 type source proceeded until plagioclase was just exhausted (Consolmagno and Drake, 1977) from the source. The REE pattern of Stannern which also plots near the 1 atm five-phase boundary, contains a negative Eu anomaly, indicating that plagioclase was retained in the source. Stolper (1977) estimates that Sioux County forms by 15-20 % partial melting and that Stannern forms by 5-10 % with plagioclase remaining in source. Eucrites such as Bereba and Cachari (Figure 2-7) could have formed by partial melting at deeper levels in the EPB. For example, Bereba, which also has a flat REE pattern (Consolmagno and Drake, 1977), could have been formed by partial melting in which plagioclase was just exhausted at about 500 bars.

Fractional crystallization

The presumed small size of the EPB has been one of the objections to the fractional crystallization model wherein main group eucrites and diogenites are related to more magnesian eucritic parent magmas through the cotectic precipitation of pyroxene and minor olivine. The change in the olivine - low-Ca pyroxene boundary from a reaction relation to a cotectic was estimated to occur at a pressure of 2 kbar or more (Longhi and Pan, 1988a). The results of the experiments reported in this chapter indicate that this change occurs at 1 kbar, which is the maximum pressure attained in a Vesta-sized parent body. Hence, the experimental results reported here provide permissive evidence for the generation of diogenite cumulates from magnesian eucrite parent magmas. If diogenites were formed by a static high pressure fractional crystallization process, a parent body larger in size than Vesta would be required. However, polybaric fractional crystallization of a magnesian eucrite parent magma, generated by partial melting at depth, during ascent from its source region could also generate diogenite cumulates. The 1 kbar olivine - low-Ca pyroxene boundary lies at low normative SiO_2. If a magnesian parent magma experienced fractionation upon ascent to the surface, the differentiated liquid is always just saturated with low-Ca pyroxene (producing diogenite cumulates), and approaches the 1 atm olivine - low-Ca pyroxene - plagioclase - spinel - liquid boundary as it rises and crystallizes.

Both Kapoeta and Yamato compositions have been proposed to be parental magmas for their respective trends (Ikeda and Takeda, 1985; Dymek et al., 1976; Hewins and Newsom, 1988) and are possible examples of magnesian eucrite magmas responsible for producing the diogenites as cumulates. The crystallization models of Hewins and Newsom (1988) reproduced Trend B from Kapoeta rho and Trend A from Y 7308 PE1 via the crystallization of pyroxene

(plus minor olivine) followed by pyroxene plus plagioclase. The experimental results reported in this chapter permit the fractionation models proposed by Hewins and Newsom (1988) and the crystallization sequence calculated by Hewins and Newsom is consistent with the 1-kbar results. Figure 2-6 shows crystallization paths calculated from the experimental data that also permit the derivation more Fe-rich eucrites from the incompatible element-poor (Yamato) and incompatible element-rich (Kapoeta) eucrite parent magmas.

Igneous activity in the eucrite parent body

Figure 2-8 illustrates magmatic processes that could relate diogenites, cumulate eucrites, magnesian eucrite clasts and the more evolved eucrites in a Vesta-sized parent body. Figure 2-8A is an enlarged portion of the Olivine - Anorthite - SiO_2 diagram used throughout this paper. The experimentally determined phase boundaries at 1 atm and 1 kbar, as well as an interpolated 500 bar boundary, are shown schematically on this diagram. Also shown is a cross section of a potential parent body with a minimum radius of 270 km and an assumed composition similar to Eu3 (Figure 2-8B). Point A on Figure 2-8A and Figure 2-8B represents a 25% partial melt at 0.9 kbar and is similar to, but more Mg-rich than, the magnesian eucrite clast Y 7308 PE1. A melt of this composition lies on the olivine - low-Ca pyroxene boundary at 0.9 kbar and will coprecipitate olivine and low-Ca pyroxene as it crystallizes at depth (not shown in figure). If this melt underwent fractional crystallization at 1 kbar, it could also produce eucrites with compositions like Cachari and Bereba. If the melt rises from its source region to the surface (path A-B-C in Figure 2-8) and experiences polybaric fractionation, olivine and low-Ca pyroxene cocrystallize in a cotectic-like relation. Such a polybaric fractionation process produces residual liquids with the composition of the main group eucrites (point C in Figure 2-8) after 18 to 22 % fractionation of pyroxene and olivine +/- Cr-

spinel. Fractionation along this polybaric path produces low-Ca pyroxenes (En_{88-65}) and olivines (Fo_{92-64}) of the compositions found in diogenite cumulates (Hewins, 1987).

If the fractionating liquid is arrested at an intermediate level within the EPB, for example at a depth of 130 km at a pressure of 500 bars, it will leave the olivine - low-Ca pyroxene boundary, which is a reaction boundary at this lower pressure, and precipitate only pyroxene, as indicated by path D in Figure 2-8A. After fractionation of 20% magnesian low-Ca pyroxene, the liquid reaches the pyroxene - plagioclase boundary and precipitates these phases in a cotectic relation. The pyroxene compositions produced during an additional 20 % fractionation along this boundary, En_{63-50}, fall within the range of pyroxenes in cumulate eucrites. The residual liquids from this process are more evolved and iron-rich than the eucrites; examples of these late stage fractionation products may be the fayalitic lithologies found in polymict eucrites (Delaney et al., 1984).

The phase equilibria provide constraints which lend support to the serial magmatism model of Hewins (1987) and Hewins and Newsom (1988), as well as the cumulate eucrite argument of Stolper (1977). Serial magmatism is more likely than the magma ocean model of Ikeda and Takeda (1985) because of the existence of two main fractionation trends with different incompatible element (IE) contents. Ten to 25 % partial melting of a magnesian chondritic source (Mg# 80) would produce the magnesian eucrite parent magmas of these trends (Dreibus and Wänke, 1980). The differences in IE content could be produced by different degrees of partial melting of the same source. Alternatively, IE poor parent magmas could be the sole primary magmas, forming the primitive IE rich liquids by magma mixing of these primary magmas with their enriched derivatives (Hewins, 1987).

Polybaric fractionation of predominantly pyroxene plus lesser olivine (path A-B-C, Figure 2-8A) from these parents during magma ascent produces the diogenite cumulates and residual liquids with the compositions of the main group eucrites (Hewins and Newsom, 1988). Thereafter, a small amount of pyroxene plus plagioclase fractionation produced the more evolved eucrites of the Nuevo Laredo trend (Stolper, 1977; Basaltic Volcanism Study Project, 1981; Warren and Jerde, 1987). Some eucrites (Sioux County, Stannern, Bouvante) could be formed by low pressure partial melting of a more iron-rich source (Stolper, 1977; Consolmagno and Drake, 1977; Christophe Michel-Lévy et al., 1987) in a heterogeneous parent body. The coincidence of the main group eucrite trend with the 1 atm olivine - low-Ca pyroxene - plagioclase - spinel - liquid reaction boundary is strong evidence for a low pressure partial melting origin for the main group eucrites, despite the fact that mass balance constraints and incompatible element contents can be explained by fractionation processes involving magnesian parents (Warren, 1985; Warren and Jerde, 1987).

While the magnesian eucrite parents could produce the diogenites as cumulates and the eucrite lavas as residual liquids through a polybaric fractionation process, the cumulate eucrites must be produced via a different path, perhaps in "constant pressure" plutonic environments within the EPB. After a small amount of olivine plus pyroxene fractionation from the parental magnesian eucrite magma during its ascent, the magma may become arrested at an intermediate level within the EPB. Since the olivine - low-Ca pyroxene boundary becomes a reaction boundary at about 0.9 kbar, liquids originally produced along this boundary will precipitate only pyroxene at lower pressures. Crystallization of pyroxene alone moves the residual liquid through the pyroxene primary phase volume until the pyroxene - plagioclase boundary

is reached. Thereafter, precipitation of pyroxene and plagioclase along this cotectic-like boundary produces cumulate minerals of the right compositions to form the cumulate eucrites. The residual liquids from this process are very iron-rich (Mg# 0.20) and do not resemble main group eucritic lavas; perhaps these liquids remained and crystallized at high levels in the intrusion (Stolper, 1977; Basaltic Volcanism Study Project, 1981). Fayalitic and ferrohedenbergitic lithologies in howardites and polymict eucrites may be examples of these late stage fractionation products (Dymek et al., 1976; Delaney et al., 1984).

CONCLUSIONS

This experimental study provides phase equilibria at elevated pressures relevant for melting and crystallization processes in the eucrite parent body. These phase relations constrain the fractional crystallization and partial melting processes that can occur over the pressure range of 1 kbar to 1 atm. The results of the experiments show the following:

1) Diogenites and pyroxene-rich clasts in howardites can form by fractional crystallization from magnesian eucrite parent compositions originating as partial melts at depth within a parent body the size of the asteroid Vesta or larger with a composition similar to that of Dreibus et al. (1977).

2) The most likely path that led from these parent magmas to the differentiated eucrites involved polybaric fractionation of predominantly low-Ca pyroxene plus olivine and spinel.

3) Cumulate eucrites are likely produced from similar parent magmas by fractionation in plutonic environments within the parent body, with the production of very iron-rich (Mg# 20) residual liquids.

REFERENCES FOR CHAPTER TWO

Albee A. L. and Ray L. (1970) Correction factors for electron microprobe microanalysis of silicates, oxides, carbonates, phosphates and sulfates. *Anal. Chem., 42,* 1408-1414.

Basaltic Volcanism Study Project (1981) *Basaltic Volcanism on the Terrestrial Planets.* Pergamon Press, New York.

Beckett J.R. and Stolper E. (1987) Constraints on the origin of eucrite melts: An experimental study (abstract). In: *Lunar and Planetary Science XVIII,* pp. 54-55. Lunar and Planetary Institute, Houston.

Bence A. E. and Albee A. L. (1968) Empirical correction factors for the electron microanalysis of silicates and oxides. *J. Geol., 76,* 382-403.

Christophe Michel-Lévy M., Bourot-Denise M., Palme H., Spettel B. and Wänke H. (1987) L'eucrite de Bouvante chimie, petrologie et mineralogie. *Bull. Soc. Fr. Mineral. Crist.,* 110, 449-458.

Consolmagno G. C. and Drake M. J. (1977) Composition and evolution of the eucrite parent body: evidence from the rare earth elements. *Geochim. Cosmochim. Acta, 41,* 1271-1282.

Delaney J.S., Prinz M., Nehru C.E. and Harlow G.E. (1981) A new basalt group from howardites: Mineral chemistry and relationships with basaltic achondrites

(abstract). In: *Lunar and Planetary Science XII*, pp. 211-213. Lunar and Planetary Institute, Houston.

Delaney J. S., Prinz M. and Takeda H. (1984) The polymict eucrites. *Proc. Lunar Planet. Sci. Conf. 15th*, in *J. Geophys. Res., 89*, C251-C288.

Dreibus G. and Wänke H. (1980) The bulk composition of the eucrite parent asteroid and its bearing on planetary evolution. *Z. Naturforsch, 35a*, 204-216.

Dreibus G., Kruse H., Spettel B. and Wänke H. (1977) The bulk composition of the moon and the eucrite parent body. *Proc. Lunar Planet. Sci. Conf. 8th*, pp. 211-227.

Dymek R. F., Albee A. L., Chodos A. A. and Wasserburg G. J. (1976) Petrography of isotopically dated clasts in the Kapoeta howardite and petrologic constraints on the evolution of its parent body. *Geochim. Cosmochim. Acta, 40*, 1115-1130.

Gaffey M. J. (1983) The asteroid (4) Vesta: Rotational spectral variations, surface material heterogeneity and implications for the origin of basaltic achondrites (abstract). In: *Lunar and Planetary Science XIV*, pp. 231-232. Lunar and Planetary Institute, Houston.

Grove T. L. (1981) Use of Fe/Pt alloys to eliminate the iron loss problem in 1-atm gas mixing experiments: theoretical and practical considerations. *Contrib. Mineral. Petrol., 78*, 298-304.

Grove T. L. and Bence A. E. (1977) Experimental study of pyroxene-liquid interaction in quartz-normative basalt 15597. *Proc. Lunar Sci. Conf. 8th*, pp. 1549-1579.

Grove T.L., Gerlach D.C., Sando T.W. and Baker M.B. (1983) Origin of calc-alkaline series lavas at Medicine Lake volcano by fractionation, assimilation and mixing: corrections and clarifications. *Contrib. Mineral. Petrol., 82*, 407-408.

Grove T.L. and Juster T. C. (1989) Experimental investigations of low-Ca pyroxene stability and olivine - pyroxene - liquid equilibria at 1-atm in natural basaltic and andesitic liquids. *Contrib. Mineral. Petrol., 103*, 287-305.

Hewins R. H. (1987) The Howardite parent body: Composition and crystallization models (abstract). In: *Lunar and Planetary Science XVIII*, pp. 417-418. Lunar and Planetary Institute, Houston.

Hewins R. H. and Newsom H. E. (1988) Igneous activity in the early solar system. In: *Meteorites and the Early Solar System* (Kerridge J.F. and Matthews M.S., eds.), pp. 73-101. University of Arizona Press, Tuscon.

Ikeda Y. and Takeda H. (1985) A model for the origin of basaltic achondrites based on the Yamato 7308 howardite. *J. Geophys. Res., 90*, C649-C663.

Jones J.H. (1987) An evaluation of proposed parental eucritic magmas (abstract). *Meteoritics, 22*, p. 95.

Juster T.C., Grove T.L. and Perfit M.R. (1989) Experimental constraints on the generation of FeTi basalts, andesites and rhyodacites at the Galapagos Spreading Center, 85°W and 95°W. *J. Geophys. Res., 94,* 9251-9274.

Larson H. and Fink U. (1975) Infrared spectral observations of Asteroid 4 Vesta. *Icarus, 26,* 420-427.

Longhi J. and Pan V. (1987) Olivine/low-Ca pyroxene liquidus relations and their bearing on eucrite petrogenesis (abstract). In: *Lunar and Planetary Science XVIII,* pp. 570-571. Lunar and Planetary Institute, Houston.

Longhi J. and Pan V. (1988a) Phase equilibrium constraints on the Howardite-Eucrite-Diogenite association. *Proc. Lunar Planet. Sci. Conf. 18th,* pp.459-470.

Longhi J. and Pan V (1988b) A reconnaissance study of phase boundaries in low-alkali basaltic liquids. *J. Petrol. 29,*115-147.

McCord T. B., Adams J. B. and Johnson T. V. (1970) Asteroid Vesta: spectral reflectivity and compositional implications. *Science, 168,* 1445-1447.

Mason B. (1962) *Meteorites.* Wiley, New York.

Mason B., Jaresowich E. and Nelen J.A. (1979) The pyroxene-plagioclase achondrites. *Smithsonian Contrib. Earth Sci., 22,* 27-45.

Morgan J.W., Higuchi H., Takahashi H. and Hertogen J. (1987) A "chondritic" eucrite parent body: inference from trace elements. *Geochim. Cosmochim. Acta, 42,* 27-38.

Morrison, D. (1976) The densities and bulk compositions of Ceres and Vesta. *Geophys. Res. Lett., 3,* 701-704.

Presnall D.C., Dixon J.R., O'Donnell T.H. and Dixon S.A. (1979) Generation of mid-ocean ridge basalts. *J. Petrol., 20,* 3-35.

Sen G. and Presnall D.C. (1984) Liquidus phase relationships on the join anorthite-forsterite-quartz at 10 kbar with applications to basalt petrogenesis. *Contrib. Mineral. Petrol., 85,* 404-408.

Stolper E. (1977) Experimental petrology of eucritic meteorites. *Geochim. Cosmochim. Acta, 41,* 587-611.

Warren P. H. (1985) Origin of howardites, diogenites and eucrites: A mass balance constraint. *Geochim. Cosmochim. Acta, 49,* 577-586.

Warren P. H. and Jerde E. A. (1987) Composition and origin of Nuevo Laredo Trend eucrites. *Geochim. Cosmochim. Acta, 51,* 713-725.

Warren P. H. and Wasson J. T. (1979) Effects of pressure on the crystallization of a "chondritic" magma ocean and implications for the bulk composition of the moon. *Proc. Lunar Planet. Sci. Conf. 10th,* pp.2051-2083.

Warren P.H., Jerde E.A., Migdisova L.F. and Yaroshevsky A.A. (1990) Pomozdino: An anomalous, high-MgO/FeO, yet REE-rich eucrite. *Proc. Lunar Planet. Sci. Conf. 20th*, pp. 281-297.

Williams D. W. (1968) Improved cold seal pressure vessels to operate to 1100°C at 3 kilobars. *Amer. Mineral., 53*, 1765-1769.

Table 2-1. Compositions of starting materials (wt.%).

	Kapoeta clast rho[1]	Synthetic analog K[2]	Yamato 7308 PE clast 1[3]	Synthetic analog Y[2]
SiO_2	49.5	49.4(2)	48.4	48.9(2)
TiO_2	0.78	0.74(2)	0.44	0.39(4)
Al_2O_3	9.88	9.91(7)	10.5	10.5(1)
Cr_2O_3	0.90	0.92(3)	0.49	0.50(3)
FeO	18.8	19.5(2)	19.3	20.1(2)
MgO	10.1	10.4(1)	11.4	11.7(1)
MnO	0.54	0.51(3)	n.d.	n.d.
CaO	9.34	9.15(6)	8.52	8.41(9)
K_2O	n.d	n.d.	0.03	0.02(1)
Na_2O	0.47	0.46	0.35	0.29(3)
Total	100.31	100.99	99.43	100.81
Mg#[4]	49	49	51	51
CaO/Al_2O_3	0.95	0.92	0.81	0.80

1. Dymek et al. (1976).

2. Microprobe analyses of fused glasses.

3. Ikeda and Takeda (1985).

4. Molar Mg/[Mg+Fe]

n.d. Oxide not determined and therefore excluded from synthetic analog.

Table 2-2A. Run conditions and phase appearance sequence for Kapoeta Series.

Run	T (°C)	P(bar)	Buffer[1]	Cont.[2]	Hours	Phases[3]	Mg# gl
KR18	1210	1	IW	a	12	gl + sp + ol + pig	0.44
KR17	1196	1	none	a	23.5	gl + sp + ol + pig	0.42
KR15	1180	1	IQF	a	42	gl + sp + ol + pig	0.38
KR19	1165	1	IQF	a		gl + sp + ol + pig	0.38
KR10	1150	1	IQF	a	70	gl + sp + ol + pig + plg	0.35
KR11	1150	1	IQF	a	81	gl + sp + ol + pig + plg	0.37
KH22	1213	1005	IW	b	8	gl + sp + ol + pig	0.40
KH8	1177	1025	IQF	b	9.3	gl + sp + ol + pig	0.35
KH7	1167	1005	IQF	b	9	gl + sp + ol + pig	0.36
KH13	1164	995	IQF	b	15	gl + sp + ol + pig + plg	0.33
KH16	1160	1005	IQF	b	16	gl + sp + ol + pig + plg	0.32
KH6	1157	1000	IQF	b	8	gl + sp + ol + pig + plg	0.35
KH11	1157	990	IQF	b	13	gl + sp + ol + pig + plg	0.34

1. IW = iron-wüstite, IQF = iron-quartz-fayalite, * = CO_2 - H_2 gas mixture.

2. Container descriptions: a) High purity iron capsules in evacuated silica glass tubes; b) High purity iron foil capsules in Pt capsules which were welded shut; c) Pt-Fe alloy wire loops.

3. Abbreviations: gl = glass, sp = spinel, ol = olivine, pig = pigeonite, plg = plagioclase.

Table 2-2B. Run conditions and phase appearance sequence for Yamato Series.

Run	T (°C)	P(bar)	Buffer[1]	Cont.[2]	Hours	Phases[3]	Mg# gl
Y7	1180	1	IW*	c	68	gl + sp + ol + pig	0.42
Y11	1170	1	IW*	c	72.5	gl + sp + ol + pig	0.42
Y6	1160	1	IW*	c	70	gl + sp + ol + pig + plg	0.38
Y2	1150	1	IW*	c	68.5	gl + sp + ol + pig + plg	0.37
Y5	1140	1	IW*	c	70	gl + sp + ol + pig + plg	0.31
YR15	1190	1	none	a	44	gl + sp + ol + pig	0.42
YR4	1170	1	IQF	a	70	gl + sp + ol + pig	0.38
YR3	1160	1	IQF	a	97.5	gl + sp + ol + pig	0.36
YR10	1150	1	IQF	a	70	gl + sp + ol + pig + plg	0.34
YR11	1150	1	IQF	a	81	gl + sp + ol + pig + plg	0.35
YR1	1140	1	IQF	a	89	gl + sp + ol + pig + plg	0.33
YH3	1167	1000	IQF	b	9	gl + sp + ol + pig + plg	0.35
YH2	1157	1005	IQF	b	9	gl + sp + ol + pig + plg	0.31

1. IW = iron-wüstite, IQF = iron-quartz-fayalite, * = CO_2 - H_2 gas mixture.

2. Container descriptions: a) High purity iron capsules in evacuated silica glass tubes; b) High purity iron foil capsules in Pt capsules which were welded shut; c) Pt-Fe alloy wire loops.

3. Abbreviations: gl = glass, sp = spinel, ol = olivine, pig = pigeonite, plg = plagioclase.

Table 2-3A. Microprobe analyses of run products from Kapoeta Series experiments.

Run	phase[1]	no.[2]	SiO_2[3]	TiO_2	Al_2O_3	Cr_2O_3	FeO	MgO	MnO	CaO	Na_2O	Total
KR10	gl	10	48.9(1)	0.88(3)	12.1(1)	0.27(3)	19.0(4)	5.83(32)	0.45(4)	10.9(2)	0.59(6)	98.9
KR10	ol	6	36.3(5)	----	0.11(20)	0.61(62)	33.6(11)	29.7(6)	0.68(3)	0.42(3)	n.d.	101.4
KR10	pig	7	53.0(4)	0.18(4)	1.19(31)	0.77(7)	19.1(3)	22.3(7)	0.65(4)	4.03(61)	----	101.2
KR10	pl	5	45.7(3)	n.d.	32.9(11)	n.d.	1.27(35)	0.46(24)	n.d.	18.4(3)	0.78(6)	99.5
KR10	sp	1	0.76	1.59	19.0	44.5	27.4	6.59	0.45	0.42	n.d.	100.7
KR11	gl	17	49.0(2)	0.86(3)	12.1(1)	0.28(2)	19.1(3)	6.17(10)	0.50(2)	10.9(1)	0.46(4)	99.4
KR11	ol	5	36.4(4)	0.03(2)	0.09(9)	0.71(61)	32.9(1)	29.9(2)	0.65(6)	0.50(6)	n.d.	101.2
KR11	pig	10	53.2(2)	0.16(4)	1.21(27)	0.81(11)	18.9(3)	22.2(4)	0.67(3)	3.97(53)	----	101.1
KR11	pl	7	45.8(3)	n.d.	33.7(3)	n.d.	0.92(11)	0.28(3)	n.d.	18.3(2)	0.78(9)	99.8
KR11	sp	1	0.45	1.51	18.1	45.6	27.2	5.91	0.48	0.38	n.d.	99.6
KR15	gl	15	49.4(2)	0.81(2)	10.7(1)	0.43(3)	20.7(4)	7.02(31)	0.50(4)	9.97(12)	0.49(5)	100.0
KR15	ol	9	36.2(2)	----	0.05(2)	0.50(4)	32.1(4)	31.3(5)	0.60(2)	0.38(2)	n.d.	101.1
KR15	pig	11	53.6(3)	0.14(4)	0.99(18)	0.85(8)	17.8(3)	23.5(6)	0.62(3)	3.21(68)	----	100.7
KR15	sp	3	0.77(66)	1.41(20)	16.6(2)	47.4(6)	27.1(3)	6.25(14)	0.42(3)	0.33(14)	n.d.	100.3
KR17	gl	15	49.7(2)	0.82(2)	10.7(1)	0.53(2)	19.6(2)	7.90(14)	0.54(4)	9.96(11)	0.47(5)	100.2
KR17	ol	9	36.8(2)	----	0.05(1)	0.57(2)	28.8(1)	33.5(4)	0.60(3)	0.37(2)	n.d.	100.7

Table 2-3A, continued (p. 2 of 3).

Run	phase[1]	no.[2]	SiO_2[3]	TiO_2	Al_2O_3	Cr_2O_3	FeO	MgO	MnO	CaO	Na_2O	Total
KR17	pig	9	53.8(3)	0.12(3)	0.99(13)	0.94(10)	17.1(3)	24.0(6)	0.61(3)	2.94(50)	----	100.5
KR18	gl	23	50.2(1)	0.77(3)	10.4(1)	0.59(2)	19.3(2)	8.67(7)	0.53(4)	9.74(9)	0.51(4)	100.7
KR19	gl	9	49.4(2)	0.85(3)	11.8(1)	0.36(2)	19.3(5)	6.75(15)	0.48(4)	10.7(1)	0.47(5)	100.1
KH6	gl	4	47.9(1)	0.91(2)	12.0(0)	0.28(2)	20.0(2)	6.15(7)	0.52(3)	10.9(1)	0.61(2)	99.3
KH6	ol	6	35.9(2)	0.03(1)	0.05(1)	0.39(4)	33.7(5)	29.8(2)	0.68(5)	0.46(3)	n.d.	101.0
KH6	pig	10	52.8(2)	0.23(4)	1.51(32)	0.75(11)	19.4(6)	21.0(4)	0.67(6)	4.72(54)	----	101.1
KH7	gl	8	48.2(4)	0.86(3)	11.5(1)	0.36(1)	21.2(6)	6.62(13)	0.53(3)	10.5(0)	0.59(3)	100.4
KH7	ol	6	36.5(1)	----	0.06(1)	0.39(2)	32.1(1)	31.2(2)	0.65(6)	0.43(2)	n.d.	101.3
KH7	pig	7	53.6(4)	0.15(3)	1.31(28)	0.81(14)	18.5(1)	22.3(4)	0.66(4)	3.64(46)	----	101.0
KH7	sp	1	0.45	1.35	19.2	44.8	26.6	6.92	0.40	0.34	n.d.	100.1
KH8	gl	8	47.8(2)	0.82(3)	10.9(1)	0.39(2)	21.7(2)	6.66(7)	0.55(3)	10.2(1)	0.53(2)	99.6
KH8	ol	5	36.1(2)	----	0.04(1)	0.42(3)	32.8(3)	29.9(3)	0.63(3)	0.40(1)	n.d.	100.3
KH8	pig	9	53.5(3)	0.15(2)	1.21(12)	0.82(10)	18.8(2)	22.4(6)	0.69(19)	3.45(76)	----	101.0
KH8	sp	1	0.22	1.30	18.1	46.7	26.1	6.45	0.45	0.32	n.d.	99.6
KH11	gl	20	47.7(3)	0.89(2)	11.9(1)	0.28(3)	21.3(2)	6.14(8)	0.53(5)	10.7(7)	0.57(5)	100.0
KH11	ol	3	35.8(2)	----	0.03(1)	0.33(4)	34.6(1)	29.1(4)	0.67(2)	0.41(1)	n.d.	101.0

Table 2-3A, continued (p. 3 of 3).

Run	phase[1]	no.[2]	SiO_2[3]	TiO_2	Al_2O_3	Cr_2O_3	FeO	MgO	MnO	CaO	Na_2O	Total
KH11	pig	9	53.1(3)	0.17(3)	1.35(3)	0.75(11)	19.4(2)	21.8(7)	0.65(3)	4.10(49)	----	101.3
KH11	sp	1	0.50	2.59	21.3	40.9	28.3	6.54	0.45	0.25	n.d.	100.8
KH13	gl	10	47.8(2)	0.96(3)	11.9(1)	0.29(1)	21.3(2)	5.89(4)	0.52(4)	10.7(0)	0.57(5)	99.9
KH13	ol	7	35.8(3)	0.02(1)	0.07(1)	0.33(2)	35.8(1)	27.9(.3)	0.69(4)	0.46(1)	n.d.	101.1
KH13	pig	7	52.9(5)	0.15(4)	1.33(34)	0.79(12)	19.6(5)	21.0(4)	0.61(2)	4.40(49)	----	100.8
KH13	pl	1	49.5	n.d.	29.6	n.d.	2.94	1.06	n.d.	15.5	1.78	100.4
KH13	sp	1	1.52	1.69	21.4	40.1	28.1	6.01	0.43	0.49	n.d.	99.7
KH16	gl	10	47.7(3)	0.94(3)	12.0(1)	0.27(2)	21.4(2)	5.75(4)	0.52(4)	10.6(1)	0.59(5)	99.8
KH16	ol	6	35.8(3)	0.02(1)	0.07(1)	0.33(3)	36.1(3)	27.6(3)	0.69(3)	0.46(4)	n.d.	101.1
KH16	pig	6	53.0(6)	0.20(4)	1.29(37)	0.76(13)	19.3(3)	21.2(9)	0.64(3)	4.48(94)	----	100.9
KH16	pl	5	46.3(2)	n.d.	31.9(8)	n.d.	1.61(36)	0.54(15)	n.d.	17.6(2)	0.91(7)	98.9
KH16	sp	1	0.07	2.44	18.7	43.4	28.6	6.12	0.51	0.40	n.d.	100.2
KH22	gl	4	47.7(1)	0.76(1)	10.1(1)	0.53(2)	21.4(2)	8.13(4)	0.48(2)	9.24(9)	0.45(4)	98.79

1. Phase abbreviations: gl = glass, ol = olivine, pig = pigeonite, pl = plagioclase, sp = spinel.
2. Number of microprobe analyses.
3. Oxides are reported in weight percent. Numbers in parentheses are 1 standard deviation of the mean in terms of least units reported. Thus 47.9(2) indicates 47.9 +/- 0.2.

n.d. indicates oxide not determined; dashes (----) indicate oxide analyzed but below detectability limits.

Table 2-3B. Microprobe analyses of run products from Yamato Series experiments.

Run	phase[1]	no.[2]	SiO_2[3]	TiO_2	Al_2O_3	Cr_2O_3	FeO	MgO	CaO	K_2O	Na_2O	Total
Y2	gl	5	49.3(1)	0.66(2)	12.5(3)	0.14(2)	19.2(3)	6.30(6)	10.4(1)	0.05(2)	0.43(6)	99.0
Y5	gl	7	48.7(2)	0.78(4)	11.8(1)	0.19(2)	21.6(3)	5.55(6)	10.2(2)	0.05(1)	0.37(7)	99.2
Y6	gl	7	49.6(2)	0.54(3)	12.9(1)	0.21(2)	19.2(3)	6.48(7)	10.2(1)	0.06(1)	0.38(7)	99.6
Y7	gl	7	50.1(2)	0.48(2)	12.6(1)	0.26(2)	18.3(3)	7.51(8)	9.85(13)	0.04(2)	0.34(5)	99.5
Y11	gl	11	50.7(2)	0.51(2)	13.0(1)	0.30(2)	18.4(3)	7.31(8)	10.0(2)	0.07(1)	0.38(6)	100.7
YR1	gl	7	48.5(2)	0.74(3)	12.0(1)	0.26(2)	21.0(2)	5.73(9)	10.3(1)	0.04(3)	0.36(2)	98.9
YR1	ol	4	35.4(2)	----	0.04(1)	0.33(6)	37.0(3)	27.4(0)	0.46(3)	n.d.	n.d.	100.6
YR1	pig	10	52.5(3)	0.11(2)	1.19(1)	0.68(4)	21.7(2)	21.4(1)	2.89(12)	n.d.	----	100.5
YR1	pl	4	45.5(3)	n.d.	33.1(7)	n.d.	1.34(48)	0.34(11)	18.6(3)	----	0.59(12)	99.5
YR1	sp	4	0.40(16)	0.97(5)	19.6(5)	44.0(2)	28.8(5)	5.72(5)	0.31(8)	n.d.	n.d.	99.8
YR3	gl	17	49.2(2)	0.51(8)	12.8(5)	0.29(3)	19.7(3)	6.24(40)	10.3(5)	0.03(1)	0.34(2)	99.4
YR4	gl	32	49.6(4)	0.50(5)	12.3(3)	0.35(4)	20.0(3)	6.76(43)	9.92(38)	----	0.31(2)	99.8
YR10	gl	10	49.0(3)	0.57(5)	12.6(1)	0.27(3)	20.4(3)	5.83(37)	10.6(2)	0.05(1)	0.33(3)	99.7
YR10	ol	4	36.4(1)	----	0.03(1)	0.34(1)	34.5(1)	29.7(1)	0.41(4)	n.d.	n.d.	101.4
YR10	pig	5	53.1(2)	0.15(2)	1.36(9)	0.74(4)	20.3(2)	22.6(2)	2.97(25)	n.d.	----	101.2
YR10	pl	5	45.3(1)	n.d.	34.0(2)	n.d.	0.99(8)	0.31(2)	18.9(2)	----	0.54(6)	100.1

Table 2-3B, continued (p. 2 of 2).

Run	phase[1]	no.[2]	SiO_2[3]	TiO_2	Al_2O_3	Cr_2O_3	FeO	MgO	CaO	K_2O	Na_2O	Total
YR10	sp	1	1.50	0.90	21.3	42.5	27.3	6.36	0.65	n.d.	n.d.	100.5
YR11	gl	14	49.0(2)	0.61(3)	12.4(1)	0.25(2)	20.3(2)	6.09(10)	10.4(1)	0.04(1)	0.34(3)	99.4
YR11	ol	6	36.2(1)	0.03(1)	0.03(1)	0.31(3)	35.2(2)	29.0(1)	0.43(1)	n.d.	n.d.	101.2
YR11	pig	10	53.0(5)	0.09(3)	1.28(25)	0.72(9)	20.6(3)	22.5(3)	2.75(19)	n.d.	----	100.9
YR11	pl	7	45.4(4)	n.d.	34.1(3)	n.d.	1.05(9)	0.29(3)	18.8(2)	----	0.53(4)	100.2
YR11	sp	1	1.14	0.88	21.8	43.0	27.9	6.33	0.42	n.d.	n.d.	101.5
YR15	gl	11	49.9(2)	0.47(2)	12.2(2)	0.44(2)	19.4(2)	7.75(23)	9.74(16)	0.04(1)	0.31(3)	100.3
YH2	gl	6	47.4(3)	0.59(3)	12.6(2)	0.22(2)	22.9(5)	5.80(17)	10.2(1)	----	0.34(4)	100.1
YH2	ol	3	35.4(3)	----	0.28(11)	0.29(3)	37.3(5)	27.7(6)	0.42(2)	n.d	n.d	101.4
YH2	pig	10	52.6(4)	0.13(3)	1.52(35)	0.63(10)	21.1(3)	21.6(6)	3.28(57)	n.d.	0.03(2)	101.0
YH2	pl	5	45.6(10)	n.d.	33.1(9)	n.d.	1.52(14)	0.49(20)	17.9(4)	0.02(1)	0.70(20)	99.3
YH3	gl	5	47.9(2)	0.55(2)	12.8(1)	0.25(2)	21.6(2)	6.38(24)	10.3(2)	0.02(1)	0.38(4)	100.2
YH3	ol	16	36.0(2)	----	0.13(5)	0.31(4)	34.3(3)	29.7(3)	0.39(2)	n.d.	n.d.	100.8
YH3	pig	15	52.7(4)	0.13(3)	1.71(43)	0.67(8)	20.4(4)	22.0(6)	3.24(48)	n.d.	----	100.9
YH3	pl	3	45.4(5)	n.d.	33.7(8)	n.d.	1.34(34)	0.42(16)	18.3(2)	----	0.59(8)	99.8
YH3	sp	1	1.13	0.66	26.8	38.2	27.1	6.85	0.39	n.d.	n.d.	101.1

1., 2., 3. See Table 1-3A for notes.

Table 2-4. Calculated phase proportions for eucrite experiments.

Run	gl	sp	ol	px	pl	ΣR^{2a}	ΔFeO^{b}	Model Mg#[c]
KR10	70	1	4	23	2	0.01	0.00	49
KR11	72	1	3	22	2	0.02	0.02	49
KR15	80	1	tr	19		1.65	2.31	47
KR17	87	1	3	9		0.24	1.12	48
KH6	65	1	tr	30	4	0.05	-0.05	49
KH11	62	1	tr	33	4	0.01	0.03	49
KH16	60	1	tr	34	6	0.01	0.02	49
KH13	60	1	tr	33	7	0.03	0.07	49
KH7	72	1	tr	27		1.10	2.09	47
KH8	71	1	tr	28		1.97	2.48	46
Y5	43	tr	7	36	14	0.01	0.01	51
Y2	62	1	10	21	6	0.01	-0.02	51
Y6	70	tr	10	16	3	0.04	0.07	51
Y7	83	tr	14	3		0.08	-0.57	51
YR1	48	tr	7	32	13	0.00	0.01	51
YR10	58	tr	9	26	8	0.02	-0.04	51
YR11	58	tr	9	25	8	0.00	0.02	51
YH2	48	tr	2	38	11	0.03	0.04	51
YH3	57	tr	3	32	7	0.01	0.03	51

a. Sum of squared residuals from mass balance calculations.

b. Relative percent difference in wt.% FeO between model calculated by mass balance and actual bulk composition.

c. Mg# for the model bulk composition calculated by mass balance.

Table 2-5. Stoichiometric coefficients (in wt.%) calculated for eucrite melting reactions.

	1 atm	1 kbar
5 Phase olivine - low-Ca pyroxene - plagioclase - spinel - liquid boundary		
Kapoeta	liq + 0.13 ol +/- tr sp = 0.84 px + 0.29 pl	liq = 0.05 ol + 0.60 px + 0.31 pl + 0.04 sp
Yamato	liq + 0.07 ol + 0.05 sp = 0.55 px + 0.57 pl	liq = tr ol + 0.39 px + 0.61 pl + tr sp
4-Phase olivine -low-Ca pyroxene - spinel -liquid boundary		
Kapoeta	liq + 0.23 ol = 1.11 px + 0.12 sp	liq + 0.11 sp = 0.03 ol + 1.00 px

Abbreviations: liq = liquid, ol = olivine, px = low-Ca pyroxene, pl = plagioclase, sp = Cr-spinel, tr = trace amounts.

Table 2-6. CIPW norms for glasses from 1 kbar eucrite experiments.

	KH22	KH8	KH7	KH13	KH16	KH6	KH11	YH3	YH2
Qz	-	-	-	0.25	0.13	0.55	-	0.26	-
Or	-	-	-	-	-	-	-	0.12	0.12
Ab	3.81	4.48	4.99	4.82	4.99	5.16	4.82	3.22	2.88
An	25.54	27.36	28.73	29.91	30.09	30.00	29.91	33.16	32.79
Di	6.42	6.43	6.55	6.02	5.71	6.70	6.17	4.89	4.38
He	10.75	13.36	13.33	13.77	13.52	13.79	13.59	10.39	10.86
En	17.04	13.56	13.36	11.88	11.68	12.21	12.11	13.63	12.40
Fs	32.75	32.30	31.18	31.17	31.71	28.86	30.59	33.23	35.26
Fo	0.17	0.03	0.07	-	-	-	0.22	-	0.01
Fa	0.36	0.09	0.18	-	-	-	0.62	-	0.03
Ilm	1.44	1.56	1.63	1.82	1.79	1.73	1.69	1.04	1.12

Table 2-7. Compositions of 10 % batch melts of eucrite parent body estimates Eu1 & Eu3.

	SiO_2	TiO_2	Al_2O_3	Cr_2O_3	FeO	MgO	MnO	CaO	Na_2O	Total	Mg#
Eu1M	48.6	0.81	12.2	0.29	18.8	7.07	0.53	11.1	0.62	100.0	40
Eu3M	49.8	0.80	12.5	0.30	13.8	10.3	0.54	11.3	0.64	99.98	57

FIGURES FOR CHAPTER TWO

Figure 2-1.

Summary of results of melting experiments at 1 atm and 1 kbar on Kapoeta and Yamato compositions (see Table 2-1). Symbols: squares = Yamato, circles = Kapoeta, solid symbols = assemblage consisting of oliv + pig + sp + plag + metal + liquid, open symbols = assemblage consisting of oliv + pig + sp + metal + liquid. Abbreviations: oliv = olivine, pig = pigeonite, sp = Cr-spinel, plag = plagioclase.

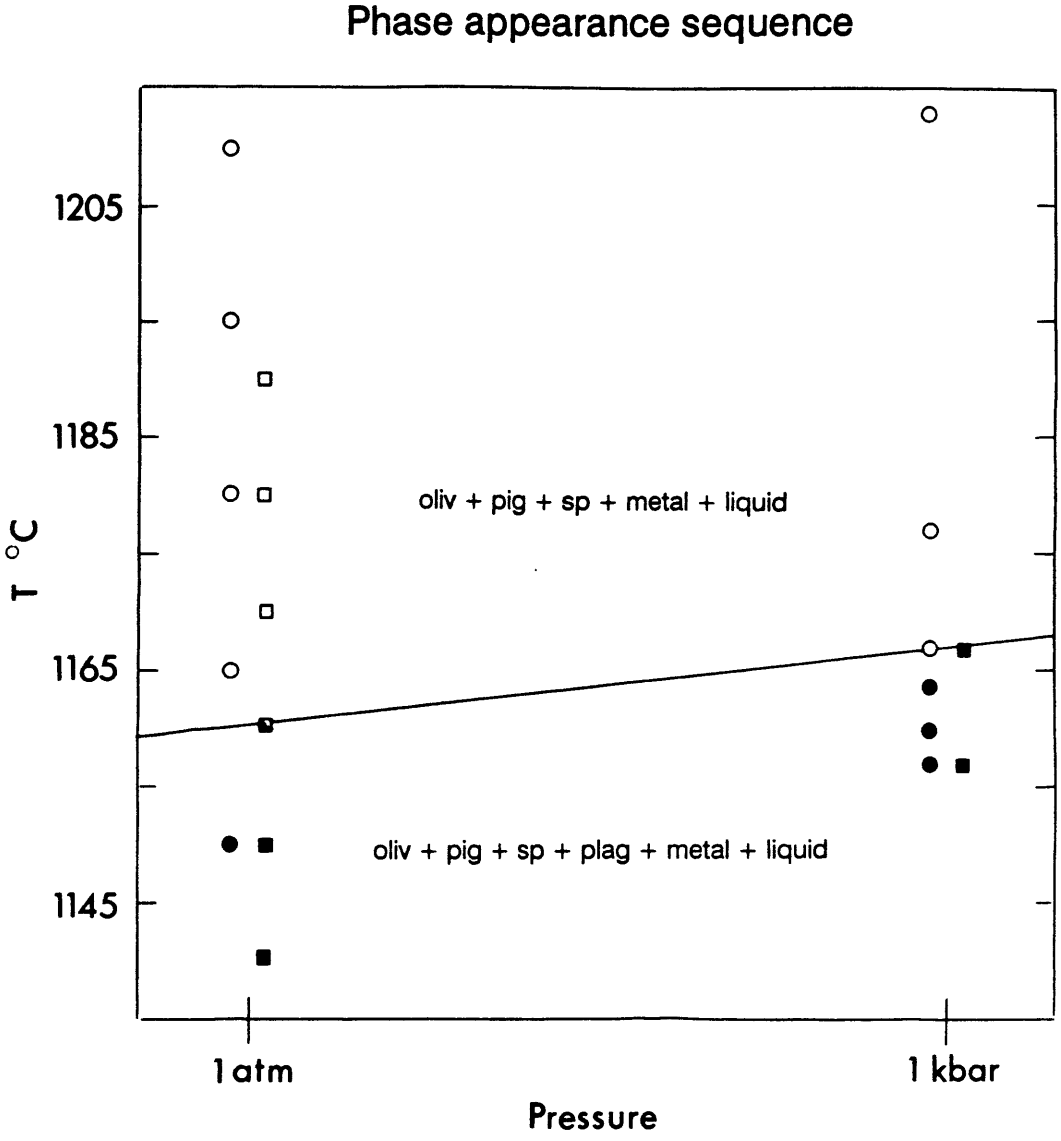
Phase appearance sequence
1205
1185
1165
1145
T °C
oliv + pig + sp + metal + liquid
oliv + pig + sp + plag + metal + liquid
1 atm
1 kbar
Pressure

Figure 2-2.

Results of melting experiments on Kapoeta and Yamato compositions at 1 atm and 1 kbar plotted in molar units on an enlarged portion of the Olivine (Oliv) - "Quartz" (Qtz) - Anorthite (An) pseudo-liquidus diagram. Projection scheme used is that of Stolper (1977). The ellipse indicates the 2 sigma error associated with replicate microprobe glass analyses. Squares (Yamato) and circles (Kapoeta) are projected positions of liquids from experiments listed in Table 2-2. Point A (open triangle) is Stolper's (1977) experimentally determined 1 atm olivine - low-Ca pyroxene - plagioclase - spinel - metal - liquid reaction boundary. Double arrows on boundary indicates a reaction boundary; a single arrow signifies a cotectic-type crystallization process.

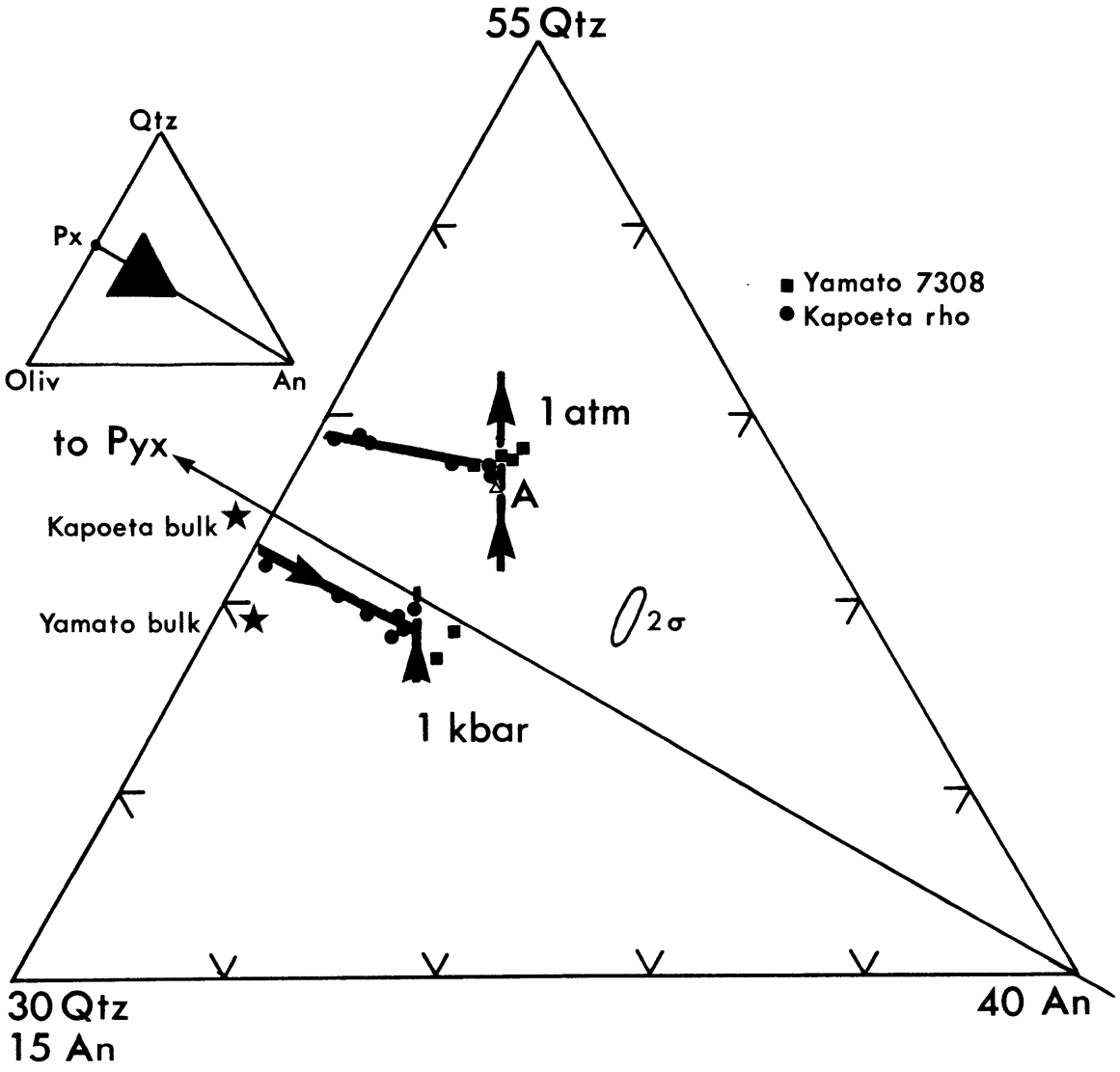
55 Qtz
Qtz
Px
Oliv
An
Yamato 7308
Kapoeta rho
1 atm
A
to Pyx
Kapoeta bulk
Yamato bulk
2σ
1 kbar
30 Qtz
15 An
40 An

Figure 2-3.

Backscattered electron images of experimental charges. The darkest gray crystals are pigeonite; the medium gray crystals are olivine; white areas are spinel and iron metal; background is glass. Both photographs cover 158 X 124 microns. A) KR17: Experiment conducted at 1 atm containing subhedral olivine crystals. B) KH16: Experiment conducted at 1 kbar containing euhedral olivine crystals.

A

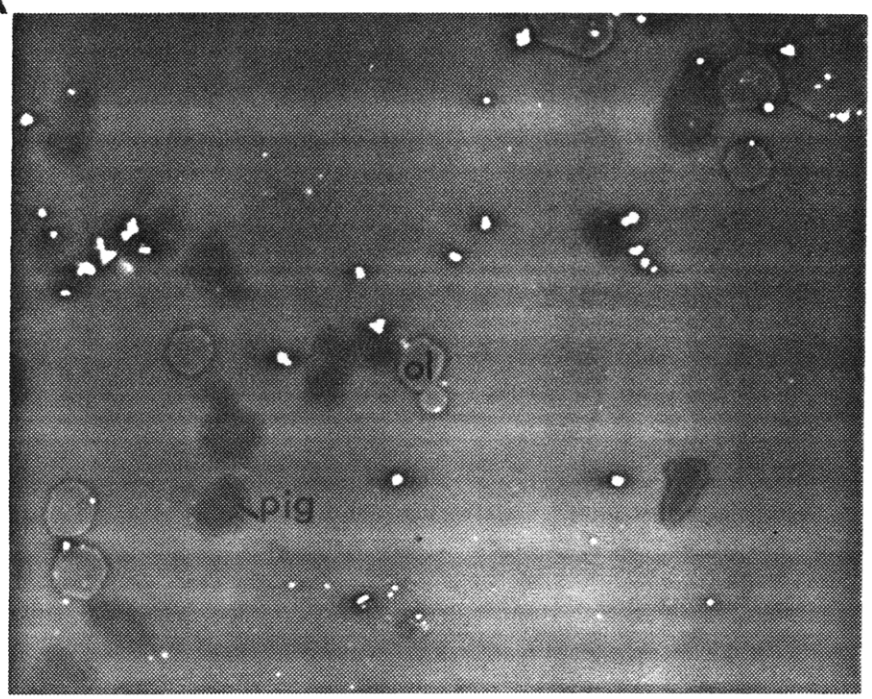

B

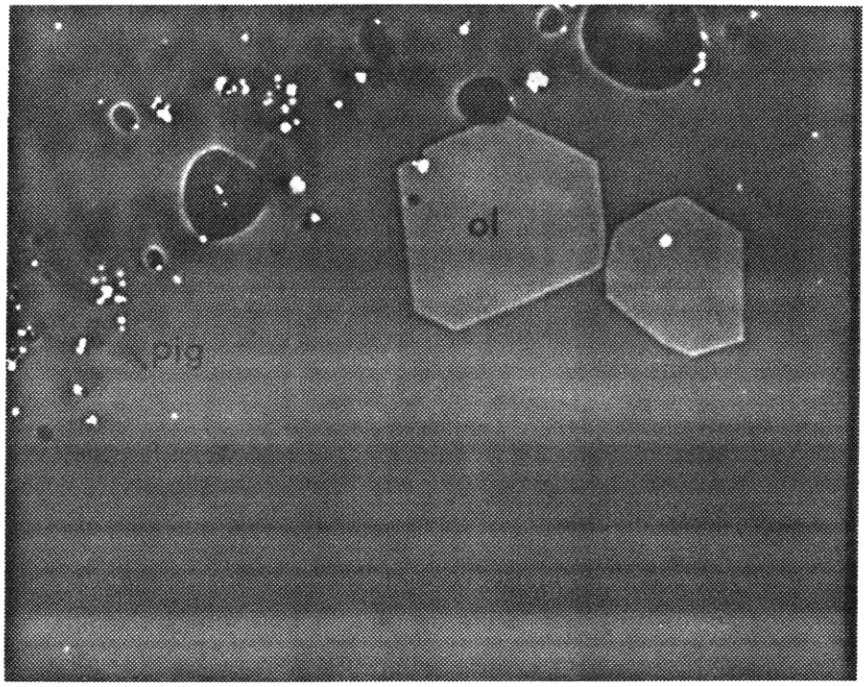

Figure 2-4

Portion of the Oliv - Qtz - An diagram showing experimentally determined phase boundaries at 1 atm and 1 kbar, compositions of experimentally produced mineral phases (pyx = pigeonite and pl = plagioclase) and model compositions of the eucrite parent body (1 - 4 are Eu1 - Eu4, BVSP, 1981). K = Kapoeta rho, Y = Yamato 7308 PE1. A) Projection scheme of Stolper (1977) using molar units. B) Projection scheme of Grove et al. (1983) using oxygen units.

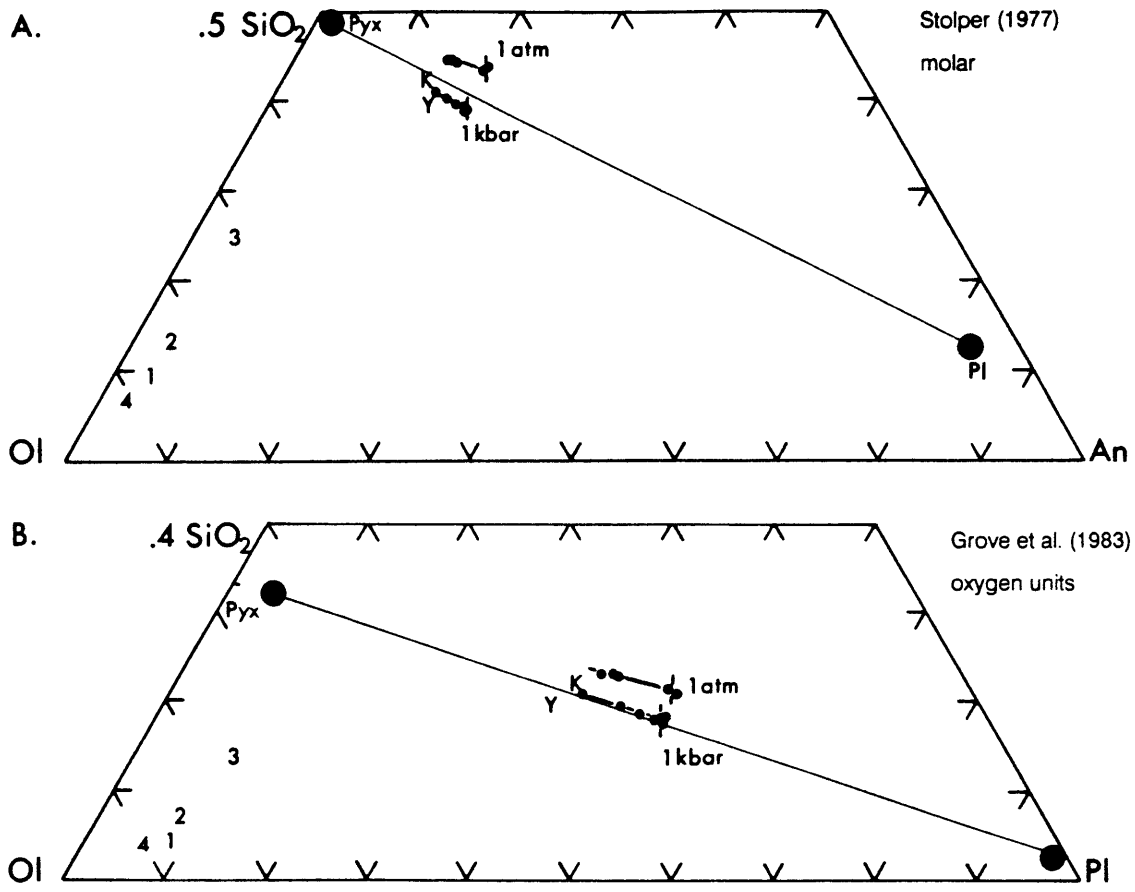
A.
.5 SiO2
Pyx
1 atm
K
Y
1 kbar
3
2
1
4
Pl
Ol
An
Stolper (1977)
molar
B.
.4 SiO2
Pyx
K
Y
1 atm
1 kbar
3
2
4
1
Ol
Pl
Grove et al. (1983)
oxygen units

Figure 2-5

Portion of the Oliv - Qtz - An diagram showing experimentally determined phase boundaries at 1 atm and 1 kbar for the magnesian eucrite compositions of this study. Projection scheme is from Grove et al. (1983) and uses oxygen units. The 1 atm and 10 kbar anorthite - enstatite cotectics as reported in Sen and Presnall (1984) are shown as near-vertical lines labelled an-en. The dotted line with arrows at the base of these boundaries shows the implied movement of liquids in CMAS saturated with plagioclase and low-Ca pyroxene and near olivine saturation. Open circles connected by arrows show the projected compositions of liquids saturated with forsterite, anorthite, enstatite and diopside at 1 atm and 7 kbar from Presnall et al. (1979). Light vectors indicate effect of increasing Fe/[Fe+Mg] on olivine - pyroxene - plagioclase saturated boundaries.

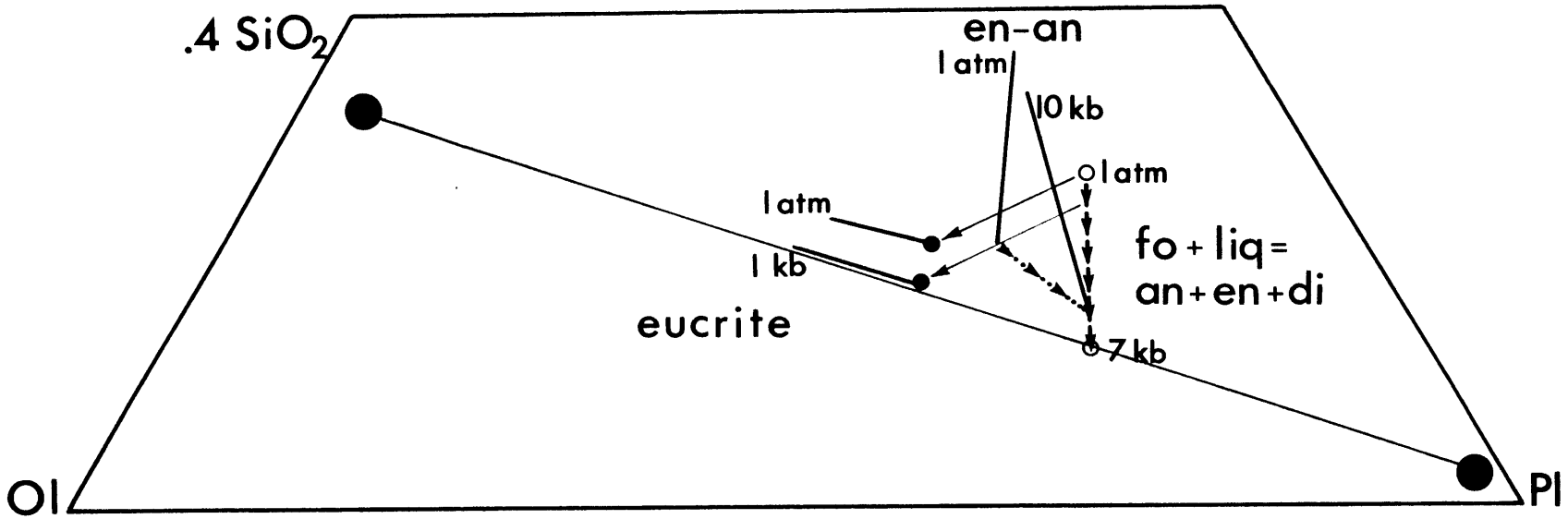
.4 SiO2
en-an
1 atm
10 kb
1 atm
1 atm
1 kb
fo + liq =
an + en + di
eucrite
7 kb
Ol
Pl

Figure 2-6

Plot of wt.% TiO_2 vs. Mg/(Mg+Fe) for eucrites, magnesian eucrite clasts and calculated models of melting and crystallization. Solid circles are noncumulate eucrites from BVSP (1981) and Warren and Jerde (1987). NL = Nuevo Laredo, St = Stannern, B = Bereba, C = Cachari, sc = Sioux County. Also shown as solid circles are magnesian eucrite clasts Kapoeta rho (K) and Yamato 7308 PE1 (Y). Solid square is the average of magnesian clasts in Pomozdino (Mason et al., 1979). Batch melting models for eucrite parent body compositions Eu1 (Morgan et al., 1978) and Eu3 (Dreibus et al., 1977) calculated using K_d's from the 1 kbar experiments. Dashed line indicates presence of olivine, spinel, and/or low-Ca pyroxene in solid. Solid lines indicate that plagioclase is also present. Melting calculations terminate at 30% melting and plagioclase disappears at about 10 % melting. Crystallization paths extending from Kapoeta and Yamato are based on 1 atm experiments.

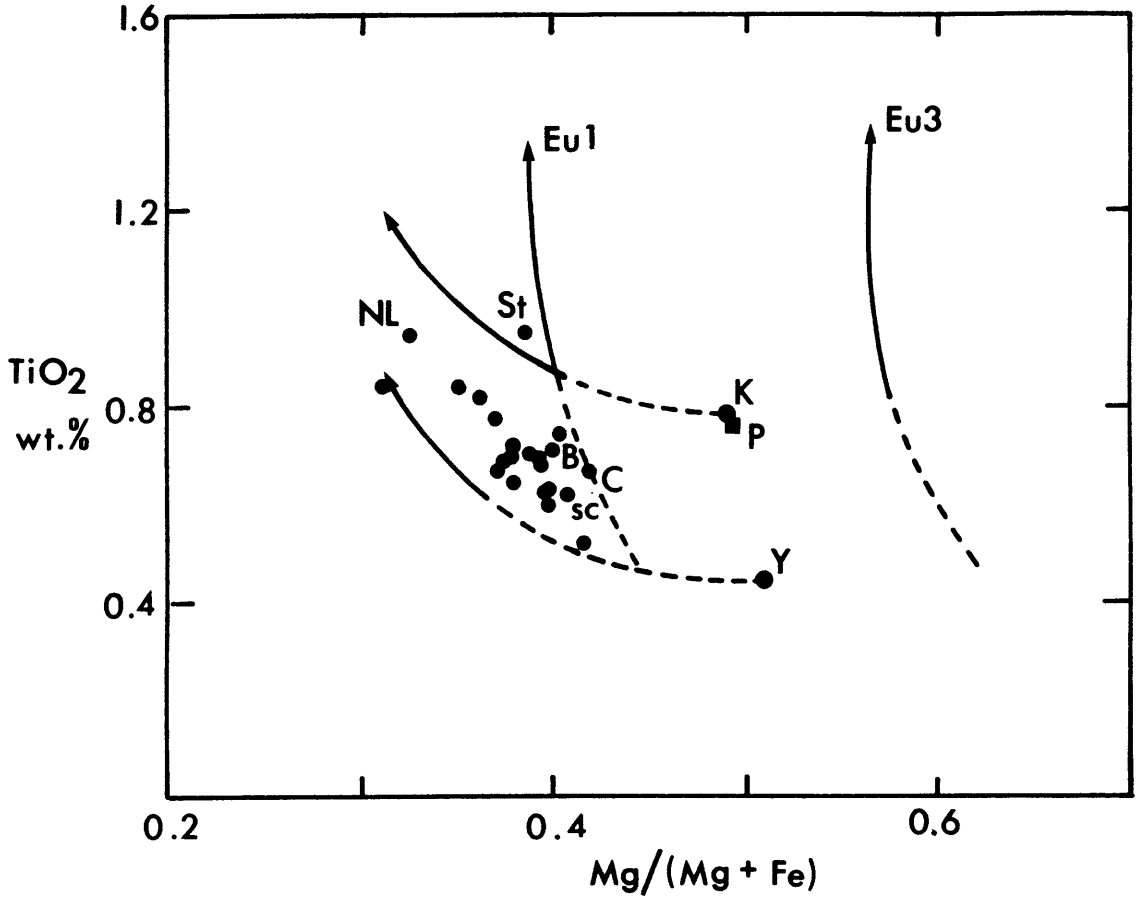
1.6
1.2
0.8
0.4
TiO2
wt.%
0.2
0.4
0.6
Mg/(Mg + Fe)
Eu1
Eu3
NL
St
K
P
B
C
sc
Y

Figure 2-7.

Portion of the Oliv - Qtz - An diagram showing experimentally determined phase boundaries at 1 atm and 1 kbar and locations of selected HED meteorites (circles) and meteorite fields (dotted outlines). Description of phase diagram is as in Figure 2-2.

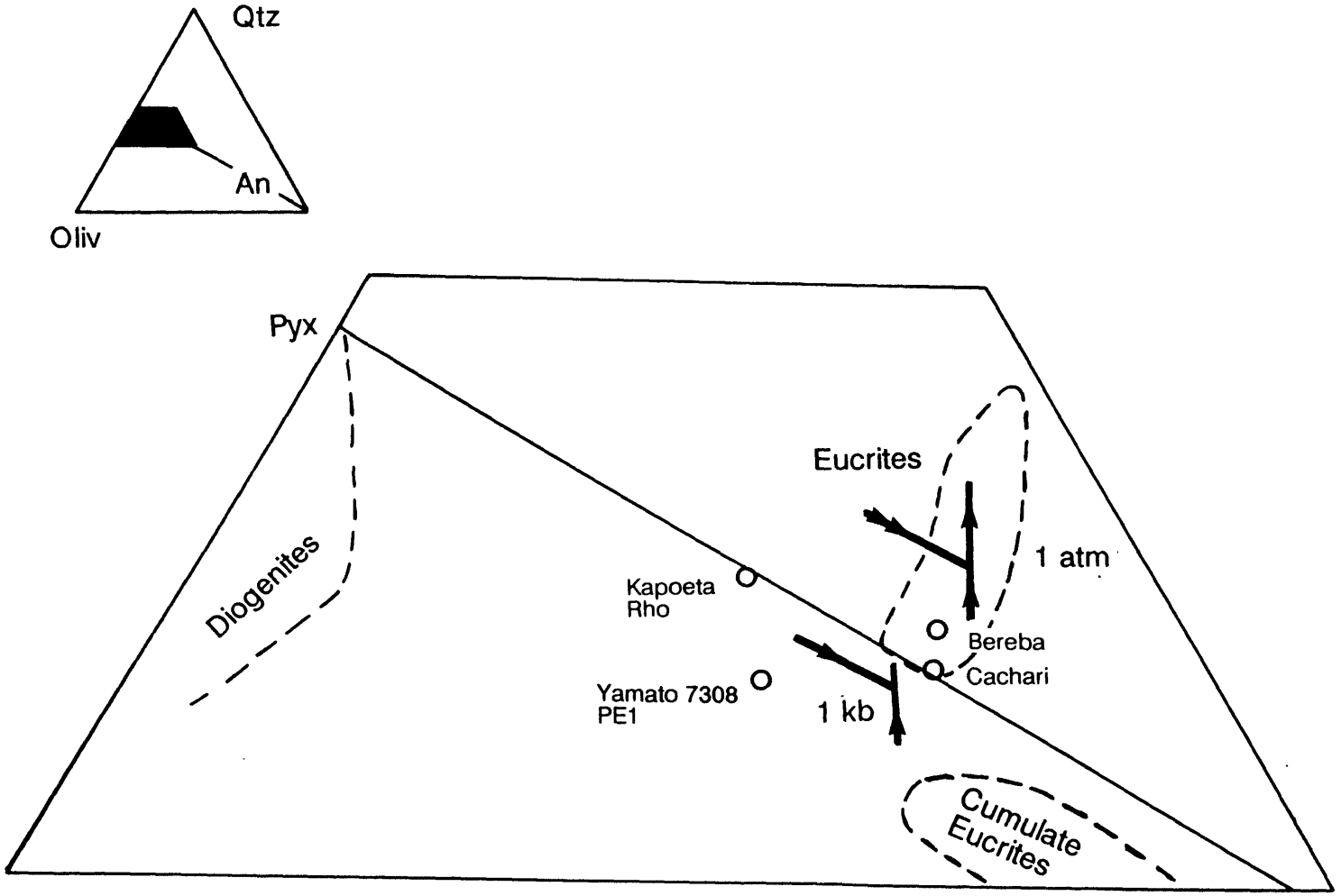
Qtz
An
Oliv
Pyx
Diogenites
Eucrites
1 atm
Kapoeta
Rho
Bereba
Cachari
Yamato 7308
PE1
1 kb
Cumulate
Eucrites

Figure 2-8.

Formation of HED meteorite components through fractional crystallization processes in the eucrite parent body (EPB). a) A portion of the Oliv - Qtz - An diagram (refer to Figure 2-2 for description) showing 1 atm, 0.5 kbar and 1 kbar phase boundaries and liquid paths (triangles) for fractional crystallization processes. b) A schematic cross section of the eucrite parent body. Igneous processes are indicated by capital letters. A) Partial melting of a magnesian chondritic source at 0.9 kbar, such that plagioclase is exhausted and the liquid lies on the olivine - low-Ca pyroxene boundary, producing magnesian eucrite magmas similar to Kapoeta rho and Yamato 7308 PE1. B) Polybaric fractionation of low-Ca pyroxene and olivine from liquid A, producing diogenites and driving the residual liquids toward C) the plagioclase saturated eucrite lavas. D) Parent magma A fractionates a small amount of low-Ca pyroxene plus olivine before becoming arrested at 130 km depth within the EPB. Here liquids leave the olivine - low-Ca pyroxene reaction boundary and precipitate only pyroxene until reaching the pyroxene - plagioclase boundary. Pyroxene plus plagioclase crystallization here produces the cumulate eucrites.

Formation of diogenites, cumulate eucrites and eucrites

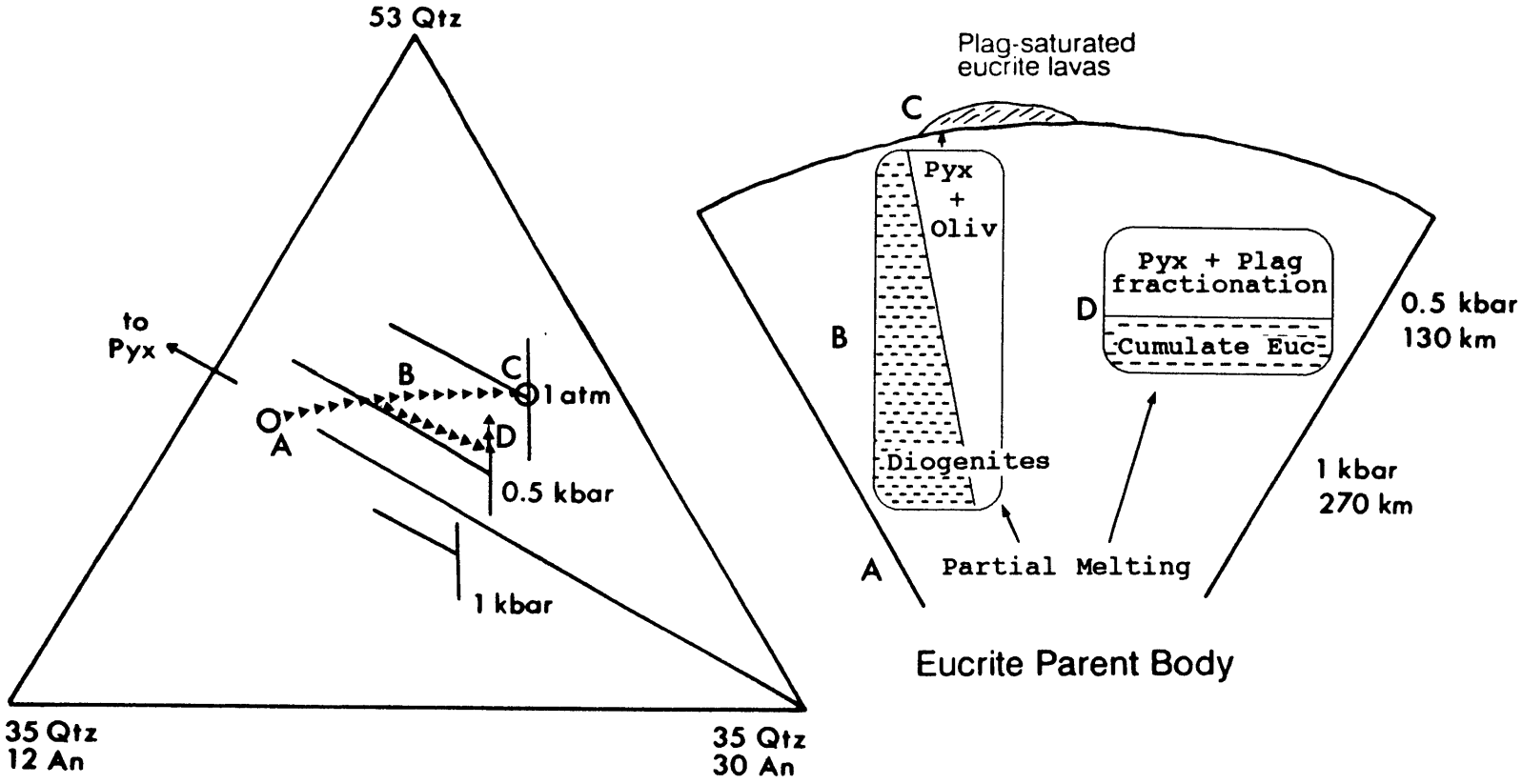

APPENDIX

Fe/Mg and Ca/Na Mineral/Liquid Exchange K_Ds

APPENDIX

This appendix contains data from both chapters for Fe/Mg mineral/liquid exchange K_Ds ($FeO_{xtl}MgO_{liq}/MgO_{xtl}FeO_{liq}$) for olivine and pyroxene and Ca/Na mineral/liquid exchange K_Ds ($CaO_{xtl}Na_2O_{liq}/Na_2O_{xtl}CaO_{liq}$) for plagioclase.

Table A Fe/Mg and Ca/Na mineral/liquid exchange K_Ds calculated from experiments

$K_D^{Fe/Mg}$	average	standard deviation
HAB olivine/liquid	0.30	0.04
HAB clinopyroxene/liquid	0.31	0.05
HAB orthopyroxene/liquid	0.26	0.06
Eucrite olivine/liquid	0.35	0.01
Eucrite pigeonite/liquid	0.26	0.08
$K_D^{Ca/Na}$	average	standard deviation
HAB plagioclase/liquid		
10 kbar	1.28	0.26
12 kbar	1.66	0.11
15 kbar	1.7	0.2
Eucrite plagioclase/liquid	1.02	0.22

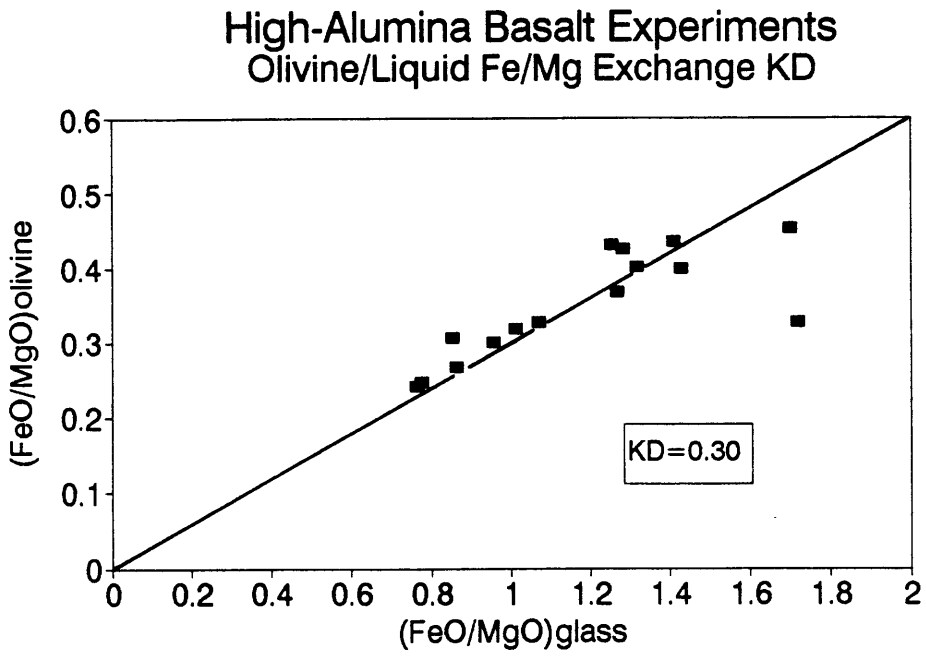
High-Alumina Basalt Experiments
Olivine/Liquid Fe/Mg Exchange KD
(FeO/MgO)olivine
(FeO/MgO)glass
KD=0.30
0
0.1
0.2
0.3
0.4
0.5
0.6
0
0.2
0.4
0.6
0.8
1
1.2
1.4
1.6
1.8
2

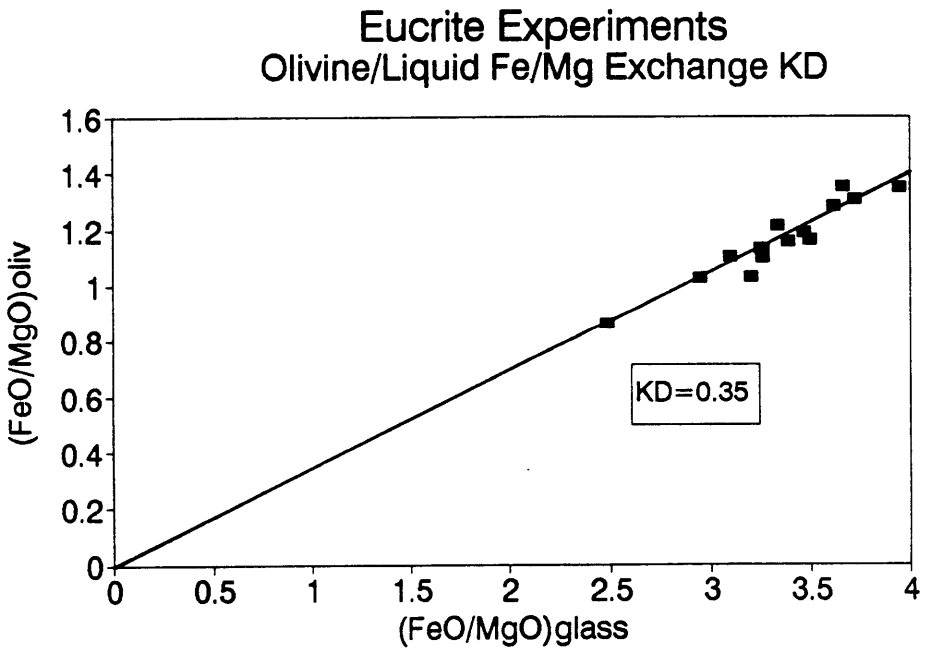
Eucrite Experiments
Olivine/Liquid Fe/Mg Exchange KD
(FeO/MgO)oliv
(FeO/MgO)glass
KD=0.35
0
0.2
0.4
0.6
0.8
1
1.2
1.4
1.6
0
0.5
1
1.5
2
2.5
3
3.5
4

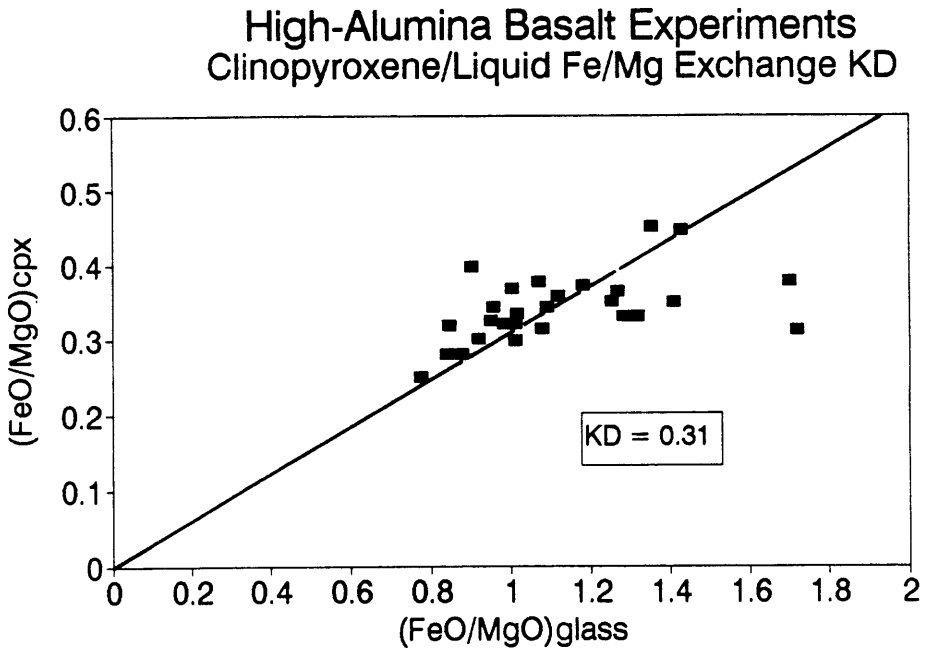
High-Alumina Basalt Experiments
Clinopyroxene/Liquid Fe/Mg Exchange KD
(FeO/MgO)cpx
(FeO/MgO)glass
KD = 0.31
0
0.1
0.2
0.3
0.4
0.5
0.6
0.2
0.4
0.6
0.8
1
1.2
1.4
1.6
1.8
2

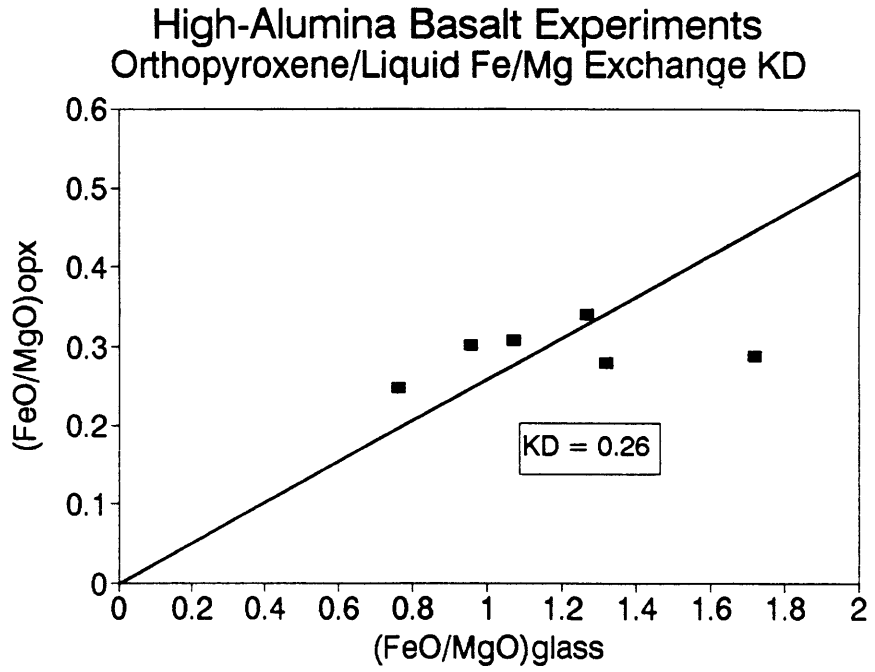
High-Alumina Basalt Experiments
Orthopyroxene/Liquid Fe/Mg Exchange KD
(FeO/MgO)opx
(FeO/MgO)glass
KD = 0.26
0
0.1
0.2
0.3
0.4
0.5
0.6
0.2
0.4
0.6
0.8
1
1.2
1.4
1.6
1.8
2

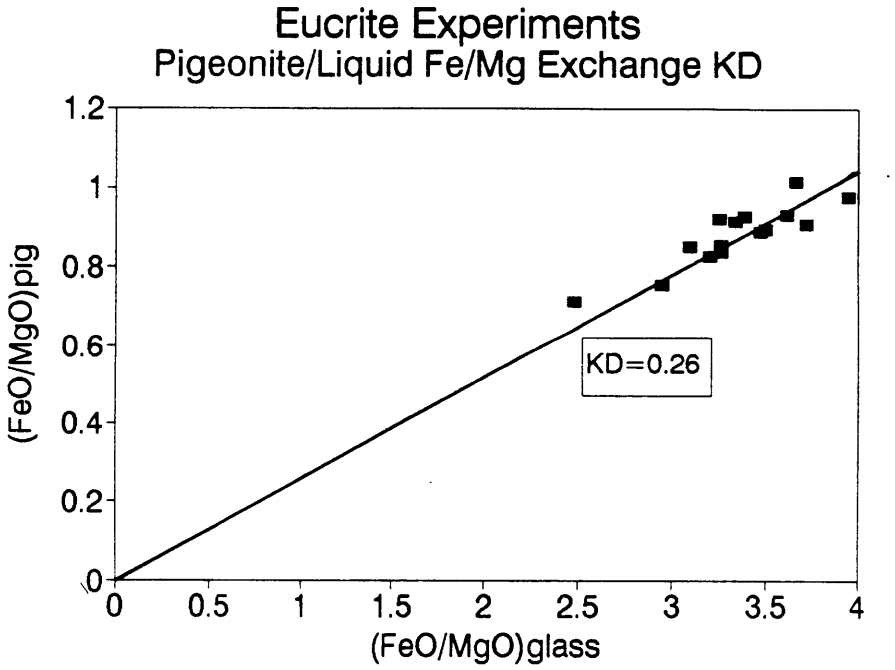
Eucrite Experiments
Pigeonite/Liquid Fe/Mg Exchange KD
(FeO/MgO)pig
(FeO/MgO)glass
KD=0.26
0
0.2
0.4
0.6
0.8
1
1.2
0.5
1
1.5
2
2.5
3
3.5
4

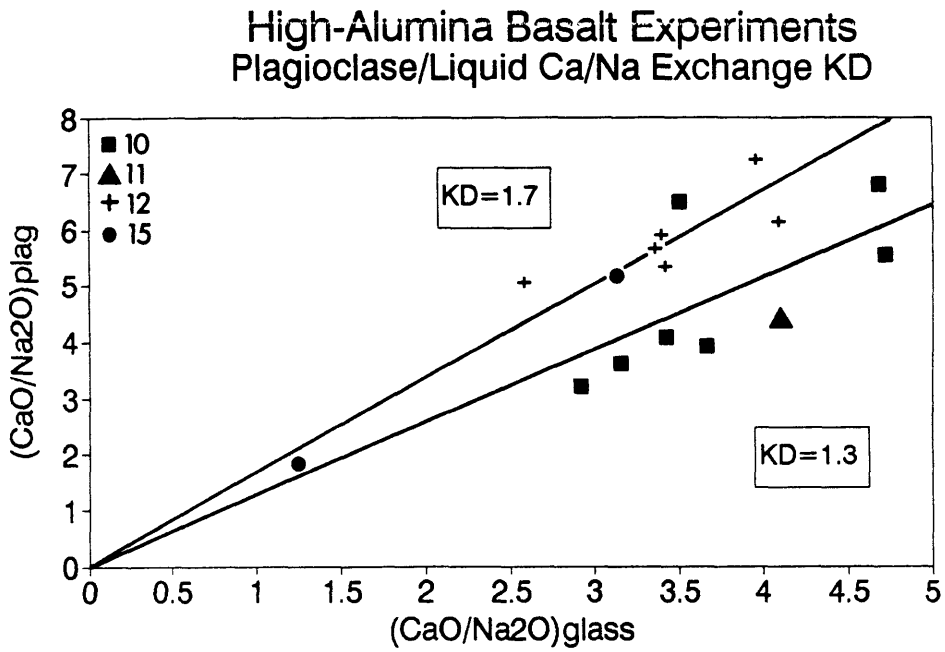
High-Alumina Basalt Experiments
Plagioclase/Liquid Ca/Na Exchange KD
■ 10
▲ 11
+ 12
● 15
KD=1.7
KD=1.3
(CaO/Na2O)plag
(CaO/Na2O)glass
0
0.5
1
1.5
2
2.5
3
3.5
4
4.5
5
1
2
3
4
5
6
7
8

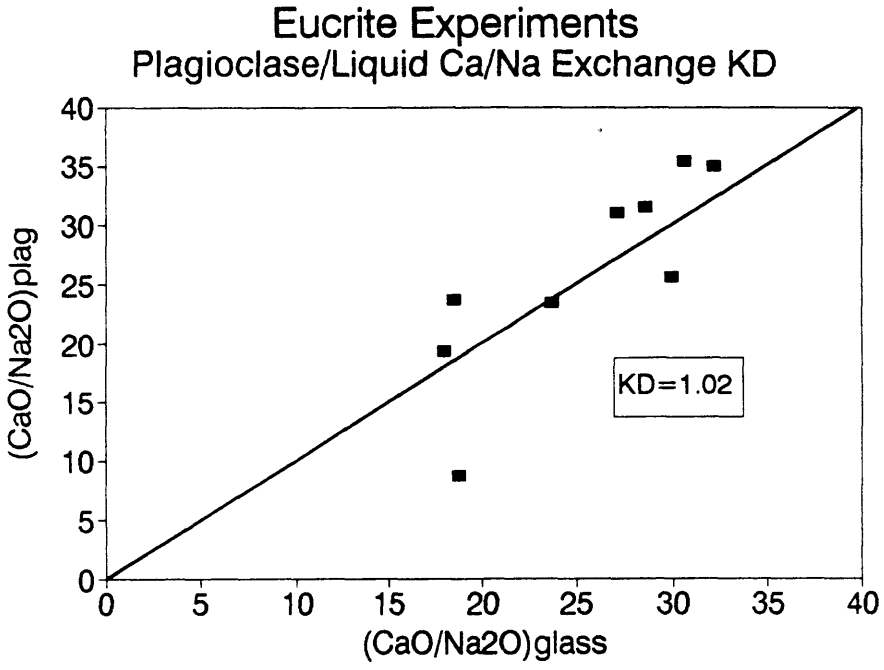
Eucrite Experiments
Plagioclase/Liquid Ca/Na Exchange KD
KD=1.02
(CaO/Na2O)plag
(CaO/Na2O)glass
0
5
10
15
20
25
30
35
40